Journal of Research of the National Bureau of Standards

Volume 90 **Number 2** **March–April**

ISSN 0160-1741 **Library of Congress Catalog Card No.: 63-37059**

The Journal of Research of the National Bureau of Standards features advances in measurement methodology and analyses consistent with the NBS responsibility as the nation's measurement science laboratory. It includes reports on instrumentation for making accurate and precise measurements in fields of physical science and engineering, as well as the mathematical models of phenomena which enable the predictive determination of information in regions where measurements may be absent. Papers on critical data, calibration techniques, quality assurance programs, and well characterized reference materials reflect NBS programs in these areas. Special issues of the Journal are devoted to invited papers in a particular field of measurement science. Occasional survey articles and conference reports appear on topics related to the Bureau's technical and scientific programs. As a special service to subscribers each issue contains complete citations to all recent NBS publications in NBS and non-NBS media.

Issued six times a year. Annual subscriptions: domestic $17.00; foreign $21.25. Single copy, $3.00 domestic; $3.75 foreign.

United States Government Printing Office, Washington: 1985
Order all publications from the Superintendent of Documents
U.S. Government Printing Office, Washington, DC 20402

The Secretary of Commerce has determined that the publication of the periodical is necessary in the transaction of the public business required by law of this Department. Use of funds for printing this periodical has been approved by the Director of the Office of Management and Budget through April 1, 1986.

Journal of Research of the National Bureau of Standards
Volume 90, Number 2, March–April 1985

New Results From Previously Reported NBS Fundamental Constant Determinations

B. N. Taylor
National Bureau of Standards, Gaithersburg, MD 20899

Accepted: December 13, 1984

A new treatment of previously reported results of three electric-unit-dependent fundamental constant experiments carried out at NBS over the last decade or so yields accurate, indirect values in SI units for a number of important quantities. These include the fine-structure constant α, the Avogadro constant N_A, the Josephson frequency-voltage ratio $2e/h$, and the quantized Hall resistance $R_H \equiv h/e^2$.

Key words: Avogadro constant; Faraday constant; fine-structure constant; Josephson frequency-voltage ratio; proton gyromagnetic ratio; quantized Hall resistance.

1. Introduction

Over the last decade or so the National Bureau of Standards (NBS) has reported the results of three high accuracy fundamental constant determinations carried out in terms of NBS as-maintained electrical units. The three quantities are the Faraday constant F_{NBS} determined in 1975 using a silver-perchloric acid coulometer [1][1]; the low field gyromagnetic ratio of the proton $(\gamma'_{p,L})_{NBS}$ measured in 1978 using the so-called weak or low field method (the prime means the protons are in a spherical sample of pure H_2O at 25 °C) [2]; and the quantized Hall resistance $(R_H)_{NBS} \equiv (h/e^2)_{NBS}$ (h is the Planck constant and e the elementary charge) determined in 1983–1984 [3][2] using the quantum Hall effect [6] in GaAs-$Al_xGa_{1-x}As$ heterostructures. Here and throughout this paper the subscript NBS indicates NBS electrical units; lack of a subscript indicates *Le Système International d'Unités* (SI) units.

The NBS as-maintained electrical units in terms of which F_{NBS}, $(\gamma'_{p,L})_{NBS}$, and $(R_H)_{NBS}$ have been measured are $(V_{NBS}/\Omega_{NBS}) = A_{NBS}$ and Ω_{NBS}. Here V_{NBS} is the NBS volt maintained constant in time since 1972 July 1 using the ac Josephson effect with an uncertainty of a few parts in 10^8, the value of the Josephson frequency-voltage ratio $2e/h$ adopted for this purpose being [7]

$$(2e/h)_{NBS} = 483593.420 \text{ GHz}/V_{NBS}. \quad (1)$$

This implies that the ratio $K_V \equiv V_{NBS}/V$, where V is the SI volt, is given by

$$K_V \equiv V_{NBS}/V \quad (2a)$$

$$= (2e/h)_{NBS}/(2e/h) \quad (2b)$$

and may be assumed to be time invariant within a few parts in 10^8.

The quantity Ω_{NBS} is the NBS ohm defined in terms of the mean resistance of five wire-wound, one-ohm resistors of the Thomas-type. Because Ω_{NBS} is based on artifact standards, one must assume that it is a time-varying unit. This implies that the ratio

About the Author: B. N. Taylor, a physicist, is chief of the Electricity Division in the NBS Center for Basic Standards.

[1]Numbers in brackets indicate literature references.

[2]The result reported in Ref. [3] supplants entirely that given in Ref. [4] since the temperature dependence of R_H, as described in Ref. [5], was not properly taken into account in the earlier work of Ref. [4]. We assume throughout this paper that the quantized Hall resistance is a legitimate measure of h/e^2, i.e., that any corrections are negligibly small.

$$K_\Omega \equiv \Omega_{NBS}/\Omega \tag{3}$$

also varies with time.

The NBS ampere A_{NBS} is not separately maintained but is defined in terms of the NBS ohm and volt: $A_{NBS}=V_{NBS}/\Omega_{NBS}$. It thus follows that A_{NBS} also varies with time as does the ratio

$$K_A \equiv A_{NBS}/A \tag{4a}$$

$$= K_V/K_\Omega \, . \tag{4b}$$

The actual NBS electrical units in terms of which F_{NBS}, $(\gamma'_{p,L})_{NBS}$, and $(R_H)_{NBS}$ were measured are, respectively, A_{NBS}, A_{NBS}^{-1}, and Ω_{NBS}. Because A_{NBS} and Ω_{NBS} are time varying units as just discussed and the three experiments were carried out over a 10-year period, the three results cannot be readily combined to obtain values for other quantities such as the fine-structure constant α and Avogadro constant N_A. This is unfortunate since, had they been measured at the same time, it would have been a straightforward procedure to derive accurate, indirect values in SI units for these constants as well as for most others of interest. The relevant equations for doing so may be obtained from the known relationships among the constants [8–11]; some of the more important expressions are:

$$\alpha^{-1} = \left[\frac{(\mu'_p/\mu_B)}{2\mu_0 R_\infty} \frac{R_H(t)_{NBS}(2e/h)_{NBS}}{\gamma'_{p,L}(t)_{NBS}}\right]^{1/3} \tag{5}$$

$$N_A = [R_H(t)_{NBS}(2e/h)_{NBS}F(t)_{NBS}]/2 \tag{6}$$

$$2e/h = \left[\frac{16^2 R_\infty^2 (\mu'_p/\mu_B)(m_p/m_e)^3}{\mu_0^4 c^6 M_p^3}\right.$$

$$\left. \times \frac{R_H(t)_{NBS}^4 (2e/h)_{NBS}^4 F(t)_{NBS}^3}{\gamma'_{p,L}(t)_{NBS}}\right]^{1/6} \tag{7}$$

$$R_H = \mu_0 c \alpha^{-1}/2 = R_H(t)_{NBS} K_\Omega(t)_{NBS} \tag{8a}$$

$$= \left[\frac{\mu_0^2 c^3 (\mu'_p/\mu_B)}{16 R_\infty} \frac{R_H(t)_{NBS}(2e/h)_{NBS}}{\gamma'_{p,L}(t)_{NBS}}\right]^{1/3} \tag{8b}$$

$$F = \left[\frac{M_p}{(\mu'_p/\mu_B)(m_p/m_e)} \gamma'_{p,L}(t)_{NBS} F(t)_{NBS}\right]^{1/2} \tag{9}$$

$$K_\Omega(t) = \left[\frac{\mu_0^2 c^3 (\mu'_p/\mu_B)}{16 R_\infty} \frac{(2e/h)_{NBS}}{R_H(t)_{NBS}^2 \gamma'_{p,L}(t)_{NBS}}\right]^{1/3}, \tag{10}$$

where the time dependencies of $(R_H)_{NBS}$, $(\gamma'_{p,L})_{NBS}$, and F_{NBS} have been explicitly indicated [$(2e/h)_{NBS}$ is time independent since V_{NBS} is defined in terms of it through eq (1)]. In these expressions $\mu_0 \equiv 4\pi \times 10^{-7}$ H/m is the permeability of vacuum; $c \equiv 299792458$ m/s is the speed of light in vacuum; μ'_p/μ_B is the magnetic moment of the proton in units of the Bohr magneton (0.012 parts-per-million or ppm current uncertainty[3]); R_∞ is the Rydberg constant for infinite mass (0.0010 ppm current uncertainty); M_p is the molar mass of the proton (0.012 ppm current uncertainty); and m_p/m_e is the ratio of the proton mass to the electron mass (0.043 ppm current uncertainty).

In the past, these and related expressions have been evaluated by assuming that Ω_{NBS} has been constant in time and by allowing an additional uncertainty of about 0.01 ppm per year for its possible drift [1,2,4]. However, recent comparisons of Ω_{NBS} with the resistance units of other national laboratories show that since about 1970 the NBS ohm has likely been decreasing by approximately 0.06 ppm/yr. In the course of reviewing the implications of such a drift on eqs (5–10), it became apparent that the problem of the time variation of Ω_{NBS} could be neatly solved by making use of one other NBS result, namely, the determination in 1973–1974 via the NBS calculable cross capacitor of the ratio $K_\Omega \equiv \Omega_{NBS}/\Omega$ [12]. With the addition of this single measurement, the drift rate of the NBS ohm may be uniquely determined, the values of $(R_H)_{NBS}$, $(\gamma'_{p,L})_{NBS}$, and F_{NBS} converted to the same measurement date, and eqs (5–10) and their numerous extensions readily evaluated. The only critical assumption required is that the drift of the NBS ohm has been linear since the time of the calculable capacitor determination of K_Ω. However, this is supported by the observed linear time dependencies of the measured differences between each of the five resistors which comprise Ω_{NBS} and their mean [13].

We now briefly summarize how the calculation proceeds. The linear drift rate assumption enables one to write

$$K_\Omega(t) \equiv \Omega(t)_{NBS}/\Omega = K_\Omega(t_\Omega)[1 + b(t - t_\Omega)], \tag{11}$$

where t is the time in years measured from some arbitrary date, t_Ω is the mean date of the NBS calculable capacitor experiment with $K_\Omega(t_\Omega)$ the mean value obtained, and b is the relative drift rate of Ω_{NBS}.[4] It then

[3] Throughout, all uncertainties are one standard deviation estimates.

[4] The time period over which K_Ω was measured was sufficiently short and the random scatter sufficiently large that the effect of the drift of Ω_{NBS} was indiscernible and hence negligible. This is also true of the measurements of F_{NBS}, $(\gamma'_{p,L})_{NBS}$, and $(R_H)_{NBS}$.

follows from this equation and the way Ω_{NBS} enters the determination of F_{NBS}, $(\gamma'_{p,L})_{NBS}$, and $(R_H)_{NBS}$ that

$$F(t)_{NBS}=F(t_F)_{NBS}[1+b(t-t_F)] \quad (12)$$

$$\gamma'_{p,L}(t)_{NBS}=\gamma'_{p,L}(t_\gamma)_{NBS}[1-b(t-t_\gamma)] \quad (13)$$

$$R_H(t)_{NBS}=R_H(t_R)_{NBS}[1-b(t-t_R)], \quad (14)$$

where t_F, t_γ, and t_R are the mean dates of the Faraday constant, proton gyromagnetic ratio, and quantized Hall resistance determinations, respectively, and $F(t_F)_{NBS}$, $\gamma'_{p,L}(t_\gamma)_{NBS}$, and $R_H(t_R)_{NBS}$ are the mean values obtained. The drift rate b may then be calculated by substituting eq (13) for $\gamma'_{p,L}(t)_{NBS}$ into eq (10) and equating the result to eq (11) with $t=t_R$. Once b is in hand, eqs (5–10) may be evaluated with the aid of eqs (12–14). Of course, the law of error propagation must be strictly obeyed in order to obtain correct uncertainties for the calculated quantities.

We have carried out such calculations with the data listed in tables 1 and 2, to which these comments apply:

Table 1. The values quoted for the nonexact constants are based on the results reported in the original references and (with the exception of m_p/m_e) analyses carried out by the author in connection with the 1985 least squares adjustment of the fundamental constants [14]. However, these analyses have generally led to only minor changes in the original results.

Table 2. Only the value of F_{NBS} has been at all changed from that originally reported. The 0.2 ppm net increase arises from a number of positive and negative corrections. New measurements of the Au and Ta impurity content of the silver used in the experiment [20] were specifically undertaken as a result of the author's reanalysis of the experiment for the 1985 adjustment. It should be noted that the 0.031 ppm uncertainty assigned $(2e/h)_{NBS}$ is an estimate of how well the NBS Josephson effect voltage standard apparatus implements the definition of V_{NBS} [see eq (1)]. The uncertainties associated with relating the working voltage standards used in the $(\gamma'_{p,L})_{NBS}$ and F_{NBS} experiments to the voltage standards used to preserve or store V_{NBS} between Josephson effect calibrations are included in the uncertainties assigned F_{NBS} and $(\gamma'_{p,L})_{NBS}$ as given in the table.

The results of the calculations are:

$$\alpha^{-1}=137.035981(12)\ (0.089\ \text{ppm}) \quad (15)$$

$$R_H=25812.8041(23)\ \Omega\ (0.089\ \text{ppm}) \quad (16)$$

$$2e/h=483597.91(32)\ \text{GHz}\cdot\text{V}^{-1}\ (0.67\ \text{ppm}) \quad (17)$$

$$N_A=6.0221438(80)\times10^{23}\ \text{mol}^{-1}\ (1.33\ \text{ppm}) \quad (18)$$

$$F=96485.381(65)\ \text{A}\cdot\text{s}\cdot\text{mol}^{-1}\ (0.67\ \text{ppm}), \quad (19)$$

Table 1. Summary of defined and electric-unit-independent constants used to evaluate eqs (5–10).

Quantity	Numerical value[1]	Uncertainty (ppm)	Refs.
μ_0	$4\pi\times10^{-7}$	defined	
c	299792458	defined	
μ'_p/μ_B	0.001520993127(18)	0.012	[15,14]
R_∞	10973731.529(11)	0.0010	[16,17,14]
M_p	0.001007276470(12)	0.012	[18,14]
m_p/m_e	1836.152470(79)	0.043	[19]

[1]The units for μ_0 are $\text{H}\cdot\text{m}^{-1}$; for c, $\text{m}\cdot\text{s}^{-1}$; for R_∞, m^{-1}; for M_p, $\text{kg}\cdot\text{mol}^{-1}$.

Table 2. Summary of NBS electric-unit-dependent data used to evaluate eqs (5–10).

Quantity	Mean date of measurement	Value[1]	Uncertainty (ppm)	Refs.
$(2e/h)_{NBS}$	Continuous since 1972 July 1	483593.420(15)	0.031	[7]
F_{NBS}	1975 March 15	96486.19(13)	1.33	[1,20,14]
$(\gamma'_{p,L})_{NBS}$	1978 March 22	2.67513229(57)	0.21	[2]
$(R_H)_{NBS}$	1983 November 27	25812.8420(12)	0.047	[3]
$K_\Omega\equiv\Omega_{NBS}/\Omega$	1973 December 2	$1-0.819(27)\times10^{-6}$	0.027	[12]

[1]The units for $(2e/h)_{NBS}$ are $\text{GHz}\cdot\text{V}_{NBS}^{-1}$; for F_{NBS}, $\text{A}_{NBS}\cdot\text{s}\cdot\text{mol}^{-1}$; for $(\gamma'_{p,L})_{NBS}$, $10^8\ \text{s}^{-1}\cdot\text{T}_{NBS}^{-1}$; for $(R_H)_{NBS}$, Ω_{NBS}. Note that in the $(\gamma'_{p,L})_{NBS}$ experiment the NBS tesla $T_{NBS}\propto A_{NBS}$.

with $b = (-0.0650 \pm 0.0102)$ ppm/yr.[5] The value for K_Ω on 1985 January 1 is $1-(1.539\pm0.107)$ ppm. While it is not the purpose of this paper to make detailed comparisons of these results with others obtained by either direct or indirect means, we do note that in most cases where other values exist the agreement is statistically acceptable. We further point out that the value of $2e/h$ derived here is (9.29 ± 0.67) ppm larger than the value used to define V_{NBS}, implying that V_{NBS} is (9.29 ± 0.67) ppm smaller than the SI volt [see eq (2b)]. This value of $2e/h$ is also (8.09 ± 0.67) ppm larger than the value 483594 GHz/V which is in use in many other national laboratories and which was recommended by the Comité Consultatif d'Electricité in 1972 [23].

In closing we emphasize that the values given here for the various constants, in particular the fine-structure constant, *are the best that can be obtained based solely on existing NBS electrical measurements*.[6] If the three quantities $(\gamma'_{p,L})_{NBS}$, $(R_H)_{NBS}$, and K_Ω had been determined at the same time, then any two would have been sufficient to determine α^{-1}. For example, eq (5) yields a value of α^{-1} from $(\gamma'_{p,L})_{NBS}$ and $(R_H)_{NBS}$. The comparable equations for the two other pairs of measurements are[7]

$$\alpha^{-1} = \left[\frac{c(\mu'_p/\mu_B)}{4R_\infty}\,\frac{(2e/h)_{NBS}}{K_\Omega(\gamma'_{p,L})_{NBS}}\right]^{1/2} \tag{20}$$

$$\alpha^{-1} = 2(R_H)_{NBS}K_\Omega/\mu_0 c. \tag{21}$$

By treating the drift rate of the NBS ohm as a variable we remove the redundancy or overdetermination inherent in the three measurements and obtain a unique value for α^{-1} and all other quantities. Since this approach eliminates the distinction between the so-called Josephson effect value of α^{-1} traditionally derived from eq (20) and the quantum Hall effect value derived from eq (21), perhaps the value given here should simply be referred to as the NBS condensed matter value.

I gratefully acknowledge helpful discussions with B. F. Field and E. R. Williams and the assistance of V. E. Bower, R. S. Davis, E. R. Williams, P. T. Olsen, M. E. Cage, R. F. Dziuba, and B. F. Field in reviewing their experiments. The data analyses carried out in connection with the 1985 least squares adjustment of the fundamental constants were performed in collaboration with E. R. Cohen.

References

[1] Bower, V. E., and R. S. Davis, J. Res. Natl. Bur. Stand. **85**, 175 (1980)/Powell, L. J.; T. J. Murphy and J. W. Gramlich, J. Res. Natl. Bur. Stand. **87**, 9 (1982)/Bower, V. E.; R. S. Davis, T. J. Murphy, P. J. Paulsen, J. W. Gramlich, and L. J. Powell, J. Res. Natl. Bur. Stand. **87**, 21 (1982).

[2] Williams, E. R., and P. T. Olsen, Phys. Rev. Lett. **42**, 1575 (1979).

[3] Cage, M. E.; R. F. Dziuba and B. F. Field, IEEE Trans. Instrum. Meas. **IM-34**, June 1985, to be published.

[4] Tsui, D. C.; A. C. Gossard, B. F. Field, M. E. Cage, and R. F. Dziuba, Phys. Rev. Lett. **48**, 3 (1982).

[5] Cage, M. E.; B. F. Field, R. F. Dziuba, S. M. Girvin, A. C. Gossard, and D. C. Tsui, Phys. Rev. B **30**, 2286 (1984).

[6] Klitzing, K.V.; G. Dorda and M. Pepper, Phys. Rev. Lett. **45**, 494 (1980).

[7] Field, B. F.; T. F. Finnegan and J. Toots, Metrologia **9**, 155 (1973).

[8] Taylor, B. N., IEEE Trans. Instrum. Meas. **IM-34**, June 1985, to be published.

[9] Taylor, B. N., Metrologia **12**, 81 (1976); Metrologia **9**, 21 (1973).

[10] Cohen, E. R., and B. N. Taylor, J. Phys. Chem. Ref. Data **2**, 663 (1973).

[11] Taylor, B. N.; D. N. Langenberg and W. H. Parker, Rev. Mod. Phys. **41**, 375 (1969).

[12] Cutkosky, R. D., IEEE Trans. Instrum. Meas. **IM-23**, 305 (1974).

[13] Dziuba, R. F., private communication (1984).

[14] Cohen, E. R., and B. N. Taylor, J. Phys. Chem. Ref. Data, to be published.

[15] Phillips, W. D.; W. E. Cooke and D. Kleppner, Metrologia **13**, 179 (1977).

[16] Amin, S. R.; C. D. Caldwell and W. Lichten, Phys. Rev. Lett. **47**, 1234 (1981).

[17] Goldsmith, J. E. M.; E. W. Weber and T. W. Hänsch, Phys. Rev. Lett. **41**, 1525 (1978).

[18] Wapstra, A. H., and G. Audi, Nucl. Phys. A, to be published.

[19] Van Dyck, R. S. Jr.; F. L. Moore and P. B. Schwinberg, Bull. Am. Phys. Soc. **28**, 791 (1983) and private communication (1983).

[20] Greenberg, R. R., private communication (1984).

[21] Thompson, A. M., Metrologia **4**, 1 (1968)/Clothier, W. K., Metrologia **1**, 35 (1965).

[22] Leclerc, G., and T. J. Witt, private communication (1984).

[23] Com. Int. Poids Mes., Com. Consult. d'Electricité Trav. 13e Session (1972) p. E-13.

[5] This value is in agreement with $b = -(0.0562\pm0.0048)$ ppm/yr which the author derived from a linear least squares fit to the results of direct and indirect comparisons of Ω_{NBS} with the unit of resistance Ω_{NML} maintained constant in time by Australia's National Measurement Laboratory (NML) with the NML calculable cross capacitor [21]. We also note that the Bureau International des Poids et Mesures unit of resistance Ω_{BIPM} is based on the mean of six resistors, two of which are of the same type used to define Ω_{NBS}. Comparisons of Ω_{BIPM} with Ω_{NML} dating back to 1964 show that Ω_{BIPM} varies quite linearly with time. Since the time dependencies of the measured differences between Ω_{BIPM} and each of the two NBS resistors which partially define Ω_{BIPM} are also observed to be linear [22], it may be concluded that the linear drift rate assumption for Ω_{NBS} is justified. If in fact one assumes the existence of a quadratic component, any reasonable estimate of its magnitude is sufficiently small that its effect is inconsequential.

[6] "Best" or "recommended" values in the traditional sense would, of course, require taking into account the relevant data available from all sources.

[7] Note that eliminating K_Ω from eqs (20) and (21) yields eq (5) while equating the two yields eq (10).

Journal of Research of the National Bureau of Standards
Volume 90, Number 2, March-April 1985

Standards for Measurement of the Critical Fields of Superconductors

F. R. Fickett
National Bureau of Standards, Boulder, CO 80303

Accepted: November 21, 1984

The origins, definitions, and measurement of the various critical magnetic fields associated with superconductors are reviewed. The potential need for a consensus standard for the measurement of these fields is evaluated. Measurement techniques as practiced both in industry and in the national laboratories and extrapolation techniques commonly used to determine the upper critical fields of the newer materials are presented. Sources of error in the experimental determination of critical fields are assessed for the various common techniques. A comprehensive bibliography of the modern literature on critical field measurement and interpretation is included.

Key words: critical field; critical parameters; magnetic field; standards; superconductors.

1. Introduction

The literature of the field of superconductivity is replete with numerous critical magnetic fields. Several (H_c, H_{c1}, H_{c2}) have universal application and acceptance, while many others are defined for subtle and specific purposes [e.g., $B^*_{c2m}(0)$]. Our goal is to evaluate whether there is a need for a measurement standard for critical field similar to one developed recently for critical current [1].[1] We consider only superconductive materials that are either commercial items now or those that have the potential of being so in the foreseeable future. This criterion might seem to allow us to ignore many of the more difficult aspects of the problem, such as the effect of surface superconductivity. Yet, our survey of the literature indicates that frequently these effects do appear in rather mundane measurements and can alter the results significantly. Thus, we have included most of the effects that have been observed to date during attempts to determine the critical fields. However, for practical purposes, effects that take place below a critical current value of about 10^4 A/cm^2 are seldom of interest, which removes us from the more esoteric regions of the J-H and T-H curves. There are, of course, exceptions such as pinning studies. Similarly, the more exotic materials, such as the Chevrel-phase conductors, are not of immediate practical importance. However, that situation could easily change. Thus, although our concentration is on the conductors that are commercially available, these new materials with great potential are also considered.

The terminology used here for the general references to the field of superconductivity is that presented in the several review documents on terminology prepared by our group [2,3] and in the new ASTM standard for superconductor terminology [4]. Definitions of the various critical fields are given both in the discussion of the theory and of the extrapolation techniques.

In the recent past, the differentiation of B and H was a matter left to those who worried about the basic physics of magnetism. Use of the cgs system was entirely acceptable and magnetism and superconductivity did not coexist. Under these conditions, the gauss and the oersted were effectively equivalent and, in fact, were often used interchangeably. At present, however, SI units are rapidly gaining acceptance and more is being written regarding the relationships of magnetism and

About the Author, Paper: F. R. Fickett is a physicist with the NBS Electromagnetic Technology Division in Boulder, CO. His work was supported by the Department of Energy through the Office of Fusion Energy and the Division of High Energy Physics.

[1]Numbers in brackets refer to literature references.

superconductivity [5]. Both situations require that we use more care in the application of these terms. The reader interested in the basics of magnetism is referred to our recent publication on magnetic effects at low temperatures [6]. Table 1 lists definitions and unit conversions for magnetic quantities.

The determining equation (in SI) is:

$$B = \mu_0(H + M), \tag{1}$$

where B is the magnetic flux density (or magnetic in-

Table 1. Units for magnetic properties.

Property	Symbol	Gaussian & cgs emu[a]	Conversion factor, C[b]	SI & rationalized mks[c]
Magnetic flux density, magnetic induction	B	gauss (G)[d]	10^{-4}	tesla (T), Wb/m^2
Magnetic flux	ϕ	maxwell (Mx), G·cm^2	10^{-8}	weber (Wb), volt second (V·s)
Magnetic field strength, magnetizing force	H	oersted (Oe)[e]	$10^3/4\pi$	ampere per meter (A/m)[f]
(Volume) magnetization[g]	M	emu/cm^3 [h]	10^3	A/m
(Volume) magnetization	$4\pi M$	G	$10^3/4\pi$	A/m
Magnetic polarization, intensity of magnetization	J, I, M	emu/cm^3	$4\pi\times10^{-4}$	T, Wb/m^2 [i]
(Mass) magnetization	σ, M	emu/g	1 $4\pi\times10^{-7}$	A·m^2/kg Wb·m/kg
(Volume) susceptibility	χ, κ	dimensionless, emu/cm^3	4π $(4\pi)^2\times10^{-7}$	dimensionless henry per meter (H/m), Wb/(A·m)
(Mass) susceptibility	χ_ρ, κ_ρ	cm^3/g, emu/g	$4\pi\times10^{-3}$ $(4\pi)^2\times10^{-10}$	m^3/kg H·m^2/kg
(Molar) susceptibility	χ_{mol}, κ_{mol}	cm^3/mol, emu/mol	$4\pi\times10^{-6}$ $(4\pi)^2\times10^{-13}$	m^3/mol H·m^2/mol
Magnetic moment	m	emu, erg/G	10^{-3}	A·m^2, joule per tesla (J/T)
Magnetic dipole moment	j	emu, erg/G	$4\pi\times10^{-10}$	Wb·m[i]
Permeability	μ	dimensionless	$4\pi\times10^{-7}$	H/m
Relative permeability[j]	μ_r	not defined		dimensionless
(Volume) energy density, energy product	W, U	erg/cm^3	10^{-1}	J/m^3
Demagnetization factor	D, N	dimensionless	$1/4\pi$	dimensionless

[a] Gaussian units and cgs emu are the same for magnetic properties. The defining relation is $B = H + 4\pi M$.

[b] Multiply a number in Gaussian units by C to convert it to SI (e.g., 1 G$\times10^{-4}$ T/G$=10^{-4}$ T).

[c] SI (*Système International d'Unités*) has been adopted by the National Bureau of Standards. Where two conversion factors are given, the upper one is recognized under, or consistent with, SI and is based on the definition $B = \mu_0(H + M)$, where $\mu_0 = 4\pi\times10^{-7}$ H/m. The lower one is not recognized under SI and is based on the definition $B = \mu_0 H + J$, where the symbol J or M is often used in place of J.

[d] 1 gauss $= 10^5$ gamma (γ).

[e] Dimensionally, oersted = gauss.

[f] *A/m was often expressed as "ampere-turn per meter" when used for magnetic field strength.*

[g] Magnetic moment per unit volume.

[h] The designation, "emu" is not a unit.

[i] Recognized under SI, even though based on the difinition $B = \mu_0 H + J$. See footnote c.

[j] $\mu_r = \mu/\mu_0 = 1 + \chi$, all in SI. μ_r is equal to Gaussian μ.

R. B. Goldfarb and F. R. Fickett, National Bureau of Standards, Boulder, CO 80303, July 1984

duction) in teslas, H is the magnetic field strength in amperes/meter, M is the (volume) magnetization in amperes/meter, and μ_0 is the permeability of free space ($4\pi \times 10^{-7}$ henrys/meter). The important distinction here is that H is an applied field, M is a property of the material and, thus, B is a mixed quantity. Because of this distinction, we suggest that the proper quantity for the critical fields discussed here is H; it is the applied field value at which the transition occurs. This choice leads to the unfortunate side effect which has plagued us for years—few researchers have an innate feel for the units of amperes/meter. This, in turn, leads to the common fix used by many authors of multiplying the number by μ_0 and then using the units of teslas, which are more familiar. As an aside: the correct abbreviation for the tesla is T and the correct plural name is teslas (not capitalized) [7].

Another subject that sometimes leads to confusion in the realm of magnetic measurements is the demagnetization factor, N. In magnetizable bodies, the poles that appear under the influence of the applied field give a return field through the body that has the effect of lowering the actual value of H within the material. This is a geometric effect and is discussed in detail in our publication [6]. It is of concern with superconductors only as long as they are in the perfect Meissner state below H_{c1}, a region that is seldom of practical interest. However, in this region the effect is important and must be accounted for either in the data processing or by choice of a sample geometry that minimizes the effect (a long ellipsoid with its long axis parallel to the applied field).

At first glance, the importance of critical field in practical applications is not obvious. Certainly high values are desired for applications in very high field magnets, but only if reasonable critical currents can also be achieved. However, the upper critical field and its behavior as a function of temperature and critical current are topics of major importance to the theoretical understanding of type II superconductivity, which in turn will almost certainly lead to better materials for the future. A prime example of this is the effort now afoot to create a higher critical field in NbTi alloys by third element additions [8]. The work is crucially dependent on accurate determination of the critical fields. Another example is the application of critical field values in the treatment of scaling of strain effects in high field superconductors.

In the remainder of this paper we will discuss how the various critical fields arise in theory and how they are related to other parameters. The techniques used for the determination of the fields are reviewed with discussion of the accuracy, precision, and experimental difficulties involved. Since high critical fields are most often determined by extrapolation rather than direct measurement, some time is spent discussing the various extrapolation schemes and their merits and problems, including controversies that have arisen related to the measurement and interpretation of modern data. The final section presents our conclusions and suggestions for how best to apply the concept of standards to this measurement problem.

2. Theory and Definitions

The theoretical background for the various definitions associated with critical magnetic fields is adequately covered in many texts on superconductivity. Cody [9] provides a particularly complete listing of the equations. Here we present just enough theory to allow us to define the terms that are essential to understanding the problems involved with the determination of critical fields. Where we have an option we will choose the simplest workable definition and leave the subtle details to the theorists. All the terms arise in one way or another from the Bardeen-Cooper-Schrieffer (BCS) or Ginzburg-Landau-Abrikosov-Gorkov (GLAG) theories. Application of these concepts to the theory of practical materials, such as the multifilamentary superconductors, is an active area of research at the present time [10–12].

Type I superconductors are included here for completeness, but are nearly totally neglected thereafter, since our concern is with the high-field type II materials.

2.1 Basic Behavior

Here we present the basics of type I and type II superconductivity. The complications that arise in the various limits are discussed in section 2.2. To start, we define five parameters:

Penetration depth, λ. This characteristic length is a measure of the depth of flux penetration into a superconductor. The currents which prevent flux penetration into the interior of the material flow in a layer of this thickness. The exact temperature dependence of this parameter is open to debate, but it decreases monotonically with increasing temperature and rapidly drops to zero near the critical temperature. Typical measured values at 4 K for NbTi and Nb_3Sn are hundreds of nanometers, but with a large spread. For elemental superconductors, λ is tens of nanometers.

Coherence length, ξ. This length is a measure of the typical size of the Cooper pairs. Looked at differently, it can be taken as the minimum thickness of the interface between superconducting and normal regions. Specifics depend on the particular theoretical treatment. The

GLAG coherence length is temperature dependent, being inversely proportional to the temperature difference from the critical value. In impure materials, the coherence length value is also influenced by the electron mean free path. Typical values are around 5 nm for type II superconductors and considerably larger for type I (A1 ~1600 nm, Pb ~83 nm).

Ginzburg-Landau parameter, κ. This is the dimensionless ratio of the two parameters above.

$$\kappa=\lambda/\xi. \tag{2}$$

It is roughly temperature independent. κ is used as the parameter that distinguishes between type I and type II superconductors; those with a value $<1/\sqrt{2}$ are type I.

Flux quantum, ϕ_0. The fundamental unit of magnetic flux.

$$\phi_0=h/2e=2.068\times10^{-15}\ \text{Wb}. \tag{3}$$

Normal state resistivity, ρ_n. The classical electrical resistivity as measured just above the superconducting transition unless stated otherwise.

The general behavior of a superconductor in a field is shown in figure 1. The shape is chosen to minimize demagnetization effects. The conductor is in the Meissner state with $B=0$ in the bulk of the material. The superconductor distorts the field lines in its vicinity.

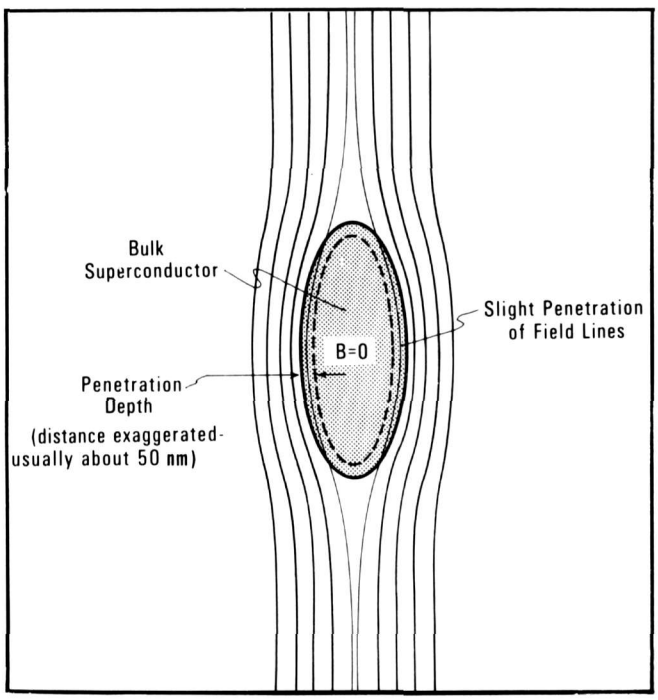

Figure 1–Superconductor behavior in the Meissner state showing the effect of the penetration depth [2].

This picture is valid for either type of superconductor at this point, i.e., below the first critical field value. The behavior of various parameters for each of the two types is shown in figure 2.

Type I superconductors. These materials are pure metals and the critical field transition is first order. The coherence length is larger than the penetration depth, and a mixed state (see below) is energetically un-

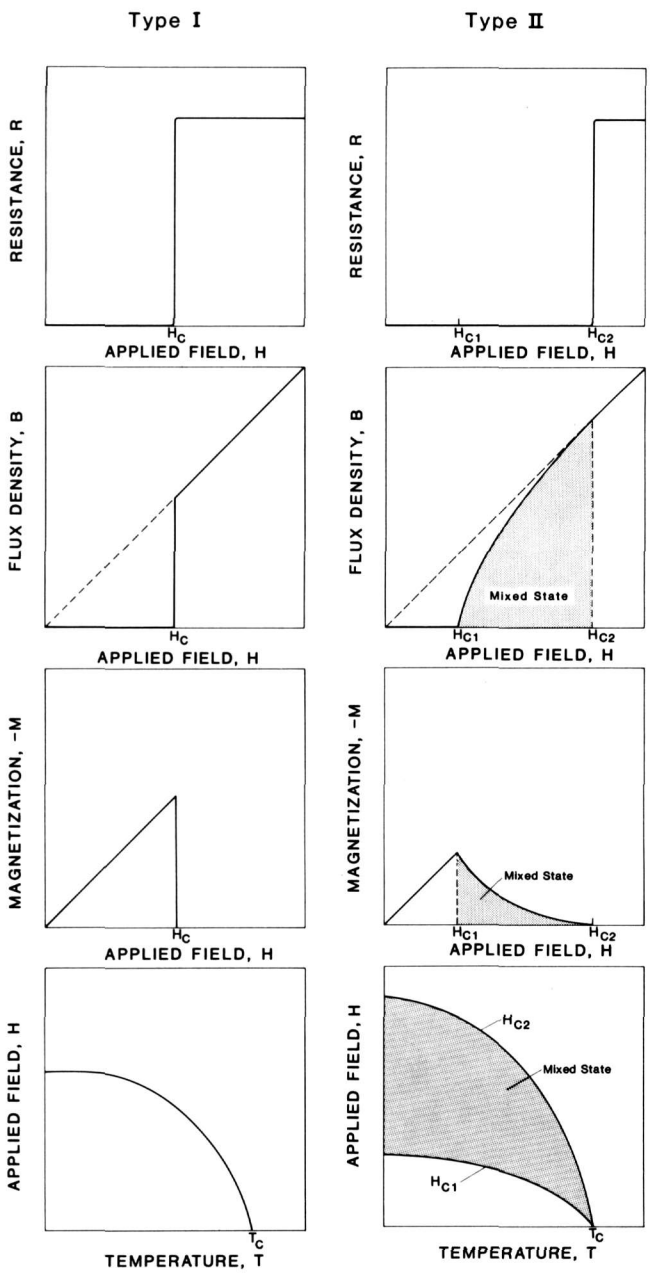

Figure 2–The parameters most often used in the determination of critical field and how they vary with field for both type I and type II superconductors.

favorable. Thus, at H_c the superconducting state collapses entirely. The critical field is temperature dependent, with an approximately parabolic dependence on T/T_c. Below the critical field the flux density is zero in the bulk and the magnetic susceptibility (M/H) is -1 (SI units), i.e., the material is perfectly diamagnetic. The resistive transition is sharp for these materials, sufficiently so that some are used as temperature standards.

Type II superconductors. These are the materials of primary commercial interest. All of the high field superconductors are a subgroup of this type. The materials tend to be alloys and compounds. They also have a region of perfect diamagnetism that extends only up to a rather small lower critical field, H_{c1}, at which a second order transition to the mixed state occurs. The behavior of the related properties is shown on the right side of figure 2. The fact that the penetration depth is greater than the coherence length gives rise to a negative surface energy between the superconducting and normal regions and the mixed state becomes energetically favorable at a relatively low field (H_{c1}). The structure of this state is as shown in figure 3. It starts when quantized flux bundles, usually of magnitude ϕ_0, penetrate the interior of the material. The flux is concentrated in the normal core which is surrounded by circulating supercurrents and, in the limit of zero applied field, it decays to zero in a distance from the core equal to the penetration depth. The density of superconducting electron pairs, which is zero in the core, reaches its equilibrium value in a distance approximately equal to the coherence length. With increasing applied field, the number of these flux vortices increases and they form a triangular array, the flux lattice, with an equilibrium separation that varies as $B^{-\frac{1}{2}}$. At the upper critical field, H_{c2}, the flux lattice vanishes and bulk superconductivity is destroyed. The effect of this scenario on the bulk properties can be seen in figure 2. The resistance (measured with sufficiently low current) does not show the transformation until H_{c2} because continuous superconducting paths still exist through the material up to this point. However, the amount of current that can be carried, the critical current density, decreases rapidly as the upper critical field is approached, as shown by the data in figure 4. H_{c2} is temperature dependent, and the slope of

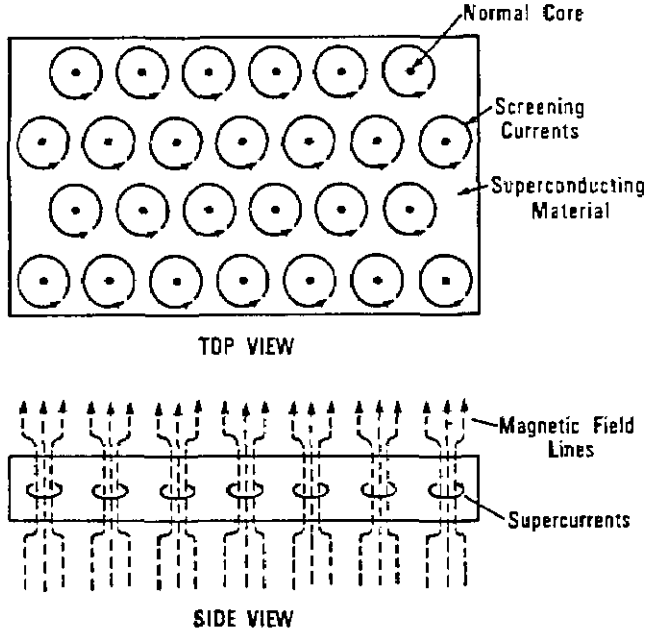

Figure 3–Flux penetration in the mixed state of type II superconductors showing the vortex structure and the flux lattice [13].

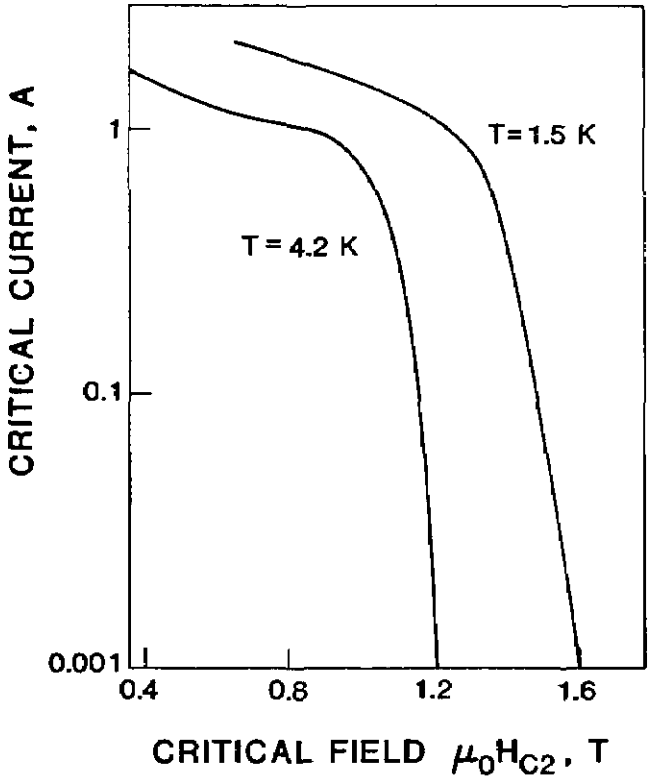

Figure 4–Variation of the critical current near the upper critical field. Data from [14].

the curve near T_c is an important parameter in the detailed theory of these materials. For some materials, very high values of H_{c2} may occur as shown in figure 5; it has been said that critical field values on the order of a 100 T are not ruled out by existing theory [15].

There are two classes of superconductors in this category, intrinsic and impurity dominated. In theory almost any superconductor can be put into the latter category by the introduction of impurities or disorder to raise the normal state resistivity. Hulm and Matthias [12] suggest as an approximate criterion for intrinsic superconductors that the critical temperature should exceed

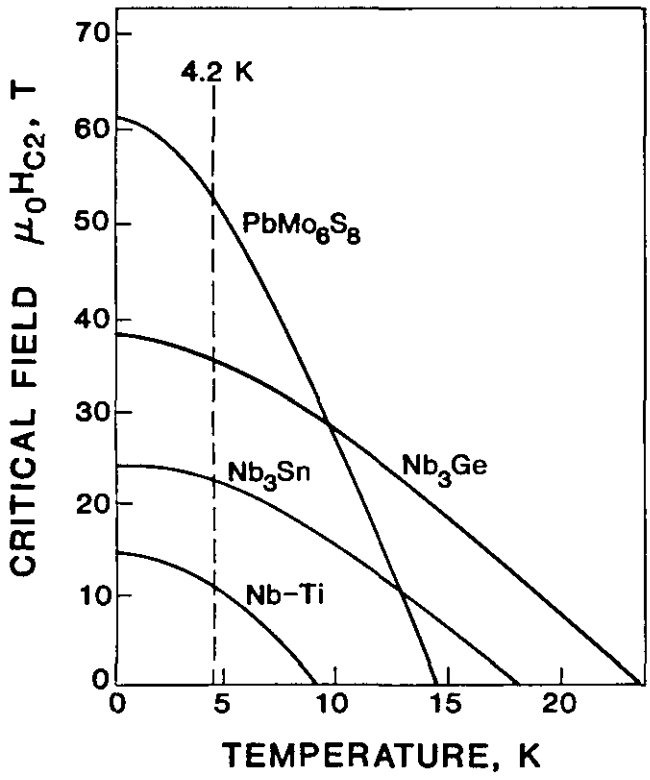

Figure 5–Behavior of critical field with temperature for several modern superconductors.

8 K. The relationship between the critical field and critical temperature of the two types is quite different. For the intrinsic materials

$$H_{c2} \propto (\gamma T_c)^2, \tag{4}$$

where γ is the electronic specific heat coefficient (proportional to the density of states). The impurity dominated materials give

$$H_{c2} \propto \rho_n \gamma T_c. \tag{5}$$

Thus it is possible (with some assumptions) to separate the two classes of materials by plotting H_{c2} against γT_c.

2.2 Complications

In addition to the rather straightforward considerations above, the type II materials have other, more complex, aspects to their behavior. The theoretical basis of most of these is presented here, again, in just enough detail to describe the effect. The interested reader should consult the pertinent references. Explanation of these effects requires the introduction of new critical fields. These fields are usually not directly measurable.

Surface critical field, H_{c3}. Above H_{c2} a material may still carry a small supercurrent in a surface layer of thickness approximately equal to the coherence length. This occurs in situations that are usually not encountered in the measurement of practical materials, such as when the field is parallel to a free conductor surface. It is not seen if the field is perpendicular to the sample nor if the sample surface is in intimate contact with normal conductor. The surface current persists with increasing field up to the surface critical field. H_{c3} is related to H_{c2} by

$$H_{c3} = \alpha H_{c2}, \tag{6}$$

where α is about 1.7. Figures 6 and 7 show the effect on the magnetization and the field-temperature plots. If the requisite conditions are met, the effect can cause serious errors in critical field determinations, especially if the measurement is made by a resistive technique.

Magnetic, spin, and scattering effects. Many effects work to alter the simple picture of the origin of the upper critical field presented above. Foremost among these is the paramagnetism of the normal state, but contributions also arise from the paramagnetism of the superconducting state, spin-orbit scattering effects, and electron-phonon coupling. Because of this, the full GLAG theory expression for the upper critical field for high values of κ,

$$\mu_0 H_{c2}^*(0) = 3.11 \times 10^3 \, \rho_n \, \gamma T_c \text{ (teslas)}, \tag{7}$$

defines a critical field that is higher than that usually measured. Normal state paramagnetism causes the

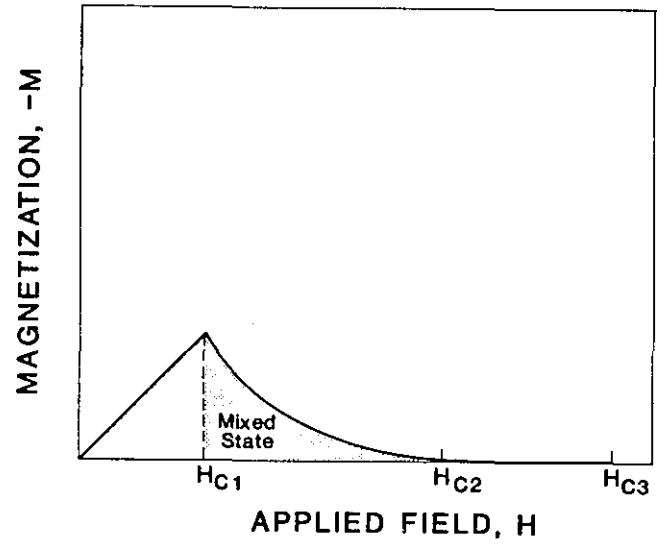

Figure 6–Magnetization curve for a type II material showing the extension to H_{c3}.

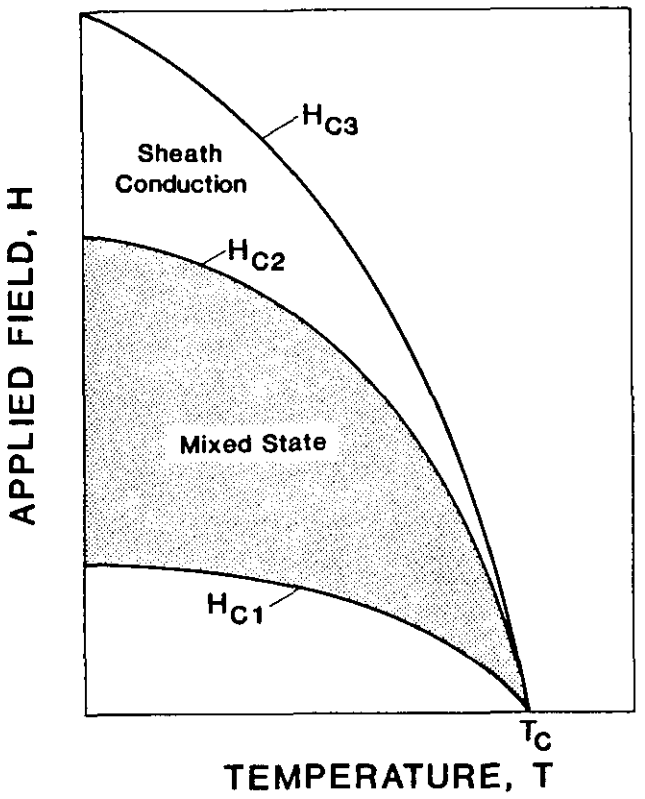

Figure 7–Applied field as a function of temperature for a type II superconductor showing the region of sheath conduction below H_{c3}.

actual value to be lower. It is possible to calculate this paramagnetically limited transition field with the result,

$$\mu_0 H_p(0) = 1.84\ T_c \text{ (teslas)}. \quad (8)$$

Another symbol for this field that is sometimes used is $H_{c2}^p(0)$. Further modifications to the theory to account for paramagnetic effects lead to another critical field,

$$H_{c2}^{**}(0) = H_{c2}^{*}(0)\ (1+\alpha^2)^{-\frac{1}{2}} \quad (9)$$

where α is the Maki parameter given by

$$\alpha = \sqrt{2}\ [H_{c2}^{*}(0)/H_p(0)] \quad (10)$$

which later theoretical development has shown to be

$$\alpha = 2.35\ \gamma\rho_n = 0.533\ [-\mathrm{d}\mu_0 H_{c2}/\mathrm{d}T]_{T=Tc}. \quad (11)$$

Flux pinning. This property determines the critical current of the high field materials, a high value of J_c requires that the fluxoid lattice be held in place. Near the upper critical field the value of J_c is strongly affected by field. The formulation originally proposed by Fietz and Webb [16] with further development by Kramer [17] is most often used to express the dependence of the pinning force (defined as $J_c B$) on applied field:

$$F_p = J_c B = \mu_0 H_{c2}^n(T)\ f(h), \quad (12)$$

where h is the ratio of the applied field to the upper critical field and n is an empirical constant that varies from $\sim$1.5 to 2.5. The function f(h) that describes the shape of the pinning curve is most often seen in the form $h^p(1-h)^q$ with the parameters p and q dependent on the specific materials.

Strain sensitivity. Practical superconducting materials, especially the intermetallics, are usually sensitive to strain. Their critical current and field are degraded by either compressive or tensile strain. Typical behavior of the measured critical field is shown in figure 8. The horizontal axis is labeled intrinsic strain, illustrating an important point from the aspect of measurement; the superconducting material in a commercial wire may already be under strain (usually compressive) because of forces exerted by the stabilizer and other components of the composite. Thus, measurement of H_{c2} on these practical materials becomes more of a problem than one might first imagine and leads to the definition of even more terminology. Most of this work comes under the heading of strain scaling studies and several empirical "laws" have emerged [19,20] to describe the behavior. These scaling laws have the exact form of eq (12), but the temperature dependence of H_{c2} is replaced by a strain dependence. Their application requires correct determination of the critical field even though, in general, they do not apply in either the low field ($<0.2\ H_{c2}$) or the high field ($>0.9\ H_{c2}$) regions. Two new defini-

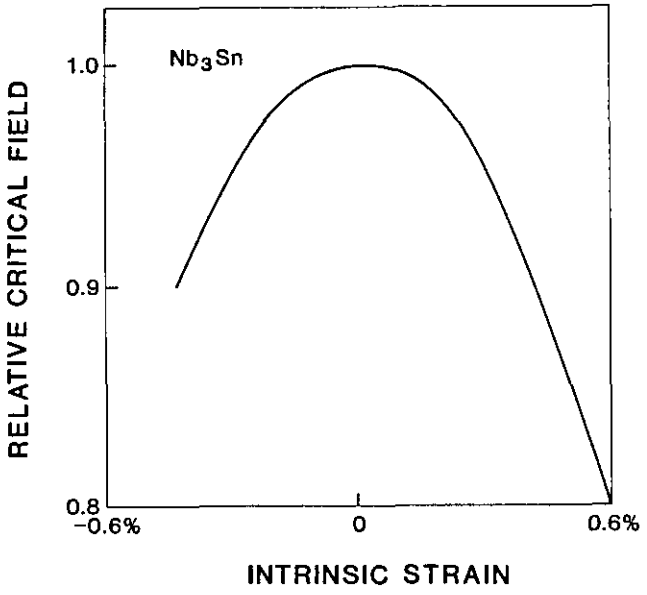

Figure 8–The effect of strain on the determination of the critical field. Data from [18].

tions appear in these writings: H_{c20}, which designates the "as received" value of H_{c2} for a practical material and H_{c2m}, which gives the maximum value of H_{c2} under strain; the peak of the curve in figure 8. This value is assumed to be that of the strain-free state of the superconductor. Since one is dealing with practical materials here, it should be pointed out that they do not often have a uniform composition or microstructure and H_{c2} may well vary throughout the material. Thus, a sufficiently high measurement current is used so that a "bulk" value will be obtained (see the discussion of extrapolation techniques below) and this fact is often brought to the attention of the reader by use of $H^*_{c2}(\epsilon)$ as the critical field designation (ϵ is the strain parameter).

3. Measurement and Data Analysis Techniques

Here we are concerned with measurement of the upper critical field, H_{c2}, although the techniques described could be applicable to the determination of other fields as well. The correct measurement of critical field, especially in practical superconductors, presents a difficult task both experimentally and in the interpretation of the resulting data. Different measurement methods may give different values for a given sample, and even the same method may give varying results depending on the choice of parameters, such as measuring current, used in a resistive determination. The cause of these variations is not an error in the concept or the measurement, but is most often due to material effects such as inhomogeneities in the superconductor. Thus, it sometimes happens that the measurement result that is most correct physically is not the most meaningful in a practical sense. Critical field determination, unlike the measurement of other superconductor parameters, suffers from the additional problem that one can seldom actually achieve the fields necessary to see the transition directly and, thus, extrapolation techniques must be used which, themselves, are subjected to interpretation.

The literature on upper critical field measurements is mixed with regard to the care given in presenting the details of the experiment and the data analysis methods. Two authors have discussed aspects of the measurement problem in detail [21,22]. Many of their ideas and observations have been incorporated into the following sections.

3.1 Defining the Transition

Transitions between the superconducting and normal states are seldom as clean as the curves of figure 2 suggest. At best, the transitions have a width to them and at worst they are nearly lost in the noise. The techniques most commonly employed involve extrapolations of parts of curves as shown in figure 9. In practice, a more elaborate system is used as illustrated in figure 10, in which the "center" of the transition is taken as the midpoint between two points that may represent 25 and 75%, as in the figure, or some other choice such as 10-90%. This approach is helpful because the early parts of the transition may be obscured by noise and because of the unsymmetrical nature of the curve, but it is an arbitrary definition. In fact, it has been suggested that, for the resistive determination of critical field in practical materials, this technique is misleading, and the proper value should be taken as that at which the transition first appears with increasing field at a properly chosen current density [21]. This arrangement is used to avoid the problem of H_{c2} variations throughout the superconducting material of the sample as discussed below. The author presents data showing that a significant difference in H_{c2} value is found by the two techniques applied to commercial-type conductors. A similar comparison using single crystal Cu-Mo-S [23] found differ-

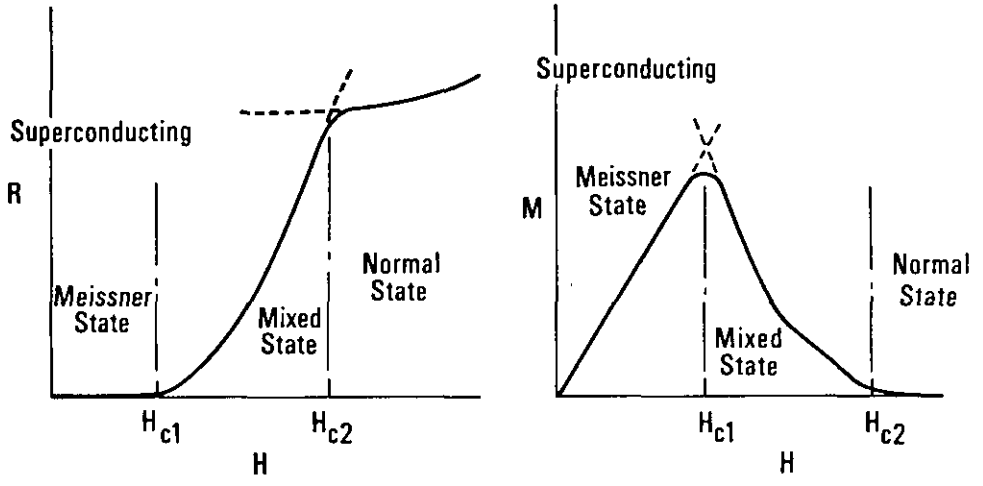

Figure 9–Techniques for determining critical field values from resistance and magnetization data plots [3].

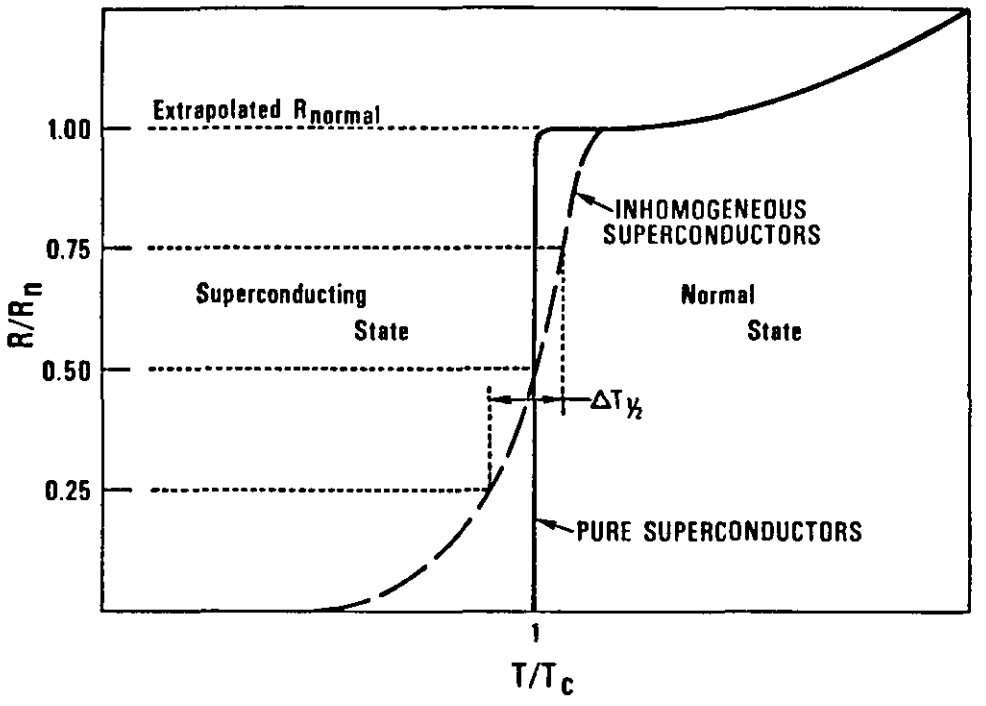

Figure 10–Illustration of method of determining the critical parameter value in the case of a broad transition [13].

ences of up to 20% between measurements using the two definitions.

A further problem can arise in the situation often encountered where one does not want to allow the sample to enter the normal state because of the possibility of damage. The approach in this case is to choose an arbitrary criterion of detected voltage over a fixed length of the wire as defining the critical parameter. This technique was chosen for the ASTM standard for critical current measurement [1]. The reasoning behind the choice and some of the related problems are discussed in an earlier publication [24]. The effect of the specific choice of criterion on the measured critical current is shown in figure 11; clearly a 1 μV criterion results in a significantly lower critical current value than a 100 μV criterion. As discussed in the reference, a low criterion is not always desirable in practical application because it may not be possible to measure it unambiguously. On the other hand, a very high one may put one too close to quenching the sample.

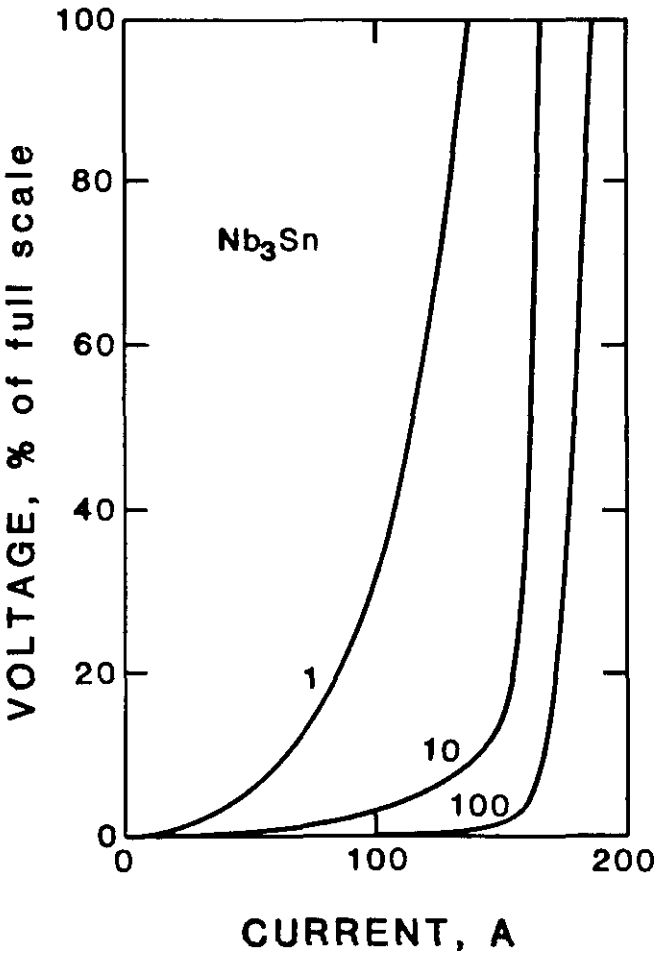

Figure 11–The effect of choice of criterion on the value reported for the critical current of a practical conductor. Numbers on the curves give the actual full-scale voltage in microvolts that corresponds to 100% on the vertical axis.

Because of its significance in understanding inhomogeneity effects, the width of the transition is an important feature of the data. All commercial materials show relatively broad transitions as indicated by the measurements shown in figure 12, especially those for the Nb_3Sn samples. The interpretation is always strongly dependent on the measurement technique.

3.2 Measurement Techniques

A wide variety of measurement techniques has been used for the detection of the upper critical field of superconductors. The choice among them depends on the goal of the measurement and the time (and money) available. As always, the easiest measurements are the most difficult to interpret and the most subject to error—another manifestation of Murphy's Law. The techniques that have been used generally fall into five classes: electrical, magnetic, electromagnetic, thermal, and acoustic. For each of these we will discuss the theory behind the measurement, the ease of use, problems with the technique, and the data interpretation required. The apparatus for each method will be touched on briefly in the next section. We do not go into great detail here because a new book on materials properties measurement at low temperatures which thoroughly covers

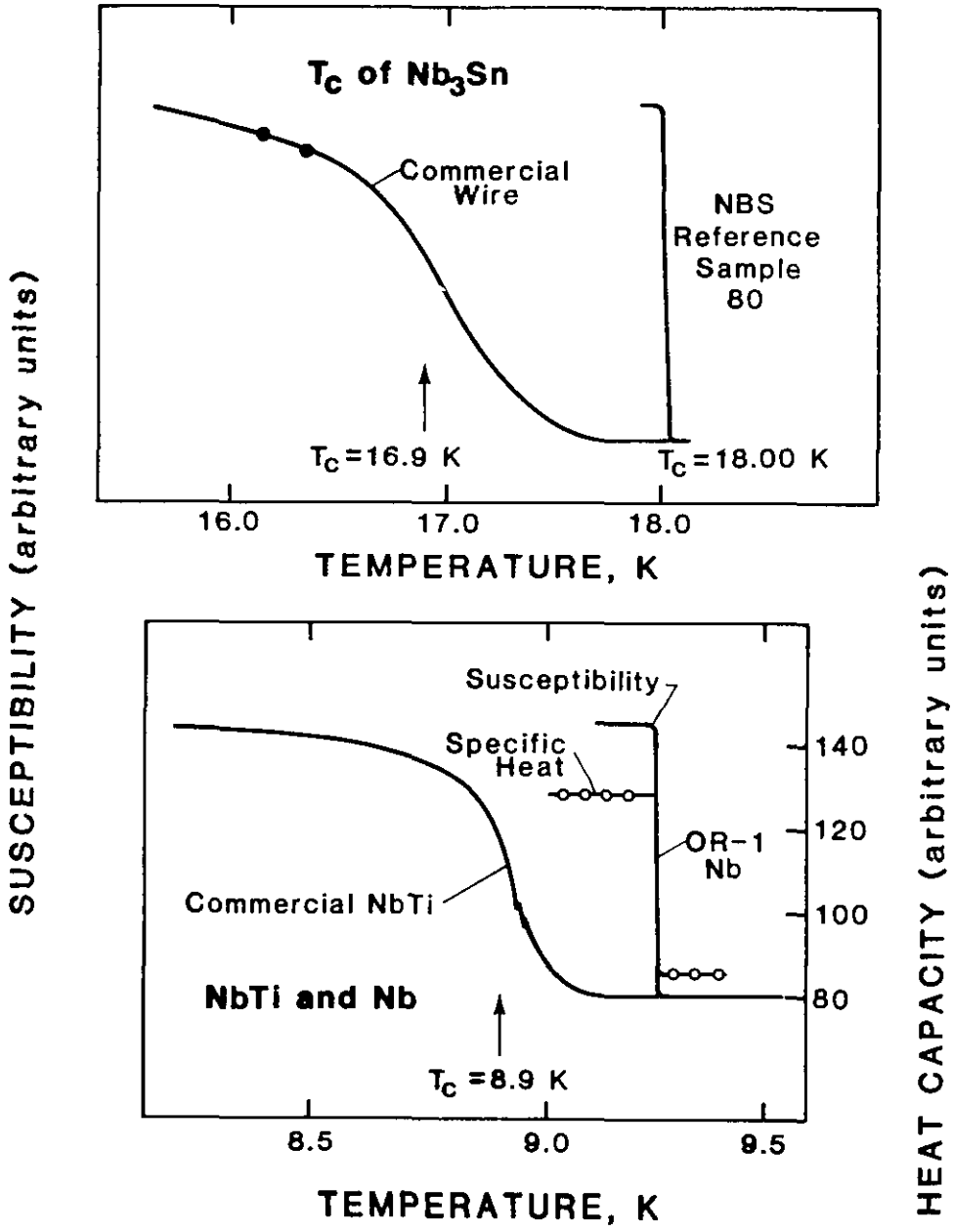

Figure 12–Comparisons between commercial materials and reference samples measured by several techniques [25].

each of the techniques, although not always their specific application to superconductors, has recently become available [26].

In the discussion that follows, one should keep in mind the fact that practical superconductors are inhomogeneous materials. The critical field of the superconductor may vary with the relative direction of the applied field and the conduction path. Isolated regions of superconducting material may occur, or regions may be coupled only through a percolation network or by the proximity effect. Normal conductor, usually copper, is almost always present, with a resistivity that is a factor of 100 or more below its room temperature value. Each of these factors will affect a given measurement method differently. The ideal measurement method would allow us to determine the microscopic variation of H_{c2} throughout the material, to measure the exact volume fraction of each superconducting species in the composite, and to determine the connectivity of the various regions. This would, of course, be accomplished with apparatus of minimum cost and greatest ease of operation. We may have to wait some time for this.

Resistive method. This measurement is by far the easiest to perform on commercial materials and it is the most commonly used. Care should be taken to have a long enough piece of wire that the minimum detectable voltage represents a reasonably low electric field criterion. Current transfer and current sharing effects can be minimized by having the voltage-measuring contacts on a significant length of the sample that is in a region of uniform field and distant from the current contacts by many wire diameters. This technique is probably the only common one that can reasonably be used in pulsed-field systems for the direct measurement of very high critical fields [27]. The values of H_{c2} measured at low current levels can be high because the voltage will remain at zero with only a few strands still superconducting. In a few unusual situations (field parallel to surface, no normal metal jacket), it is also possible for surface superconductivity effects to cause the transition to be observed at very high field values. Even when surface effects are not of concern, the choice of measuring current is not a trivial problem. Larbalestier [21] presents data showing the value of H_{c2} for cold-worked NbTi to vary from more than 11.6 T to less than 10.9 T as the measuring current density is raised from 0.005 to 10 A/cm^2, and the curve is not leveling out even then.

Magnetic methods. A number of techniques use detection of the change in magnetization of a sample as a means of monitoring the critical field transition. Early methods are described by Hein and Falge [28] and more recent ones in the book mentioned above [26]. At H_{c2} both the magnetization and the susceptibility become effectively zero. Magnetometer techniques measure the magnetization of the sample directly. The sample is inserted into a pickup coil in the field region. The field is set to a fixed value and the sample is moved either out of the coil completely (ballistic method) or caused to oscillate within the coil (vibrating sample). The voltage induced in the coil is integrated to give the magnetization. A variation of this system is found in the swept-field technique in which the sample remains fixed within the pickup coil and the magnetic field is ramped at a fixed rate. Use of a balanced coil system (see below) allows extraction of the magnetization signal.

The various inductive techniques all use susceptometers; they measure the incremental susceptibility ($\Delta M/\Delta H$) by applying a small low-frequency ac field to the sample in the presence of a large background dc field and detecting the induced signal, either with a secondary coil (mutual inductance) or by the change in inductance of the primary (self inductance). The mutual inductance method is the most commonly used, and most often the secondary coil system is made up of two counterwound coils that are connected in series with the sample contained in one of them. This arrangement allows canceling of the primary field signal with the sample in the normal state prior to a measurement. Such systems are said to be balanced.

All of the systems just described require calibration if they are to be used for direct measurements rather than for tracking the sample through a transition. The easiest method uses a properly shaped test specimen of type I superconductor, such as lead, and assumes it is perfectly diamagnetic at 4 K. Room temperature standards of susceptibility and magnetic moment are also available from the National Bureau of Standards. Magnetic methods are seldom actually used to determine H_{c2} of practical materials, but they are used extensively in the determination of ac losses in superconductors. They are useful for samples of bulk material and for chips or powders. When used with wires, the samples are either bundles of cut wires with their axes parallel to the applied field or noninductively-wound coils in which the wire axis is normal to the field. Again, the inhomogeneous nature of practical superconducting materials can give problems in magnetic measurements. The most common occurs in superconductors where a high-H_{c2} phase precipitates at the grain boundaries of lower critical field material. The magnetic techniques see this layer, and the resulting signal is indistinguishable from that which would be seen if the entire grain were actually in the superconducting state. In the "normal" situation of simply inhomogeneous superconductors, the inductive signal will tend to have a broader spread than the resistive one and, in general, will give a lower

critical field value for a given material. Also, the magnetization change, ΔM; tends to be very small for high-H_{c2} materials.

Specific heat. Measurement of the variation of the specific heat as a function of temperature through the superconducting transition is generally considered to be the best experimental method for characterizing superconducting materials of all sorts. It is the only one that can potentially indicate the amount of superconducting material present and, at least in concept, indicate the presence of superconductors with different transition temperatures or fields. However, it requires a relatively complex experimental apparatus for accurate measurements. Its use in the measurement of critical fields is further complicated by the effect of the field on the thermometry and the lengthy measurement times, but it has been used successfully for measurements on Nb_3Sn in an 18 T field [29]. The temperature variation of the specific heat for an idealized superconductor is shown in figure 13. An excellent review of the theory and experiment with specific applications to superconductors is given by Stewart [30] and a general treatment of specific heat at low temperatures by Sparks [26]. Briefly, the discontinuity at the critical temperature arises from the different contributions to the specific heat made by normal and superconducting electrons. The lattice contribution is small at these temperatures; it varies as T^3 and is unaffected by the transition. The electronic contribution, on the other hand, is linear in T in the normal state and takes an exponential form in the superconducting state with the exponent given by $-\Delta/kT$, where Δ is the energy gap associated with the superconducting state. Furthermore, BCS theory gives the result

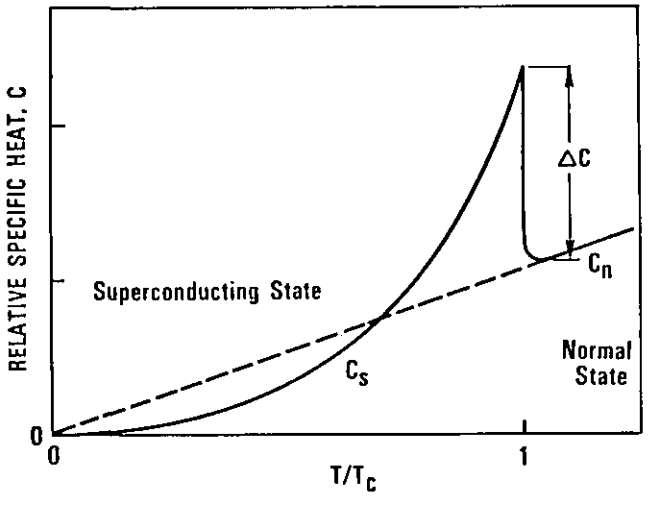

Figure 13–Behavior of the specific heat with temperature through a superconducting-to-normal transition [3].

$$ae^{-\Delta/kT}c/\gamma T_c = 2.43 \qquad (13)$$

for the ratio of the specific heats of the superconducting and normal states at T_c in zero field. This allows one to estimate the amount of the sample that is superconducting, although the exact number may not hold true for some of the more exotic materials [30]. Furthermore, if data can be taken to well below the transition temperature, a much more accurate determination of the normal component of the sample can be made. Because of the temperature dependences just described, the only component of significance well below the transition is the γT term of the normal material. The ratio of this term to the value of γT above the transition is then a direct measure of the fraction of the sample that is not superconducting.

Other methods. The three techniques just mentioned are the only ones in common use for critical field determination. However, a few other methods have been used on occasion. Foner and colleagues [31,32] describe an rf (5 to 20 MHz) technique, useful for measuring H_{c2} in powdered or odd-shaped samples, in which losses in an induced rf current are measured with a bridge arrangement. The technique is said to effectively monitor only the superconducting regions of the sample so that, in concept, it would allow determination of multiple critical field values of materials within a composite. The first of the papers also makes reference to a microwave technique.

The use of ultrasonics for critical field determination is discussed by Neuringer and Shapira [33]. The paper presents an in-depth analysis of the theory and experimental data showing the rapid increase in the attenuation of a 10 MHz signal on field-induced transition to the normal state in a NbZr alloy.

Comparisons. A few experiments have compared the critical temperature (not critical field) of a single sample as determined by several of the methods outlined above. They have (wisely) used samples of either pure type I material [34], carefully prepared niobium [25, see fig. 12], or single-phase alloys [33]. In all cases quite good agreement was obtained between measurements by all of the techniques, indicating that, in general, lack of agreement among different techniques applied to complex materials is due to the inhomogeneous nature of the composite rather than problems with technique. In fact, differences between the inductive and resistive methods have been used recently to investigate crack formation in the reaction layer of a Nb_3Sn multifilamentary composite [35].

3.3 Apparatus

The specific apparatus required for the measurement of critical field by any of the techniques discussed here are adequately described in the references. General low temperature experimental methods are the subject of numerous texts (see [26] and references therein). Here we mention only two apparatus topics that are specific to critical field measurements, sample configuration and high-field magnet systems. For ease of discussion we assume that the sample is a wire and we use the resistive technique as our model, although the comments should usually apply to any other arrangement.

The measurement of critical parameters requires that the sample be mounted in such a manner that it will be as strain-free as possible after cooldown, but which assures that it will not be able to move under the effect of the applied field and current, while still maintaining good thermal contact with the bath. Figure 14 shows the most common sample mounting schemes. Each has its own pros and cons which have been discussed in detail elsewhere [24]. A particularly difficult problem has to do with the transfer of current in and out of the filaments in response to proximity to current contacts and to changes in field magnitude or orientation. Care must be taken that the measurement region is one in which the current has attained a stable distribution. If the measurement involves sweeping a field, one should be aware that current transfer among filaments will be occurring during the sweep.

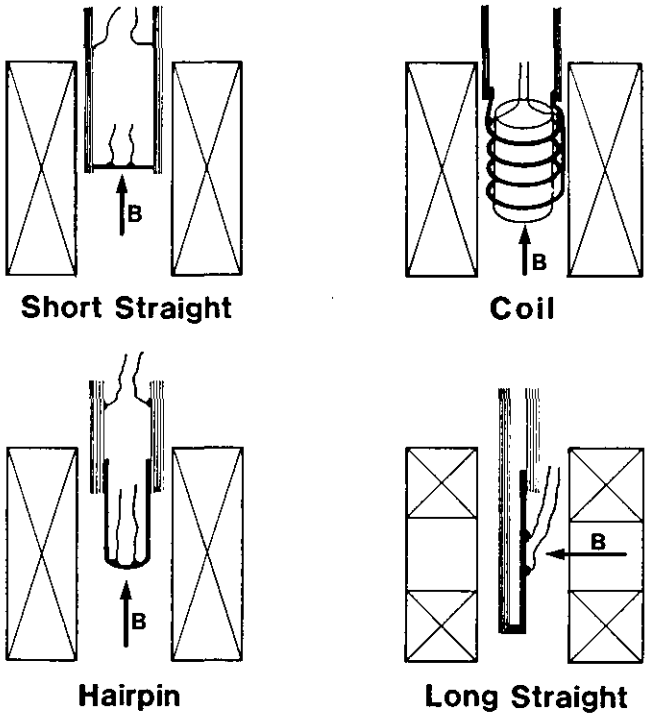

Figure 14–Commonly used configuration for samples for the measurement of critical parameters by the resistive method.

Magnet systems that attain fields much in excess of 10 T are not generally available. This makes direct measurement of the critical field of the more interesting materials at low current densities impossible. Thus, most laboratories use approaches that involve the extrapolation techniques discussed below. In the larger laboratories, steady fields of 12 T are available in reasonable volumes using superconducting magnets and fields to 20 T with normal magnets. Hybrid superconducting-normal systems exist that reach fields as high as 30 T. Beyond that is the region attainable only with pulsed magnet techniques. These magnets allow one to achieve fields in the 50 T range for very short periods of time (tens of ms) and the rapid field changes introduce a whole new set of problems into the measurement.

3.4 Sources of Error

It is possible to do a detailed error analysis for each of the critical field measurement methods described. However, it will nearly always show that the measurement itself can easily be made with an accuracy near 5% and somewhat better precision (near 2%) if care is taken in the determination of the magnetic field and its uniformity and in the suppression of electronic noise. This level of accuracy is usually quite adequate for most purposes outside of the basic research laboratory. The real problem is the uncertainty in the critical field due to stress and nonuniformity of material in the sample and the effect of choices of criterion and measuring current or other experimental parameters on the final result, be it H_{c2} or the transition width. Reasonable care in the preparation, characterization, and mounting of the samples is called for here. In pulsed field techniques care must be taken to prevent inductive heating of the material. Other rise-time effects appear to be negligible in the pulsed measurements [27]. In the more conventional measurements, slowly sweeping field or temperature seems to introduce no errors. At least it has been shown that the value and width of the transition is essentially the same whether one holds temperature fixed and sweeps the field or vice versa [36].

3.5 Extrapolation Methods

The value of the critical field for modern superconducting materials at the temperatures of interest is usually very high and, thus, unattainable in most laboratories. Several extrapolation methods are commonly used to allow determination of H_{c2} at 0 or 4 K from other data on the critical parameters. The two common meth-

ods are the use of data on the variation of H_{c2} with T near the critical temperature, where H_{c2} is relatively low, and extrapolation using pinning theory of the critical current-versus-field behavior. Each of these methods depends critically on the use of theory to guide the extrapolation and each has reasonable success with certain materials and fails rather dramatically with others. For this reason, it is not possible to say that any one technique is "correct." It depends on the material to which it is applied. Also, these problems with correctness of the extrapolation are in addition to the problems already discussed related to the determination of the transition value from the experimental data. A small problem with terminology arises here also in that the extrapolated upper critical field is nearly universally designated H^*_{c2}, a term already used (see eq (7)) to indicate the theoretical critical field in the absence of paramagnetic limiting. In some cases there is no problem with this dual usage, but in others there definitely is the opportunity for some confusion.

Critical field versus temperature. This technique relies on the result from GLAG theory:

$$H^*_{c2}(0)=a\,[\mathrm{d}H_{c2}/\mathrm{d}T]_{T=T_c}\cdot T_c, \tag{14}$$

where a is a constant equal to 0.69 for dirty materials and to 0.72 for clean ones. To use this method, the critical field value is measured in the region near T_c and the resulting plot is used to get the slope and the critical temperature. Typical data from the literature are shown in figure 15. The success of this method depends on how closely the material obeys the simple GLAG theory. The relationship in eq (14) can also be modified to account for various effects like paramagnetic limiting before the extrapolation is made, but this requires a knowledge of the material properties that may not exist. Also, the value of the differential is strongly dependent on the measuring current, with changes of as much as 30% reported for an order of magnitude change in the current [22]. As an example, note the widely different values obtained for the critical field of Nb_3Sn in the two plots in figure 15. One cannot really say that current density was the cause of the difference, but it is a strong possibility. Thus, the chance of agreement of an extrapolated measurement of this type with the upper critical field measured directly depends on the measurement parameters and also on the extent to which the subject material can be described by the various theoretical treatments available. In this latter situation, the common materials are in not too bad shape. Commercial quality Nb_3Sn is agreed to be a simple GLAG-theory material, while the NbTi alloys show only a small amount of paramagnetic limiting of H_{c2}. On the other hand V_3Ga has a strong paramagnetic limit and the more exotic materials, such as Pb-Mo-S, cannot in general be fit to the theory even with the extensive modifications available for use in the literature.

There is another reason that one desires to have accurately measured data on the quantity $\mathrm{d}H_{c2}/\mathrm{d}T$ near T_c: it allows an experimental determination of the electronic specific heat coefficient, γ, that figures prominently in much of the theory. Comparison of eqs (15) and (5) show that the differential divided by the normal resistivity gives the value for gamma, assuming the proper theoretical value has been used for the proportionality coefficient. Application of this concept to numerous NbTi alloys is given by Hawksworth and Larbalestier [8].

Critical current versus field. Methods of assuring that a sample is at a fixed temperature other than that of a liquid helium bath are not easy to achieve experimentally. This fact makes the measurements just described quite difficult. An alternative technique is to use critical current data taken as a function of magnetic field at relatively modest fields and use pinning theory to extrapolate the data to zero critical current, which should occur at H_{c2}. The success of this method depends not only on the correct measurement of the critical current, but also on knowledge of the exact behavior of the pinning force with field strength. For NbTi alloys, the expression,

$$F_p=\mathrm{c}\,H_{c2}^{2.5}\mathrm{h}(1\text{-}\mathrm{h}), \tag{15}$$

has proven useful in some instances [39], although the value of the exponent is not certain, being in the range 2.0 to 2.5 in most cases. Under the proper circumstances a simple linear extrapolation of J_c to zero is acceptable [22]. The material most investigated by this technique is probably Nb_3Sn. The pinning force expression as derived by Kramer (see the discussion for eq (12)) for this material is

$$F_p=K_s\,\mathrm{h}^{\frac{1}{2}}(1\text{-}\mathrm{h})^2, \tag{16}$$

where K_s is a constant for the conductor. The value of K_s and its dependence on H_{c2}, κ and other parameters may change slightly depending on the particular theoretical modification chosen for the scaling [11]. In any event, it is conventional to rewrite eq (16) as

$$(J_c\,H^{\frac{1}{2}})^{\frac{1}{2}}=K_s^{\frac{1}{2}}H_{c2}^{-5/2}(H_{c2}-H), \tag{17}$$

so that the equation becomes effectively linear in H. The quantity on the left hand side of the equation is then plotted as a function of applied field and a linear extrapolation made to zero. This method is illustrated by the

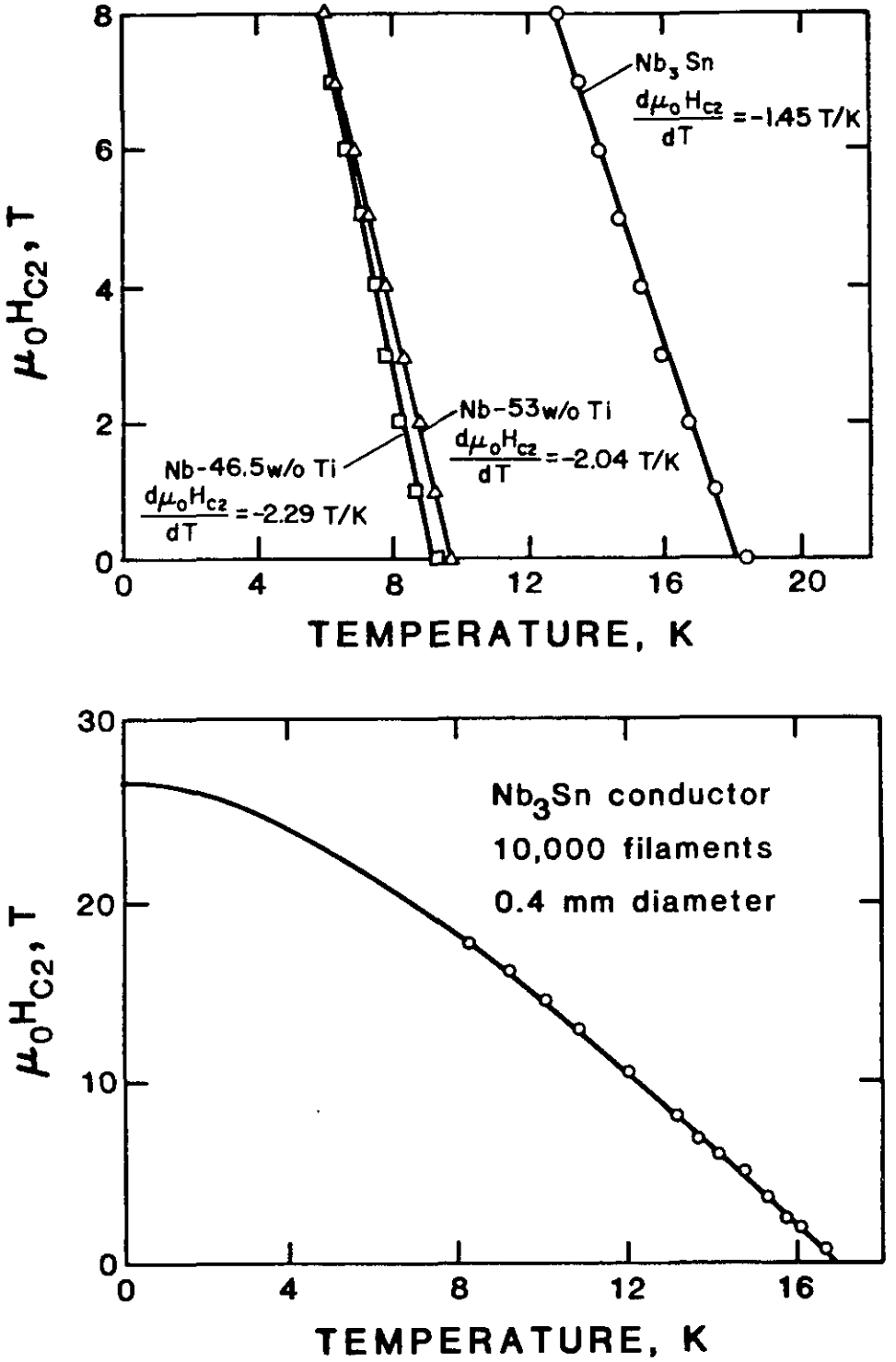

Figure 15–Typical data showing the behavior of the slope of H_{c2} versus T near T_c for several common materials. The upper graph is from [37] measured with a current density of 1.0A/mm^2. The extrapolated value of $\mu_0 H_{c2}$ for the Nb_3Sn sample is 18.45 T. The lower graph, from [38], shows data taken at a current density of 0.02 A/mm^2 and a fit to those data using the simple GLAG theory expression (eq (14)).

plot of 4.2 K data shown in figure 16 in which the actual behavior of the curve is also shown, indicating the departure observed at low current values. This conductor is the same one as shown in the lower part cf figure 15. The present extrapolation results in a significantly lower value for H_{c2}. In another instance the same author observed this method to give values for Nb_3Sn that were too high compared to those obtained by direct measurement [20]. Furthermore, it has been seen that the extrapolation is not useful for highly aspected conductors such as tapes [11]. Application of the method to other high field materials requires a reevaluation of the

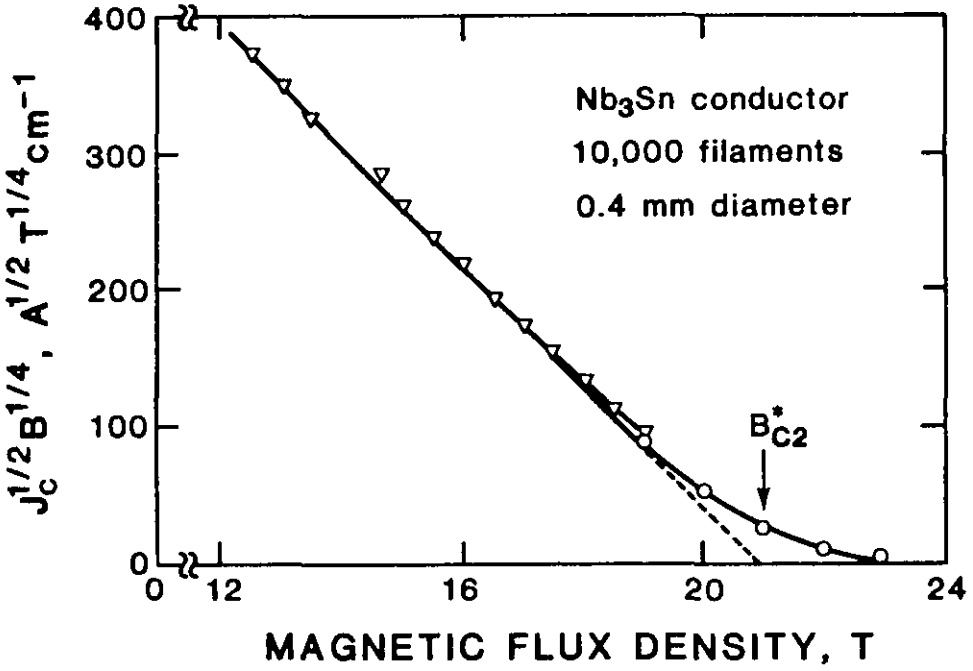

Figure 16–Determination of the upper critical field of Nb_3Sn by the Kramer plot extrapolation [38]. The dashed line shows the extrapolation. Measured values are also shown in this region. Note that this sample is also the one for which data are shown in the lower part of figure 15.

constants used in eq (12) and effectively requires a more detailed analysis than the linear plot [19].

3.6 Reporting of Data

Since part of our goal is to evaluate the structure of a standard for critical field measurement, one consideration that is always of importance is the content of an adequate report of measurement. The many problems (or potential problems) outlined above seem to call for a very detailed report if an adequate assessment of the results is to be made by a reader interested in applying them to his own problem or evaluation. We suggest the following listing be used as a guide to the necessary components of a report. Clearly, not all parts will be required in every case.

Results

The critical field with correct symbol [e.g., $H_{c2}(T)$, $H^*_{c2}(0)$, etc.].

Measured directly or extrapolated.

Temperature of stated value (may or may not be temperature of measurement).

Estimated accuracy of the value given.

Experiment

Measurement technique used.

How the transition was determined from the raw data, including voltage or electric field criteria (where appropriate) and the point on the transition curve chosen for the reported value.

Width of the transition between stated limit points.

Details of sample geometry, internal structure, orientation with respect to the measuring field, mounting method considering questions of induced strain and thermal contact (for variable temperature methods).

Variable temperature methods require careful assessment of the effect of magnetic fields on the thermometry. Methods of calibration used to account for this effect should be described.

Each measurement method has its own set of reporting requirements. Most are the typical error and parameter choices related to any measurement with such a system. A few are of prime importance for critical field measurement reports.

Resistive transition—the current density, voltage probe separation, distance of voltage taps from the current contacts.

Magnetic technique—the exact method used, sample mass, magnitude of measurement fields (for inductive methods), calibration technique and accuracy, noise on unprocessed signal.

Specific heat—thermometer calibration and relationship to sample temperature, sample mass, addenda loss evaluation, heater power levels.

Modern data collection techniques frequently involve processing of the data very early, perhaps even before it is seen by the experimenter. All such processing steps should be mentioned.

A point that is often neglected is the accuracy of the applied magnetic field measurement. Calibration of magnets, including evaluation of field inhomogeneity and, in the case of superconducting magnets, the effect of frozen-in flux is a difficult task. It is suggested that a calibration check be made every several months and certainly when the magnet system is first put into service.

Extrapolation

Details of an extrapolation technique should be given including:

The exact method used, including modifications to the theory employed and the actual equations.

The range of actual data used in the extrapolation.

If at all possible, a graph showing the data and the result of the extrapolation (see fig. 16).

4. Conclusions

As we mentioned at the beginning, the purpose of this investigation is to evaluate the desirability and feasibility of creating a standard for measurement of the critical field of practical superconducting materials. The type of standard under consideration is that typically produced by organizations such as ASTM to assist in commerce. Two standards already exist in the field of superconductivity, one for general definitions [4] and the other for the measurement of critical currents below 600 A [1]. Such standards are created by consensus among all interested parties and must be able to be used by industrial laboratories in their day-to-day operation. A further consideration is that there should be a demonstrated need for the standard, at least in the forseeable future.

A standard of this type can take several forms. It may be any of the following: a list of definitions; a manual outlining accepted measuring and reporting methods; a detailed method of measurement in which apparatus, technique, and report format are specified; or it may be an artifact or standard reference material. Whatever the form, it is essential that the standard be backed up with adequate research to document the need for each requirement of the standard. This is not a trivial problem, and it is often neglected in the rush to create a standard to solve a particular problem. Our feelings regarding the need for and structure of a standard are given below. In summary it seems that the time is not yet ripe for a full-fledged standard, but there is some justification for creating a list of standard definitions and, perhaps, an "operation manual" or similar document. A standard reference material approach might also prove useful, but would be quite expensive.

4.1 Need for a Standard

Standards of the sort discussed here are usually created in response to a need expressed by the community. In the case of critical field, there has been a limited expression of need. The commercial materials now in use are, in general, adequately characterized by their critical current versus field characteristic. Critical field information is of most use to that group of researchers who are trying to construct better practical materials for high field applications by modification of the crystallographic or electronic structure of various existing materials. This group should agree among themselves on the requirements for an acceptable measurement of the critical field, but that is not adequate reason for creating a standard. It is entirely conceivable that very high field materials may become feasible in the future, and the need could become great for a critical field standard for commercial versions of those superconductors. We do feel that a few definitions related to the critical field measurement should be added to the general definitions standard, mostly the various modifications of H_{c2} discussed above. Furthermore, it is possible that certain groups, such as DoE, might want to specify a critical field measurement method and data analysis technique for a particular material. This could be done, but it would require that some of the research mentioned below be performed first if the document were to have very wide application.

4.2 Measurement Standards

As should be clear from the analysis above, the creation of a detailed single measurement standard for critical field is probably impossible given the current state of knowledge regarding the factors that influence H_{c2} and the inhomogeneous nature of the superconducting portion of the practical conductor composite. However, if an attempt were to be made, there are a few items that should be considered. The only measurement technique that is likely to be widely used in industry is the resistive method applied at 4.2 K. A clever application of an inductive technique might also be possible, but none has

appeared to date. Similarly, the possibility of routine direct measurement is remote because of the expense of high field magnets. Thus, extrapolation techniques would have to be used and most likely those would be critical current versus field extrapolations with the measurements made at 4.2 K. Extensive research on the pinning force phenomenon would be necessary. Significant advances in understanding the effect of crystallographic and metallurgical variations on the critical field would be required. All these requirements could be mitigated somewhat by the use of a standard reference material as discussed below, but research on the measurement methods and their related errors would still be needed. A standard method should use a relatively high current density, probably in excess of 100 A/mm^2, which would avoid some of the problems, but would result in lower critical field values.

4.3 Standard Reference Materials

This approach to the standardization of critical field measurements is probably the most appealing for the present circumstances. Unfortunately, it is also a very expensive solution. The idea is to make a series of very well characterized materials that could then be distributed for the calibration of apparatus. Such materials could also be used to evaluate the various extrapolation techniques. The characterization would require very careful work, expertise in several measurement and analysis techniques, access to high field magnets, and a consensus as to the proper choices for the important parameters. However, considerable progress is now being made in understanding the interactions between the metallurgy and the superconducting properties of these materials which may well result in an advanced (practical) superconductor with well-documented homogeneity and internal structure in the near future. This conductor, if it can be made in significant quantities, would be an ideal candidate for a critical field SRM.

It is a pleasure to acknowledge the help of the entire NBS Superconductors and Magnetic Materials group, headed by A. F. Clark, through many conversations and suggestions. Special thanks are due R. B. Goldfarb for assistance with the subtleties of the field of magnetic units and J. W. Ekin for helping to keep the practicalities of the topic in the foreground. Much of the information on early experimental techniques was obtained from unpublished notes carefully prepared by D. T. Read. Mrs. V. Grulke cheerfully prepared the manuscript, with only occasional comments about amateur word-processor users.

References

Listed here are references from the recent literature in which the measurement or interpretation of critical field data are discussed. Those used as text references are numbered and make up the first part of the listing. The others, listed alphabetically following the text references, serve to provide background information. Only a few of the many excellent theoretical treatments are included.

[1] ASTM Standard for the Measurement of Critical Current (1983).

[2] Powell, R. L., and A. F. Clark, Definitions of terms for practical superconductors, 1. Fundamental states and flux phenomena, Crogenics **17**, 697-701 (1977).

[3] Powell, R. L., and A. F. Clark, Definitions of terms for practical superconductors, 2. Critical parameters, Cryogenics **18**, 137-141 (1978).

[4] ASTM Standard for Superconductor Terminology (1983).

[5] Matsumoto, H., and H. Unezawa, Interplay between magnetism and superconductivity, Cryogenics **23**, 37-51 (1983).

[6] Fickett, F. R., and R. B. Goldfarb, Magnetic properties, Chapter 6 of *Materials at Low Temperatures*, American Society for Metals, Metals Park, Ohio (1983).

[7] Nelson, R. A., SI: The international system of units, published by the American Association of Physics Teachers, Stony Brook, NY (1983).

[8] Hawksworth, D. G., and D. C. Larbalestier, Enhanced values of H_{c2} in NbTi ternary and quaternary alloys, Adv. Cryo. Eng. **26**, 479-486 (1980).

[9] Cody, G. D., Phenomena and theory of superconductivity, Chapter 3 of *Superconducting Magnet Systems*, H. Brechna, ed., Springer-Verlag, New York, pp. 159-229 (1973).

[10] Beasley, M. R., New perspective on the physics of high-field superconductors, Adv. Cryo. Eng. **28**, 345-359 (1982).

[11] Suenaga, M., and D. O. Welch, Flux pinning in bronze-processed Nb_3Sn wires, in *Filamentary A15 Superconductors*, M. Suenaga and A. F. Clark, eds., Plenum Press, New York, pp. 131-142 (1980).

[12] Hulm, J. K., and B. T. Matthias, Overview of superconducting materials development, Chapter 1 of *Superconducting Materials Science*, S. Foner and B. B. Schwartz, eds., Plenum Press, New York, pp. 1-61 (1981).

[13] Ekin, J. W., Superconductors, Chapter 13 of *Materials at Low Temperatures*, American Society for Metals, Metals Park, Ohio (1983).

[14] Hulm, J. K.; J. E. Kunzler and B. T. Matthias, The road to superconducting materials, Physics Today, pp. 34-44 (Jan. 1981).

[15] Hulm, J. K., and B. T. Matthias, High-field, high-current superconductors, Science **208**, 881-887 (1980).

[16] Fietz, W. A., and W. W. Webb, Hysteresis in superconducting alloys-temperature and field dependence of dislocation pinning in niobium alloys, Phys. Rev. **178**, 657-667 (1969).

[17] Kramer, E. J., Scaling laws for flux pinning in hard superconductors, J. Appl. Phys. **44**, 1360-1370 (1973).

[18] Ekin, J. W., Mechanical properties and strain effects in superconductors, Chapter 3 of *Superconductor Materials Science*, S. Foner and B. B. Schwartz, eds., Plenum Press, New York, 1981, pp. 455-509.

[19] Ekin, J. W., Four-dimensional J-B-T-ϵ critical surface for superconductors, J. Appl. Phys. **54**, 303-306 (1983).

[20] Rupp, G., Parameters affecting prestrain and B_{c2} in multifilamentary Nb_3Sn conductors, Adv. Cryo. Eng. **26**, 522–529 (1980).

[21] Larbalestier, D. C., Superconducting materials—A review of recent advances and current problems in practical materials, IEEE Trans. Mag. **MAG-17**, 1668–1686 (1981).

[22] Evetts, J. E., The characterization of superconducting materials—Conflicts and correlations, IEEE Trans. Mag. **MAG-19**, 1109 (1983).

[23] Lee, Z. H., K. Noto, Y. Watanabe, and Y. Muto, A new anisotropy of the upper critical fields H_{c2} in the $Cu_{1.8}M_6S_8$ single crystal, Physica **107B**, 297–298 (1981).

[24] Goodrich, L. F., and F. R. Fickett, Critical current measurements: A compendium of experimental results, Cryogenics **22**, 225–241 (1982).

[25] Schooley, J. F., and R. J. Soulen, Definition of the critical temperature of practical superconductors, in *Development of Standards for Superconductors*, F. R. Fickett and A. F. Clark, eds., NBSIR 80-1629 (1979) pp. 20–26.

[26] *Materials at Low Temperatures*, R. P. Reed and A. F. Clark, eds., American Society for Metals (1983).

[27] Fischer, O.; H. Jones, G. Bongi, M. Sergent, and R. Chevrel, Measurements of critical fields up to 500 kG in the ternary molybdenum sulphides, J. Phys. C; Solid State Phys. 7, L450-L453 (1974).

[28] Hein, R. A., and R. L. Falge, Differential paramagnetic effect in superconductors, Phys. Rev. **123**, 407–415 (1961).

[29] Stewart, G. R.; B. Cort and G. W. Webb, Specific heat of A15 Nb_3Sn in fields to 18 Tesla, Phys. Rev. B **24**, 3841 (1981).

[30] Stewart, G. R., Measurement of low-temperature specific heat, Rev. Sci. Instrum. **54**, 1 (1983).

[31] Foner, S.; E. J. McNiff, Jr., B. T. Matthias, and E. Corenzwit, Properties of high superconducting transition temperature $Nb_3Al_{1-x}Ge_x$ alloys, Proc. Eleventh International Conference on Low Temperature Physics II, 1025–11032 (eds. J. F. Allen, D. M. Finlayson, and D. M. McCall) St. Andrews (1968).

[32] Foner, S., High field superconductors, Colloq. Int'l. CNRS **242**, 423–429 (1975).

[33] Neuringer, L. J., and Y. Shapira, Nb-25%Zr in strong magnetic fields: magnetic, resistive, ultrasonic, and thermal behavior, Phys. Rev. **148**, 231-246 (1966).

[34] Soulen, R. J., and J. H. Colwell, Equivalence of the superconducting transition temperature of pure indium as determined by electrical resistance, magnetic susceptibility, and heat-capacity measurements, J. Low Temp. Phys. **5**, 325–333 (1971).

[35] Cave, J. R., and C. A. F. Weir, Cracking and layer growth in Nb_3Sn bronze route material, IEEE Trans. Mag. **MAG-19**, 1120 (1983).

[36] Habermeier, H.-U., Disorder and the upper critical field of Nb_3Ge, IEEE Trans. Mag. **MAG-17**, 1657–1659 (1981).

[37] Spencer, C. R.; P. A. Sanger and M. Young, The temperature and magnetic field dependence of superconducting critical current densities of multifilamentary Nb_3Sn and NbTi composite wires, IEEE Trans. Mag. **MAG-15**, 76–79 (1979).

[38] Rupp, G.; E. J. McNiff, Jr. and S. Foner, Upper critical field in multifilamentary Nb_3Sn conductors, IEEE Trans. Mag. **MAG-17**, 370–373 (1981).

[39] Hillmann, H., and K. J. Best, New measurements of critical data of optimized NbTi superconductors, IEEE Trans. Mag. **MAG-13**, 1568-1570 (1977).

Critical Field Determination for Practical Superconductors

Braginski, A. I., and H. C. Freygardt, Workshop on superconductors for magnets: Frontiers of technology, IEEE Trans. Mag. **MAG-17**, 2343–2354 (1981).

Bulakh, I. E.; S. V. Drozdova, C. A. Kalyushnaya, V. M. Pan, V. F. Primachenko, A. D. Shevchenko, N. V. Shevchuk, and M. V. Shubaev, Ultrahigh critical magnetic field superconductors $Pb_{0.9}Mo_6S_{7.5}$, IEEE Trans. Mag. **MAG-17**, 1642–1644 (1981).

Dew-Hughes, D., Practical superconducting materials, Chapter 2 of *Superconducting Machines and Devices*, S. Foner and B. B. Schwartz, eds., Plenum Press, New York, pp. 87–137 (1974).

Fietz, W. A., and C. H. Rosner, Advances in superconductive magnets and materials, IEEE Trans. Mag., pp. 239–259 (June 1974).

Flukiger, R.; S. Foner, E. J. McNiff, Jr., and B. B. Schwartz, Effects of material parameters on H_{c2} in A15 superconductors, J. Mag. Mag. Mater. **11**, 186–188 (1979).

Flukiger, R., Phase relationships, basic metallurgy, and superconducting properties of Nb_3Sn and related compounds, Adv. Cryo. Eng. **28**, 399-413 (1982).

Flukiger, R.; W. Schauer, W. Specking, L. Oddi, L. Pintschovius, W. Mullner, and B. Lachal, The phase relationships in Nb_3Sn wires at low temperatures as detected by crystallographical (neutron and x-ray diffraction) and by physical [B_{c2}(T), J_c vs. ϵ] measurements, Adv. Cryo. Eng. **28**, 361-370 (1982).

Fujii, G., Present practices in Japan for the measurement and definition of various superconducting parameters, Cryogenics **21**, 21-38 (1981).

Geballe, T. H., and J. K. Hulm, Superconductors in electric-power technology, Scientific American (November 1980).

Goncharov, I. N., and I. S. Khukharova, Investigation of the resistive behavior of a type-II superconductor near the upper critical field strength, Sov. Phys. JETP **35**, 331–336 (1972).

Hoard, R. W.; R. M. Scanlan, G. S. Smith, and C. L. Farrell, The effect of strain on the martensitic phase transition in superconducting Nb_3Sn, IEEE Trans. Mag. **MAG-17**, 364–367 (1981).

Khan, H. R., and W. Schauer, Microstructure and superconductivity of some C15 laves phase alloys: V_2Hf, $V_2Hf_{.51}Nb_{.49}$ and $V_2Hf_{.51}Ti_{.28}$, IEEE Trans. Mag. **MG-17**, 1017–1020 (1981).

Landwehr, G., Problems connected with the generation of continuous magnetic fields above 15 Tesla, IEEE Trans. Mag. **MAG-17**, 1768-1774 (1981).

Larbalestier, D. C., Nb-Ti alloy superconductors—Present status and potential for improvement, Adv. Cryo. Eng. **26**, 10-36 (1980).

Larbalestier, D. C., Niobium-titanium superconducting materials, Chapter 3 of *Superconductor Materials Science*, S. Foner and B. B. Schwartz, eds., Plenum Press, New York, pp. 133–199 (1981).

Morohashi, S.; K. Noto, N. Kobayashi, and Y. Muto, Thermodynamic properties and fundamental parameters of single crystal $Cu_{1.8}Mo_6S_8$, Physica **1088**, 929-930 (1981).

Orlando, T. P.; J. A. Alexander, S. J. Bending, J. Kwo, S. J. Poon, R. H. Hammond, M. R. Beasley, E. J. McNiff, Jr., and S. Foner, The role of disorder in maximizing the upper critical field in the Nb-Sn system, IEEE Trans. Mag. **MAG-17**, 368-369 (1981).

Roberts, B. W., Survey of superconductive materials and critical evaluation of selected properties, J. Phys. Chem. Ref. Data **5**, 581-821 (1976).

Scanlan, R. M., Superconducting materials, Afin. Rev. Mater. Sci. **10**, 113-132 (1980).

Schauer, W., and W. Schelb, Improvement of Nb_3Sn high field critical current by a two-stage reaction, IEEE Trans. Mag. **MAG-17**, 374–377 (1981)

Tachikawa, K., Recent developments in filamentary compound superconductors, Adv. Cryo. Eng. **28**, 29–40 (1982).

Journal of Research of the National Bureau of Standards
Volume 90, Number 2, March–April 1985

Spectral Transmittance Characteristics of Holmium Oxide in Perchloric Acid Solution

Victor R. Weidner, Radu Mavrodineanu, Klaus D. Mielenz, Rance A. Velapoldi, Kenneth L. Eckerle, and Bradley Adams

National Bureau of Standards, Gaithersburg, MD 20899

Accepted: November 28, 1984

The work describes the methods and procedures used to determine the wavelengths of minimum transmittance of holmium oxide in perchloric acid solution. Measurements of spectral transmittance of the solutions were made by means of a high precision spectrophotometer over the wavelength range 200 nm to 680 nm. The wavelength scale accuracy of this instrument was verified by extensive measurements of mercury and deuterium emission lines. The measurements of spectral transmittance of the holmium oxide solutions were made as a function of temperature, purity, concentration, and spectral bandwidth. Analysis of the uncertainties associated with these parameters and the uncertainties associated with the calibration of the instrument wavelength scale and the data analysis have resulted in an estimated uncertainty of ±0.1 nm for the determination of the wavelengths of minimum transmittance of the holmium oxide solution.

Key words: holmium oxide; spectral bandwidth; spectrophotometer calibration; spectral transmittance; wavelength calibration; wavelength standard.

1. Introduction

This work describes the methods and procedures used to determine the wavelengths of minimum spectral transmittance of holmium oxide (Ho_2O_3) in perchloric acid ($HClO_4$) solution in the spectral region 200 to 680 nm. The object of this activity was to develop a standard for verifying the wavelength scale of uv/visible spectrophotometers, and to provide assistance toward improving the accuracy of measurements in the fields of molecular absorption spectrometry or spectrophotometry [1][1].

Holmium oxide in a glass matrix has been issued by the National Bureau of Standards (NBS) as a wavelength standard for the ultraviolet and visible spectrum since 1961 [2]. Didymium glass wavelength standards have been issued since 1945. The didymium glass wavelength standards are available from NBS as Standard Reference Material 2009; 2010; 2013; and 2014 [3].

About the Authors: Victor R. Weidner is with NBS' Radiometric Physics Division, headed by Klaus D. Mielenz and served also by Kenneth L. Eckerle; Radu Mavrodineanu is associated with the Bureau's Inorganic Analytical Research Division as a reemployed annuitant; Rance A. Velapoldi is deputy director of the NBS Center for Analytical Chemistry; and Bradley Adams served the Bureau as a student worker.

2. Experimental

2.1 Instrumentation

Measurements of spectral transmittance of the holmium oxide solutions were made by means of a Varian Cary Model 2390 recording spectrophotometer[2].

[1]Numbers in brackets indicate literature references.

[2]Certain commercial equipment or products are mentioned in this paper in order to adequately document the work. In no case does this imply that the equipment or product is being endorsed by NBS or that it is necessarily the best equipment or product for the application.

The optical system of this double beam instrument consists of a filter predisperser and a double-pass double-sided grating monochromator. A deuterium lamp is used over the wavelength range 185 to 340 nm and a tungsten-halogen lamp is used over the wavelength range 340 to 3150 nm as a source. The spectral bandwidths are selectable from 0.07 nm to 3.6 nm. Data can be recorded by a digital readout system with thermal printer and an analog chart display.

2.2 Materials

2.2.1 Holmium Oxide

The holmium oxide solutions were prepared by dissolving the powder in a 10% perchloric acid in distilled water. The purity of the holmium oxide specimens used in the preparation of these solutions was indicated by the manufacturer [4] to be 99.99% (Lot No. Ho-0-4-007) and 99.999% (Lot No. Ho-0-5-007). Solutions were prepared with 2%, 4%, and 6% holmium oxide. These solutions were placed in 10 mm pathlength nonfluorescent fused silica cuvettes.

The actual form in which Ho is formed when Ho_2O_3 is dissolved in $HClO_4$ is that of an aquo ion of the general formula $Ho(H_2O)_n^{3}+$. The term "holmium oxide" and the spectral transmittances reported in the manuscript refer to this chemical species. Aqueous solutions of perchloric acid are used in this study to dissolve Ho_2O_3 since the resulting aquo ion is least likely to form complexes when subjected to changes in temperature and concentration [5].

The holmium oxide powder is stated by the manufacturer to have an average particle size of about 2 micrometers. The perchloric acid was a nominal 70-72% reagent grade (considered here as 100%). The distilled water was produced by thermal distillation. The aqueous solutions of holmium oxide in 10% perchloric acid were prepared by weighing 2, 4, or 6 g of the oxide and adding 10 mL of distilled water and 10 mL of perchloric acid. The holmium oxide was dissolved by heating at about 80 °C for one hour. The clear solution was transferred quantitatively to a 100 mL volumetric flask and was brought to volume with distilled water at room temperature.

2.2.2 Cells

The cells used for the transmission measurements of the holmium oxide solutions were conventional nonfluorescent, fused silica, cuvettes with a nominal pathlength of 10 mm. These cuvettes were provided with graded quartz-to-pyrex tubes with rubber caps.

2.3 Measurement Techniques

2.3.1 Calibration of the Spectrophotometer Wavelength Scale

The spectophotometer wavelength scale error was evaluated by measuring the emission spectrum of the instrument's deuterium lamp and the emission spectrum of a mercury pen lamp [6,7,8].

The wavelength calibration was performed at the beginning of the holmium oxide solution measurements and again at the completion of the measurements. A number of emission lines of mercury and two emission lines of deuterium were used over the wavelength range 230 nm to 690 nm (see fig. 1). The wavelength scale errors were determined for spectral bandwidths of 0.1 nm, 1 nm, 2 nm, and 3 nm.

Each emission line was scanned at a rate of 0.01 nm per second and recorded on a scale of 0.2 nm per centi-

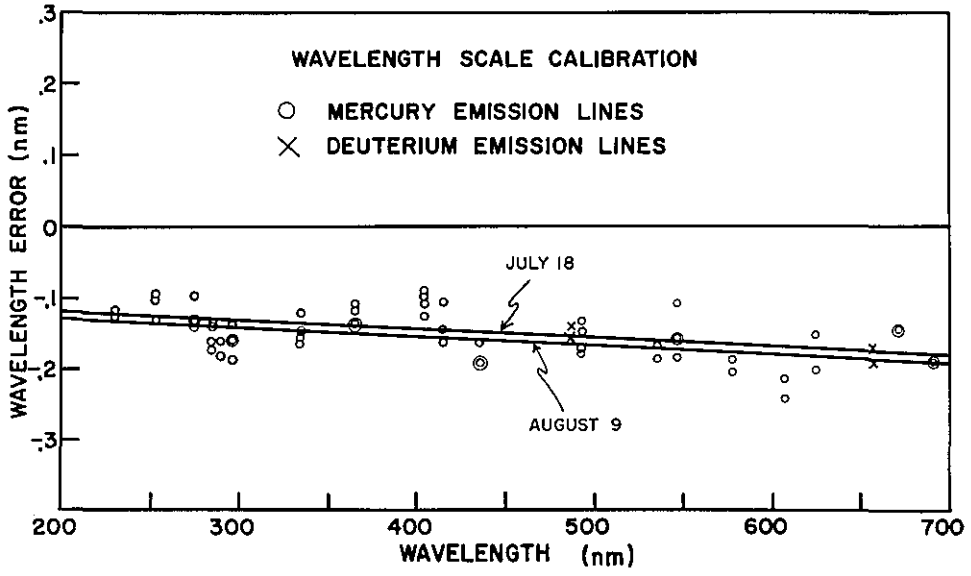

Figure 1–Wavelength scale calibration of the spectrophotometer.

meter. The recorded emission peaks were bisected, using a proportional divider, to determine the wavelengths at the center of the recorded triangular lines. Using this technique, the wavelength scale was read to the nearest 0.01 nm with a precision of ±0.005 nm. The differences between the measured wavelengths of mercury emission lines and the true wavelengths are plotted in figure 1. A linear least squares fit of these wavelength differences for the two dates July 18 and August 9 (also shown in fig. 1) was used to correct the measured values of the holmium oxide transmission minima for errors in the wavelength scale of the instrument.

The wavelength error of the instrument was essentially the same for spectral bandwidths less than 1 nm. However, at spectral bandwidths of 2 nm and 3 nm, the wavelength error was slightly different and a different correction was required.

The deuterium lamp emission lines were measured at two wavelengths each day during the holmium oxide solution characterization to verify the accuracy of the wavelength scale. These measurements showed that the calibration of the wavelength scale is constant to ±0.02 nm after a nominal warm-up of one hour. These results, as well as the repeatability of the calibration with the mercury line source, indicate that the overall stability of the instrument wavelength scale was better than ±0.05 nm during the period of time required to complete the wavelength characterization of the holmium oxide solution.

The mercury pen lamp is mounted in the lamp positioning device that ordinarily holds the deuterium lamp of the spectrophotometer. The arc tube of the mercury pen was aligned parallel to the entrance slit of the monochromator. The lamp holder is equipped with screw adjustments for vertical and horizontal alignment of the source. The entrance slit cannot be directly observed. Therefore, the source was adjusted with instrument operating in the single-beam mode until a maximum signal is observed. To test the effect of the positioning of the mercury line source on the observed emission line maxima, the pen lamp was moved horizontally across the field of view of the entrance slit to the monochromator in approximately 0.22 mm steps for a total of 12 steps or a 2.64 mm distance. The results of this experiment showed that the recorded emission maxima varied by less than ±0.01 nm for lamp positions within ±1 mm of the center position. The center position corresponded to the position of maximum signal.

2.3.2 Confirmation of Spectral Bandwidths

The mercury line source was used to confirm the spectral bandwidth settings of the spectrophotometer. The mercury emission line at 435.8 nm was scanned for spectral bandwidths of 0.1 nm, 0.25 nm, 0.5 nm, 1 nm, 2 nm and 3 nm. The emission peak was normalized to 100% on the chart recorder by adjusting the instrument gain. The bandwidth at half peak height is approximately equal to the spectral bandwidth. The natural bandwidth of the emission line is much less than the instrument bandwidth. The recorded curve has a triangular symmetry for all settings of the monochromator slitwidths. For the above-mentioned nominal spectral bandwidth settings of the spectrophotometer, the measured spectral bandwidths were 0.092 nm, 0.228 nm, 0.468 nm, 1.04 nm, 2.18 nm, and 3.20 nm, respectively. This technique for determining spectral bandwidths has some uncertainties due to assumptions made. However, it serves to confirm that the desired spectral bandwidths are closely approximated when the instrument is programmed to provide those settings; hence the effect on the transmittance minima is negligible.

2.3.3 Determination of the Wavelengths of Minimum Transmittance

The spectral transmittance of holmium oxide in an aqueous solution of perchloric acid exhibits many absorption bands in the ultraviolet and visible spectrum. The spectrum is shown in figure 2 for a 0.1 nm spectral bandwidth scan. The total number of observed absorption bands varies as a function of the spectral bandwidth used during the recording of the spectrum. There are approximately 14 major absorption features or bands between 200 and 650 nm that can be observed clearly for a wide range of spectral bandwidth settings. Most of the major absorption bands have lesser bands between them or in close association. These smaller bands are better resolved at bandwidths less than 1 nm. Only the major absorption bands that could be of use as possible wavelength standards were selected for detailed study. The various parameters affecting the measured wavelengths of minimum transmittance of the holmium oxide solution are discussed in section 3. These include such parameters as temperature, purity, concentration, and spectral bandwidth.

The spectral transmittance of the holmium oxide solution was digitally recorded on a thermal printer at 0.1 nm intervals with the monochromator scanning at a rate of 0.05 nm/s. The transmittance was simultaneously recorded on a chart with a wavelength display of 0.5 nm/cm.

The holmium oxide solution was contained in a 10 mm pathlength fused silica cuvette. The transmittance of the solution in this cuvette was measured relative to an air-only path in the reference beam.

The determination of the wavelengths of the transmittance minimum of the holmium oxide solution was derived from an analysis of the recorded digital output. The 0.1 nm interval transmittance data were plotted on

Figure 2–Spectral transmittance of a 4% solution of holmium oxide in 10% perchloric acid in water, beginning at right.

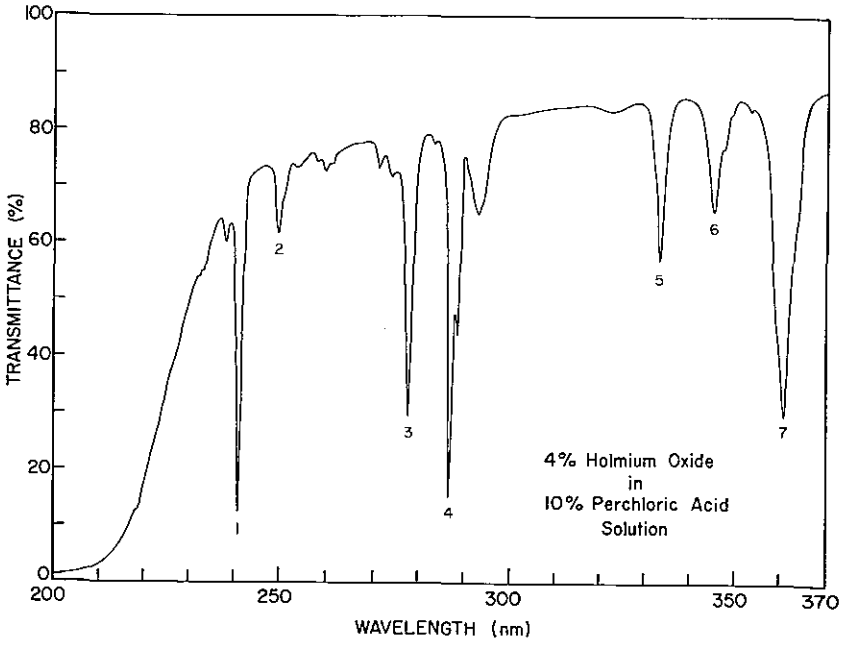

2-1

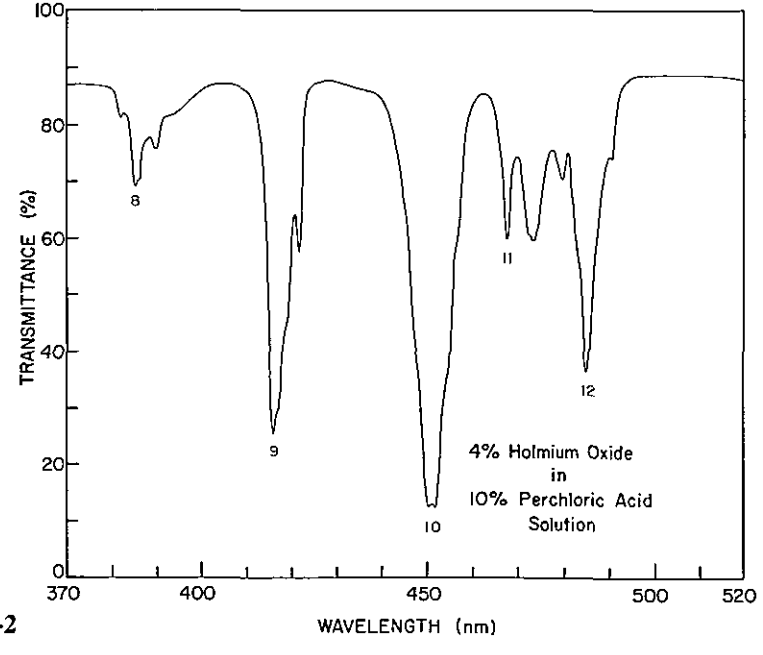

2-2

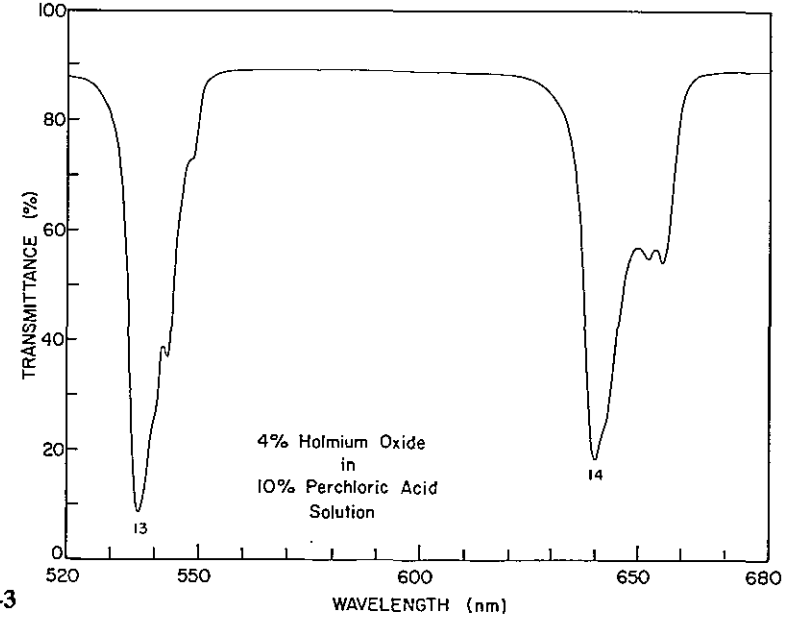

2-3

graph paper on a scale of 0.1 nm per cm with subdivisions of 0.01 nm per mm so that the wavelength interval of this plotted digital data could be read to the nearest 0.01 nm between the measured data points. The location of the wavelength of minimum transmittance for a given holmium oxide band was determined graphically (fig. 3) by drawing a curve through the data points and bisecting the horizontal grid lines between the two slopes of the curve representing the absorption feature. Several of these bisection points locate the line between the two slopes that intersects the minimum transmittance point, (usually at the lowest point of the curve). The wavelength at this point of intersection was taken as the measured wavelength of minimum transmittance for the absorption feature. The true wavelength of the minimum was determined by applying a wavelength correction to the instrumental wavelength scale, as determined in section 2.3.1.

2.3.4 Accuracy of the Wavelengths of Minimum Transmittance

The overall uncertainty in the location of the wavelengths of minimum transmittance is believed to be no greater than ±0.1 nm at the 95% confidence limit. This conclusion is based on the reproducibility of the following calibration procedures:

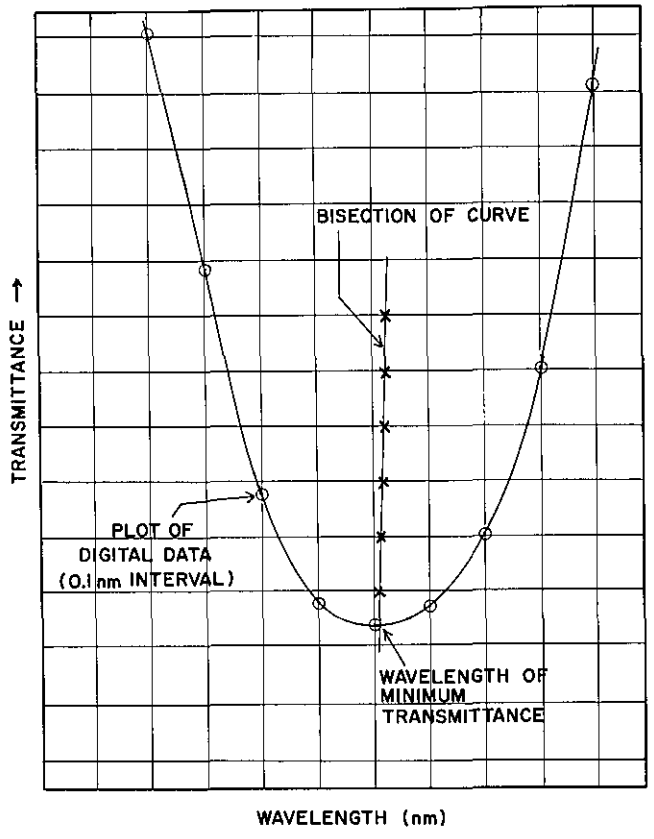

Figure 3–Graphical technique used to determine the transmittance minima from digital spectral transmittance data.

- The uncertainty of the calibration of the instrument wavelength scale using the mercury and deuterium lamps, and the long-term and day-to-day instabilities of the instrument wavelength scale (less than ±0.05 nm).
- The imprecision of the graphical technique for deriving the measured wavelengths of minimum transmittance. (±0.02 nm).
- The dependence of the measured wavelengths of minimum transmittance on variations in temperature or concentration of the solution. (±0.02 nm).

These uncertainties have been discussed in section 2.3.1. The imprecision of the graphical technique is illustrated in table 1, where data are shown for three absorption features. Ten sets of digital results were produced by the instrument for each of these features. The digital data were plotted and the wavelengths of minimum transmittance for each absorption feature were determined for the 10 sets of data by the graphical technique. The standard deviation and standard error for the 10 determinations is also given in table 1.

3. Measurements

3.1 Influence of the Blank Cuvette, Solvent, and Water

The spectral transmittances of an empty fused silica cuvette, a cuvette filled with distilled water, and a

Table 1. Ten cycle repetitive measurements of three holmium oxide transmittance minima. Listed minima are obtained by graphical techniques, using the digitally recorded 0.1 nm interval transmittance measurement.

	(spectral bandwidth=0.1 nm)		
Cycle	Minima No. 1	Minima No. 12	Minima No. 14
1	240.88 nm	485.08 nm	640.28 nm
2	240.87	485.10	640.30
3	240.86	485.11	640.30
4	240.84	485.11	640.30
5	240.85	485.10	640.29
6	240.84	485.11	640.30
7	240.85	485.11	640.29
8	240.85	485.11	640.30
9	240.84	485.10	640.30
10	240.85	485.11	640.29
Average:	240.853	485.104	640.295
Standard Deviation:	0.0134	0.0097	0.0071
Standard Error:	.0042	.0031	.0022

Note: The data shown in this table have not been corrected for the wavelength scale error of the spectrophotometer.

cuvette filled with the diluted perchloric acid (without holmium oxide) are illustrated in figure 4. These measurements are relative to an air path in the reference beam.

Measurements of the wavelength of minimum transmittance for the band at 241 nm were made with the holmium oxide in perchloric acid solution versus a cuvette containing only the perchloric acid in the reference beam. The wavelength of minimum transmittance of this band was found to be the same when the holmium oxide solution was measured relative to air in the reference beam and when it was measured relative to a cuvette containing the perchloric acid solution. Since the 241 nm band is within the spectral range showing a slope in the transmittance of the cuvette–perchloric acid spectra, (see fig. 4) it was considered to be the band most likely to be influenced by this slope. However, no measurable influence was detected in the location of the wavelength of minimum transmittance of this band due to these spectral features associated with the solvent or cuvette.

3.2 Influence of Temperature

The wavelengths of minimum transmittance of the holmium oxide solution were determined at 20 °C, 25 °C, and 30 °C for spectral bandwidths of 0.1 nm and 1 nm. If there is a temperature-related influence on the location of the wavelengths of minimum transmittance, it was not detected within these temperature ranges. The measured differences were attributed to random uncertainties.

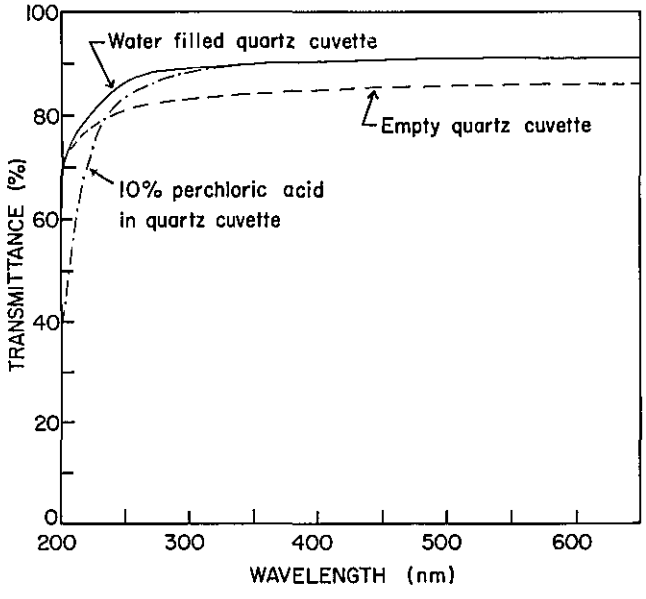

Figure 4–Spectral transmittances of an empty fused silica cuvette, a cuvette filled with water, and a cuvette filled with a solution of 10% perchloric acid in water.

3.3 Influence of Purity

Complete spectral scans of solutions made with the 99.99% and 99.999% purity holmium oxides showed no spectral differences except in the extreme ultraviolet cut-off at wavelengths less than 230 nm. The differences are illustrated in figure 5 for the wavelength range 200 to 300 nm. The wavelengths of the minimum transmittances for the 14 selected absorption bands were found to be the same for solutions prepared from these two lots of holmium oxide.

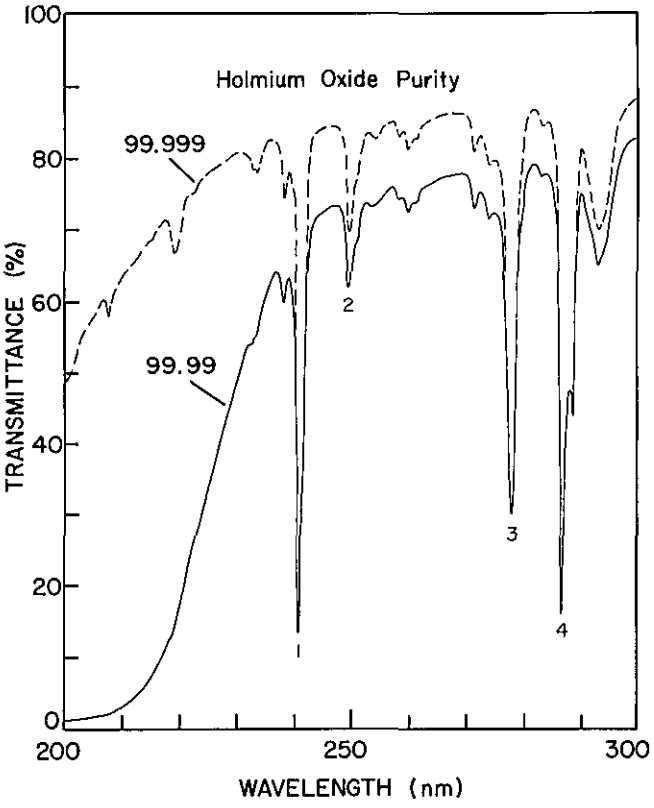

Figure 5–Spectral differences of solutions prepared from holmium oxide specimens of 99.99% purity and 99.999% purity.

3.4 Influence of Concentration

The location of the wavelengths of minimum transmittance of the holmium oxide solution as a function of concentration was tested with concentrations of 2%, 4%, and 6% in the perchloric acid solution. The general spectral scan indicated that the changes in concentration affected the measured transmittance as would be expected but did not influence the location of the transmittance minima. To verify this further, three of the bands were evaluated by the graphical technique described in section 2.3.1. The results of these concentration measurements for these bands are shown in table 2.

Table 2. Influence of holmium oxide concentration on the wavelengths of minimum transmittance.

	(spectral bandwidth = 0.1 nm)		
Holmium oxide concentration	Minima No. 1	Minima No. 12	Minima No. 14
2 %	240.84 nm	485.11 nm	640.30 nm
4 %	240.86	485.11	640.32
6 %	240.84	485.12	640.31

Note: The data shown in this table have not been corrected for the wavelength scale error of the spectrophotometer.

3.5 Influence of Spectral Bandwidth

The wavelengths of minimum transmittance of the holmium oxide solution were determined for spectral bandwidths of 0.1 nm, 0.25 nm, 0.5 nm, 1 nm, 2 nm, and 3 nm. Measurement of the instrumental spectral bandwidths is discussed in section 2.3.2. The influence of spectral bandwidth was by far the most important parameter affecting the location of the measured wavelengths of minimum transmittance. The results of this study are shown in figures 6 through 19 for the 14 minima identified in figures 2-1, 2-2, and 2-3. The data for bandwidth effects are also listed in tables 3 and 4. The measurements indicate that for most of the holmium oxide bands, the location of the wavelengths of minimum transmittance does not change significantly for spectral bandwidths of less than 1 nm. From these data it can be seen that a 0.1 nm spectral bandwidth is adequate to define the wavelengths of minimum transmittance within the stated uncertainties. For some bands the location of the minimum transmittance shifts only slightly for spectral bandwidths greater than 1 nm. However, many do show large shifts for larger bandwidth settings. These results indicate that for instruments with spectral bandwidth settings of less than 1 nm, the holmium oxide solution can serve as an excellent wavelength standard. For instruments having bandwidth settings between 1 nm and 3 nm the standard can still be of use if the instrument bandwidth is known.

4. Results

4.1 Transmittance of Holmium Oxide Solution

The general spectral signature of the holmium oxide solution is illustrated in figures 2-1, 2-2, and 2-3 for a spectral bandwidth of 0.1 nm. Some of the finer spectral features shown in these figures will be absent when the spectrum is recorded at bandwidths greater than 1 nm. The major transmittance minima selected for this study are indicated by numbers 1 through 14 as shown in these figures. These band numbers are used throughout the manuscript as a key to associate the data in the tables with the spectral features illustrated in the figures.

4.2 Selection of Useful Wavelengths of Minimum Transmittance

The selection of holmium oxide bands that are considered useful for calibration purposes was based on the influence of spectral bandwidth on the location of these minima. The transmittance minima of small side bands associated with major absorption features usually shift in wavelength with bandwidth setting or are not resolved over the normal instrumental bandwidth range. The 14 major absorption bands are listed in tables 3 and 4. The absorption bands not listed in the tables are not considered useful for wavelength calibration purposes.

4.3 Numerical Data

The wavelengths of minimum transmittance of the 4% holmium oxide solution are listed in tables 3 and 4 for six spectral bandwidths. The results of the measurements as a function of temperature are also listed for 0.1 nm and 1 nm spectral bandwidths at temperature settings of 20 °C, 25 °C, and 30 °C.

The shift in wavelengths of minimum transmittance as a function of spectral bandwidth is shown in figures 6 through 19 for the 14 selected minima. The recommended values of minimum transmittance are listed in table 3 and 4 for the measurements made at 25 °C.

4.4 Uncertainty of Measured Wavelengths

The uncertainties associated with the data listed in tables 3 and 4 have been discussed in section 2.3.4. The uncertainty in the determination of the wavelengths of minimum transmittance for the holmium oxide solution is believed to be no greater than ±0.1 nm at the 95% confidence limit using the instrumentation and techniques described in this paper.

4.5 Comparison of Results with Measurements Made on the NBS Reference Spectrofluorimeter

The wavelengths of minimum transmittance of several absorption bands of holmium oxide solution were determined by analysis of spectral data obtained with the NBS Reference Spectrofluorimeter [9]. This reference instrument is primarily designed to be used as a research tool for high accuracy spectral analysis of fluorescent materials and in the development of standards for use in this area of research. The versatile design of the instrument allows for its use as a high accu-

Figures 6–19—Fourteen holmium oxide transmittance minima as a function of spectral bandwidth.

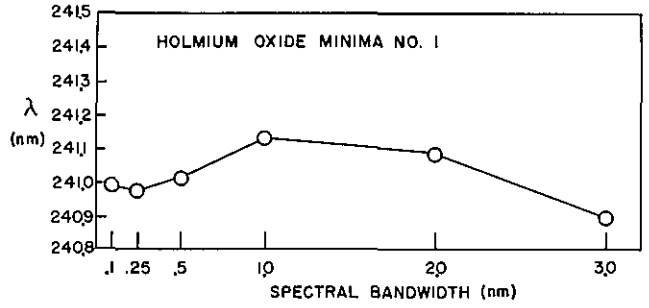

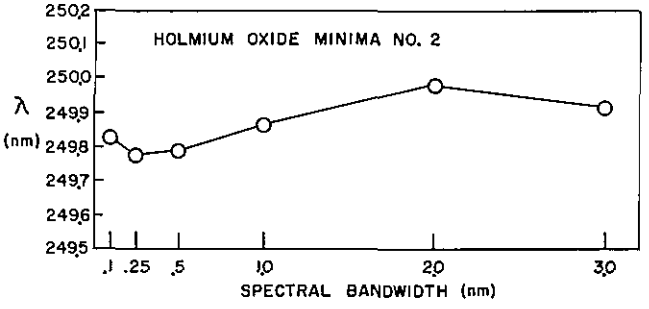

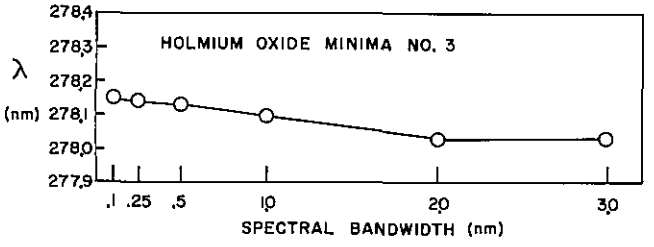

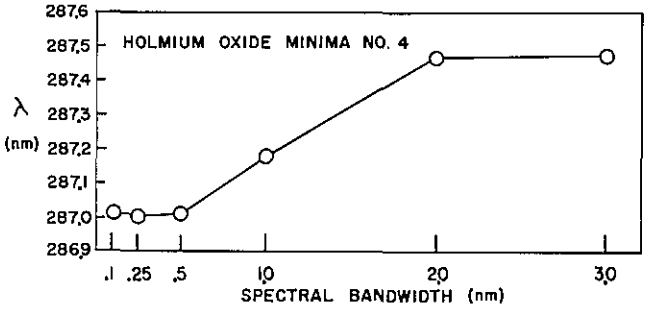

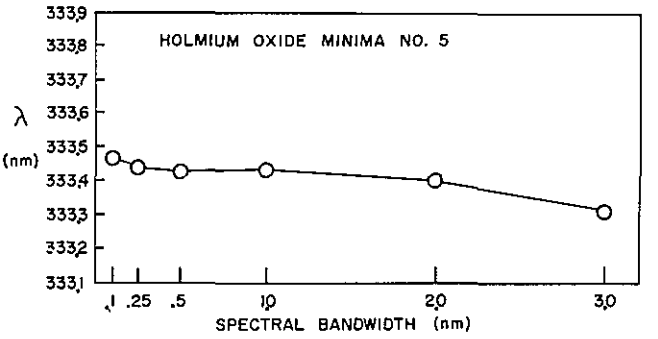

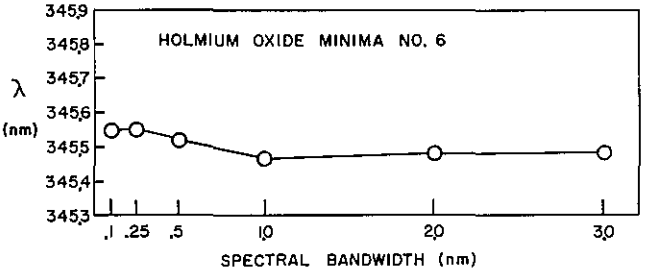

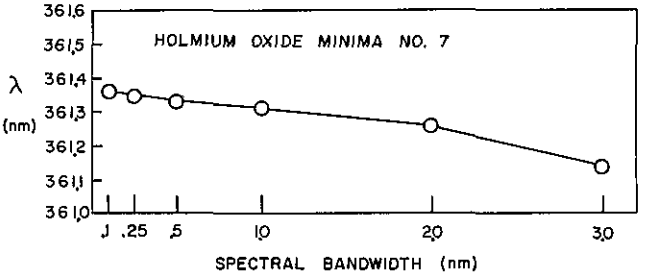

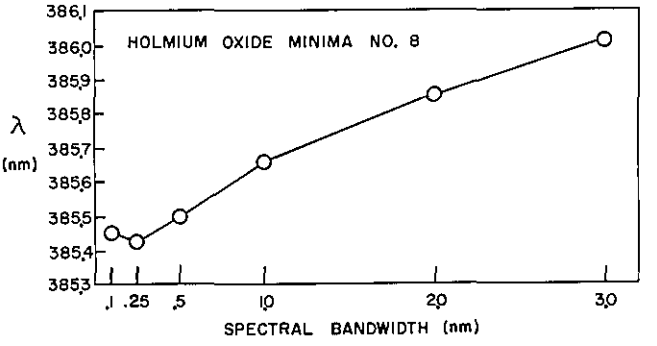

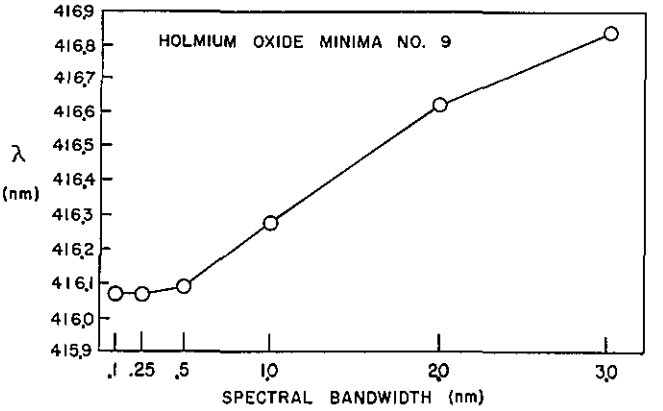

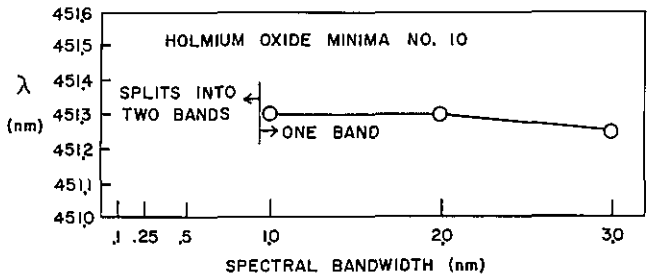

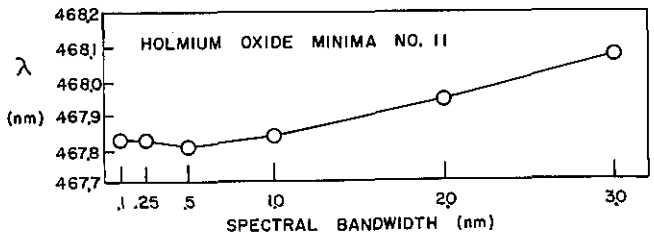

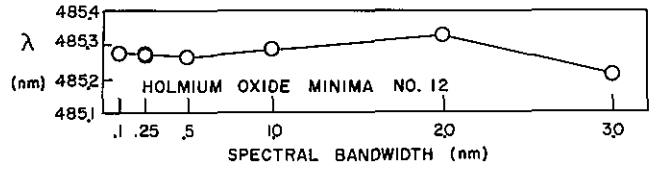

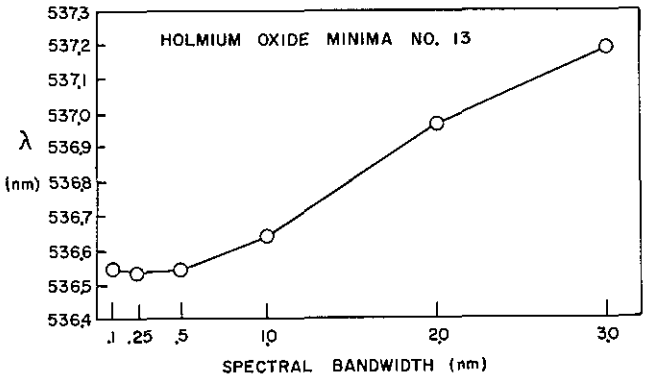

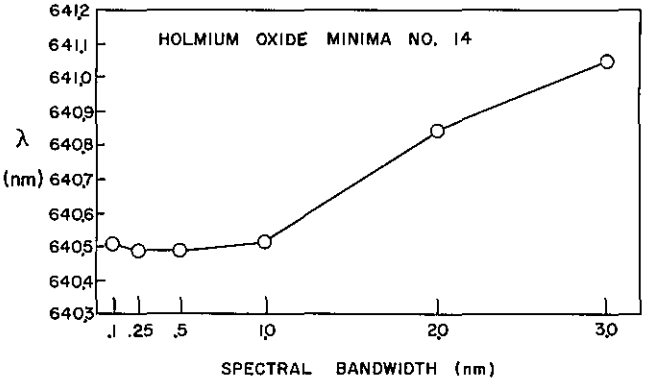

Table 3. Results of holmium oxide solution analysis for transmittance minima 1 through 7 for spectral bandwidths of 0.1, 0.25, 0.5, 1, 2, and 3 nm. 4% holmium oxide in a 10% perchloric acid solution.

Minimum No.	Temp. (°C)	Spectral Bandwidths 0.1 nm	0.25 nm	0.5 nm	1 nm	2 nm	3 nm
1	20	240.99 nm			241.13 nm		
1	25	240.99	240.97 nm	241.01 nm	241.13	241.08 nm	240.90 nm
1	30	240.99			241.15		
2	20	249.79			249.88		
2	25	249.83	249.78	249.79	249.87	249.98	249.92
2	30	249.79			249.86		
3	20	278.14			278.09		
3	25	278.15	278.14	278.13	278.10	278.03	278.03
3	30	278.14			278.09		
4	20	286.99			287.17		
4	25	287.01	287.00	287.01	287.18	287.47	287.47
4	30	287.01			287.18		
5	20	333.48			333.45		
5	25	333.47	333.44	333.43	333.44	333.40	333.32
5	30	333.48			333.45		
6	20	345.57			345.47		
6	25	345.55	345.55	345.52	345.47	345.49	345.49
6	30	345.62			345.49		
7	20	361.38			361.33		
7	25	361.36	361.35	361.33	361.31	361.16	361.04
7	30	361.38			361.31		

Note: The uncertainty in the wavelengths of minimum transmittance is ±0.1 nm. An extra decimal place is given for rounding purposes.

Table 4. Results of holmium oxide solution analysis for transmittance minima 8 through 14 for spectral bandwidths of 0.1, 0.25, 0.5, 1, 2, and 3 nm. 4% holmium oxide in a 10% perchloric acid solution.

Minimum No.	Temp. (°C)	Spectral Bandwidths 0.1 nm	0.25 nm	0.5 nm	1 nm	2 nm	3 nm
8	20	385.45 nm			385.66 nm		
8	25	385.45	385.42 nm	385.50 nm	385.66	385.86 nm	386.01 nm
8	30	385.44			385.68		
9	20	416.10			416.27		
9	25	416.07	416.07	416.09	416.28	416.62	416.84
9	30	416.13			416.30		
10	20	-----*			451.30		
10	25	-----*	-----*	-----*	451.30	451.30	451.24
10	30	-----*			451.34		
11	20	467.83			467.84		
11	25	467.82	467.82	467.80	467.83	467.94	468.07
11	30	467.84			467.84		
12	20	485.30			485.29		
12	25	485.28	485.28	485.27	485.29	485.33	485.21
12	30	485.31			485.30		
13	20	536.53			536.65		
13	25	536.54	536.53	536.54	536.64	536.97	537.19
13	30	536.45			536.63		
14	20	640.48			640.52		
14	25	640.51	640.49	640.49	640.52	640.84	641.05
14	30	640.52			640.49		

* Splits into 2 minima for spectral bandwidths less than 1 nm.

Note: The uncertainty in the wavelengths of minimum transmittance is ±0.1 nm. An extra decimal place is given for rounding purposes.

racy spectrophotometer in some applications. The wavelength scale of the spectrofluorimeter has been carefully calibrated by extensive measurements of emission line sources and is known to have an uncertainty of ±0.1 nm for spectral bandwidth of 0.1 nm.

This reference instrument was used to confirm the results obtained with the calibrated high-precision commercial spectrophotometer used for the holmium oxide measurements. A comparison was made to confirm the results for three of the transmittance minima at one spectral bandwidth setting. The results of this comparison are shown in table 5. The two instruments provided data for these three transmittance minima that agree to within 0.1 nm. The wavelength scale uncertainty for both instruments is ±0.1 nm.

Table 5. Comparison of values for holmium oxide transmittance minima with values obtained with *the NBS Reference Spectrofluorimeter.*

Instrument	(spectral bandwidth = 0.1 nm) Minima No. 1	Minima No. 7	Minima No. 14
Varian (Cary) Model 2390	240.995 nm	361.361 nm	640.507 nm
NBS Reference Spectrofluorimeter	240.970 nm	361.313 nm	640.469 nm

4.6 Other Measurements Outside NBS

A list of the wavelengths of minimum transmittance of the holmium oxide solution reported by other workers is given in table 6. (Ref. 10 offers details of these measurements.)

The data shown in table 6 indicate that workers in other laboratories are in generally good agreement with one another and that the NBS data also agree well with these workers' previously published data. These workers also found that the wavelengths of minimum transmittance of holmium oxide in similar solution in perchloric acid are not sensitive to variations in temperature and concentration. They also concluded that the wavelengths of minimum transmittance were least affected by changes in spectral bandwidth for band-

Table 6. Comparison of values for holmium oxide transmittance minima with values obtained by other workers (see Reference 11).

Min. No.	NBS Transmittance Minima		(1)	(2)	(3)	(4)
1	240.99 nm	*	241.15 nm	241.0 nm	241.1 nm	241.1 nm
2	249.83	*	249.75	250.0	249.7	249.7
3	278.15	*	278.2	277.8	278.7	278.2
4	287.01	*	287.15	287.5	287.1	287.2
5	333.47	*	333.5	333.3	333.4	333.3
6	345.55	*	345.6	345.5	345.5	345.0
7	361.36	*	361.5	361.0	361.5	361.2
8	385.45	*	385.6	385.6	385.5	385.6
9	416.07	*	416.2	416.0	416.3	416.6
10	451.30	#	450.7	450.4	450.8	451.0
11	467.82		467.75			468.0
12	485.28		485.25	485.2	485.8	485.2
13	536.54		536.3			536.8
14	640.51		640.5			

* Spectral bandwidth=0.1 nm
\# Spectral bandwidth=1 nm

widths less than 1 nm, but that large shifts can be encountered at bandwidths in excess of 1 nm.

5. Conclusions

The reported wavelengths of minimum transmittance of the holmium oxide solution appearing in tables 3 and 4 are estimated to be uncertain by no more than ±0.1 nm at the 95% confidence limit. These wavelengths of minimum transmittance were found to be essentially unaffected by changes in temperature at 25 °C ±5 °C. They were also unaffected by variations in the concentration for solutions containing 2%, 4%, and 6% holmium oxide. The critical parameter affecting the measured values of minimum transmittance was found to be the spectral bandwidth setting of the spectrophotometer. For spectral bandwidths less than 1 nm the wavelength shift is generally less than 0.2 nm. Users can most effectively determine the wavelength error associated with their instrument by using the NBS data listed in tables 3 and 4 that are representive of the spectral bandwidth setting ordinarily used with the instrument. The wavelengths of minimum transmittance of the holmium oxide solution for spectral bandwidths greater than 3 nm have not been evaluated.

The authors gratefully acknowledge the assistance of Chenq-Tsong Chang, guest worker from Taiwan, for his contribution in measuring the transmittance minima of the holmium oxide solution on the NBS Reference Spectrofluorimeter; Jack J. Hsia, for constructive discussions; Robert W. Burke, for assistance in the preparation of various Ho_2O_3 solutions; and the NBS Optical Shop for preparation of the fused silica cuvettes.

6. References

[1] The terminology used in this work was defined earlier by K. D. Mielenz in Anal. Chem. **48**, 1093 (1976).

[2] Keegan, H. J.; J. C. Schleter and V. R. Weidner, Ultraviolet Wavelength Standard for Spectrophotometry, J. Opt. Soc. Am. **51**, 1470 (1961), (abstract).

[3] Venable, W. H., Jr., and K. L. Eckerle, Standard Reference Material: Didymium Glass Filters for Calibrating the Wavelength Scale of Spectrophotometers (SRM 2009, 2010, 2013, 2014).

[4] The holmium oxide was obtained from Research Chemicals, a Division of Nucor Corp., Phoenix, Arizona.

[5] Gschneider, K. A., Jr., and L. E. Yring, Handbook of the Physics and Chemistry of Rare Earths, Vol. 3 North-Holland (1979).

[6] Harrison, G. R., MIT Wavelength Tables, MIT Press, Cambridge, MA (1960).

[7] ASTM Manual on Recommended Practices in Spectrophotometry, Published by American Society for Testing and Materials, 1916 Race St., Philadelphia, PA 19103 (1969).

[8] CRC Handbook of Chemistry and Physics, 63d Edition, CRC Press, Inc., (1982-1983).

[9] Mielenz, K. D., in "Measurement of Photoluminescence" (K. D. Mielenz, Editor), pp 17–19, Academic Press (1982).

[10] Burgess, C., and A. Knowles, Eds. Standards in Absorption Spectrometry, Chapter 7, Wavelength Calibration, Chapman and Hall, London (1981).

Journal of Research of the National Bureau of Standards
Volume 90, Number 2, March–April 1985

An Apparatus for Direct Fugacity Measurements on Mixtures Containing Hydrogen

Thomas J. Bruno
National Bureau of Standards, Boulder, CO 80303

Accepted: January 7, 1985

An apparatus has been designed and constructed to allow measurements of fugacities in gaseous mixtures containing hydrogen. The apparatus makes use of a semipermeable membrane to allow a direct measurement of the partial pressure of a permeating component (in this case, hydrogen) in a mixture with a nonpermeating component. In this study, measurements were made on mixtures of hydrogen/methane and hydrogen/propane.

The apparatus is designed to operate at moderate and high temperatures (ambient to 250 °C) and moderate and high mixture pressures (3 to 50 MPa). The actual pressure range that is experimentally accessible is dependent on the fluid mixture under study, due to its influence on the pressure gradient across the semipermeable membrane.

The pressure measurements are done isothermally on a series of concentrations of the binary. Each mixture is characterized using a developmental gas-chromatograph which has been built especially for this work. The gas-chromatograph was calibrated using standard mixtures of hydrogen/methane and hydrogen/propane, prepared gravimetrically in our laboratory.

Using measured values of the mixture pressure, hydrogen partial pressure and mixture mole fraction at a given temperature, fugacity coefficients were determined using the virial equation. The measured values are compared with some previous data and general trends are discussed.

Key words: fugacity coefficients; fugacity measurements; gas-chromatograph; gas mixtures; hydrogen/methane; hydrogen/propane.

1. Introduction

The concept of fugacity owes its origin to Lewis [1,2][1], who desired some measure of "escaping tendency" upon which to base his idea of equilibrium. His original use of partial molar free energy suffered from a negative infinity in the case of a gas in the limit of low pressure [3]. The concept of fugacity, which was devised to remedy this difficulty, is a convenient way to express the chemical potential of a substance in experimentally accessible terms. Since defining equations and useful functional relationships are presented in a variety of sources [4–6], a discussion of the basics of fugacity will not be repeated here.

Fugacity is a most important quantity in experimental thermodynamics because of its theoretical significance and general usefulness. The phase equality of temperature, pressure, and component fugacity is the criterion for physical equilibrium of a system. In a system involving chemical reactions, fugacities appear in the equilibrium constants describing the multicomponent system. Departures from equilibrium can be described in terms of fugacity gradients [7]. Since fugacity is a measure of nonideality of a gaseous system, measurements of fugacity and fugacity coefficients are of value in research on equations of state, especially work involving mixtures.

There are several techniques by which fugacities in gas mixtures may be measured experimentally. The most generally used method involves consideration of the P-V-T surface of gas mixtures of composition y_i. The component fugacities f_i are then obtained from [8,9]:

About the Author, Paper: Thomas J. Bruno is a physical chemist in the Chemical Engineering Science Division of NBS' National Engineering Laboratory. The work described was supported financially by the Gas Research Institute.

[1]Numbers in brackets refer to literature references.

$$\ln f_i = \ln P x_i + \int (V_i/RT - 1/P)\, dP \qquad (1)$$

where V_i is a partial molar volume, and x_i is the mole fraction of component i, and P, T and R have their usual meanings. The P-V-T-x data used in this type of measurement must be very precise, because of the loss of precision of derived thermodynamic functions. In addition, large quantities of PVT data are necessary for the successful exploitation of the above equation. One can also use the above equation with various equations of state as a predictive tool for fugacity.

There are more accurate techniques for experimental determination of fugacities in gas mixtures [10]; however these are applicable only in specific instances. One such case involves mixtures containing hydrogen. For these mixtures, a physical equilibrium technique using a semipermeable membrane is applicable. The principle of this technique is quite simple and is illustrated in figure 1. An experimental chamber is divided into two regions by a membrane permeable only to component i. The fugacity of pure component i at partial pressure P_i will be equal to the fugacity of component i at P_m, the total mixture pressure, after equilibrium has been established. The three general criteria for equilibrium are thus satisfied: the equality of temperature, pressure, and fugacity. The permeation through the membrane, and hence the approach to equilibrium is driven by the equalization of chemical potential on both sides of the membrane.

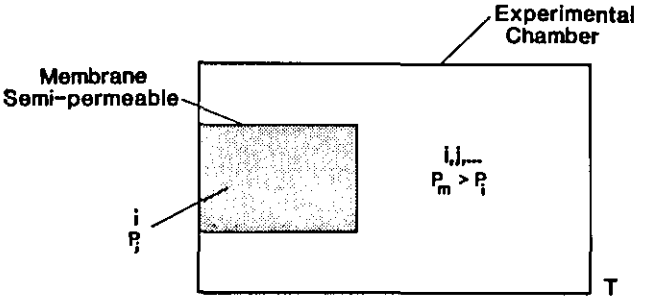

Figure 1-Principle of the semipermeable membrane technique.

The observance and measurement of hydrogen partial pressure was originally done using a semi-permeable membrane by Ramsay [11] and Tsakalotos [12]. The first application of this technique to measurement of gas mixture component fugacities was due to Krishnamurty [13] at Columbia University. His original study of hydrogen-helium mixtures was followed by several studies of hydrogen-propane mixtures [14,15], and a few studies of ternary mixtures containing butane and ammonia with hydrogen-propane [15,18]. The present apparatus differs markedly from the original Columbia University instrument, with many of the difficulties [19,20] encountered with the Columbia design being addressed and described in the experimental section.

Once a hydrogen partial pressure has been measured across the semipermeable membrane at a particular temperature, the fugacity of this single component can be determined. It is more convenient to deal with a dimensionless quantity called the fugacity coefficient, ϕ_i, defined by

$$\phi_i = f_i/(x_i P_i) \qquad (2)$$

where P_i is the partial pressure of component i [6]. The fugacity coefficient of this single component can be determined using the virial equation (truncated after the third virial coefficient) [17,18],

$$\ln \phi_i = \frac{B}{R}\left(\frac{P_i}{T}\right) + \frac{C - B^2}{2R^2}\left(\frac{P_i^2}{T^2}\right). \qquad (3)$$

The above quantities are for pure hydrogen only. To determine the fugacity coefficient of hydrogen in the mixture, we use the defining equation for the fugacity coefficient [10]:

$$\phi_{H_2}^m = f_{H_2}/x_{H_2} P_m \qquad (4)$$

where x_{H_2} is the mole fraction of hydrogen in the mixture, and P_m is the total pressure of the mixture. The value of P_m is necessarily greater than that of P_i, since it also includes the partial pressure of the nonpermeating component.

2. Test Systems

The systems chosen for the initial studies on this instrument are gaseous binary mixtures of hydrogen/methane and hydrogen/propane. These were chosen for several reasons. First, there was no evidence that either mixture would be detrimental to the membrane, or that temporary poisoning of the membrane would cause slow diffusion rates. Second, preliminary predictions made using the Redlich-Kwong equation indicated that these systems would be quite informative [8]. Hydrogen/propane is expected to have appreciable nonideality [15], while hydrogen/methane, on the other hand, would be expected to show a smaller change of fugacity coefficient with mole fraction. This second system, therefore, provides a test of the overall sensitivity of the apparatus, since the total expected change is more comparable to the experimental error. Third, there are previous data on hydrogen/propane with which to compare the present data [18,19].

Hydrogen/methane and hydrogen/propane mixtures pose no unfavorable analytical requirements. The chromatographic separations are easily done using one

column for each mixture. Heart-cutting or multi-dimensional techniques are unnecessary. The retention times are quite reasonable, and well-shaped peaks are obtained at experimentally convenient column and injector temperatures. The analytical conditions for both mixtures are thus very conducive to precise quantitation.

3. Experimental

3.1 Pressure Vessel

A schematic diagram of the essential features of the apparatus is given in figure 2. The heart of the apparatus is a large, thick-walled pressure vessel which serves as the experimental chamber. The vessel has a relatively large internal volume (2050 ml), so that the removal of small aliquots of mixture for analysis will cause minimal disturbance of equilibrium. The opening of the vessel is also large (11.43 cm diameter), to accommodate the membrane manifold, a mixer, and required feed-throughs. The vessel was machined from a section of work hardened 316 stainless steel barstock, with final dimensions and clearances exceeding the requirements set forth by the ASME [21,22]. A bolted closure is employed in the vessel, using eight bolts machined from 4340 (AISI designation) steel. The high loading on the

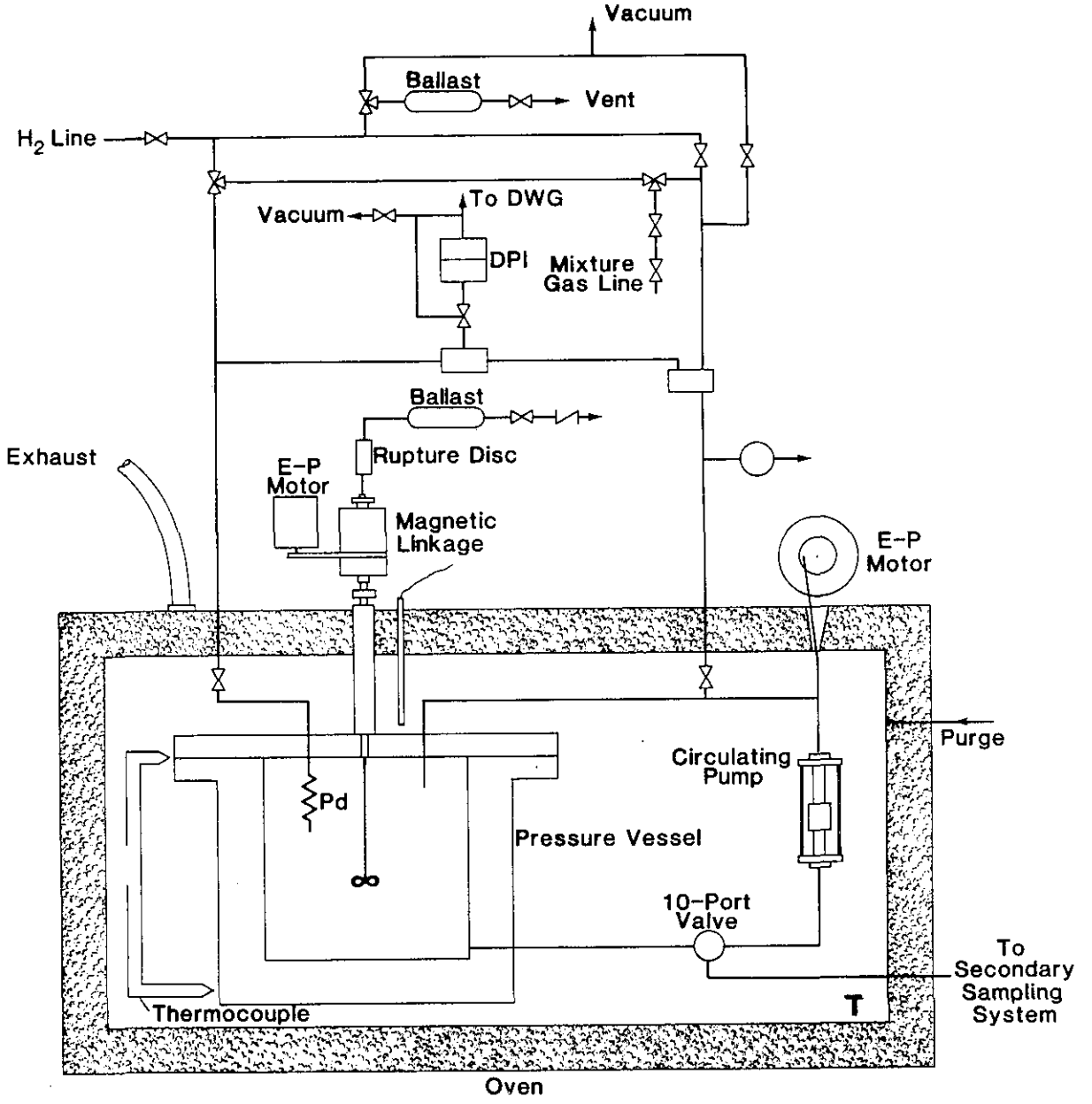

Figure 2–Schematic diagram of the apparatus.

11.43 cm diameter closure required the use of an ultra-high strength steel for the bolts. Sealing is provided by either a 25% glass-filled PTFE gasket or 316 stainless steel gasket (the stainless steel gasket is used for temperatures above 220 °C). The vessel with its closure is capable of containing a pressure of 50 MPa at 340 °C. The lid of the vessel also accommodates a thermometer probe well, and a provision for a safety head (equipped with a 41 MPa rupture disk) and supports a propeller-type mixer. The mixer is a commercial magnetic linkage type with air cooled magnets.

3.2 Membrane Manifold

Due to the importance of the membrane manifold for this experiment, and its attendant complexities of fabrication, a detailed discussion is provided. The semipermeable membrane manifold, pictured in figure 3, is suspended from the underside of the vessel lid using a compression fitting.

As stated previously the working principle of the semi-permeable membrane method depends upon the separation of the mixture (i, j, . . .) and a pure, permeating component (i) into two separate "compartments" within the experimental chamber. The "wall" separating the two components is permeable to i (in the present case, i is hydrogen), but not to the other mixture components. Many materials are known to allow permeation of hydrogen. The best material for this purpose is palladium [23], a fact which has led to commercial exploitation in hydrogen purifiers. Palladium itself has little mechanical strength, however, and in practical applications, one must usually resort to the use of an alloy containing 25% silver. Palladium-silver, 75/25, is easily fabricated into useful forms such as rod, foil and tubing. Due to geometrical and support considerations, tubing is the most suitable form for use at high pressures.

The Pd-Ag tubing was obtained from a commercial processor and had an outside diameter of 0.160 cm, and a wall thickness of 0.008 cm. The material is annealed to a dead soft condition in a tube furnace, and tested for pinholes using a helium leak detector. At present, the material is available only in 396 cm long sections, due to limitations of the drawing die. The thin wall of the tubing was necessary to achieve reasonable gas diffusion rates. Indeed, if the wall thickness were much greater, diffusion may not be observed at all [24]. It was necessary to increase the strength of this rather thin and weak tubing, since it must support pressure gradients of 7 MPa or more. For this purpose, 400 cm length coil springs were fabricated from 0.025 cm diameter stainless steel wire. The springs were wound to have a nominal relaxed o.d. of 0.145 cm, and are easily inserted into the Pd-Ag tubes. The spring is then under a low tension

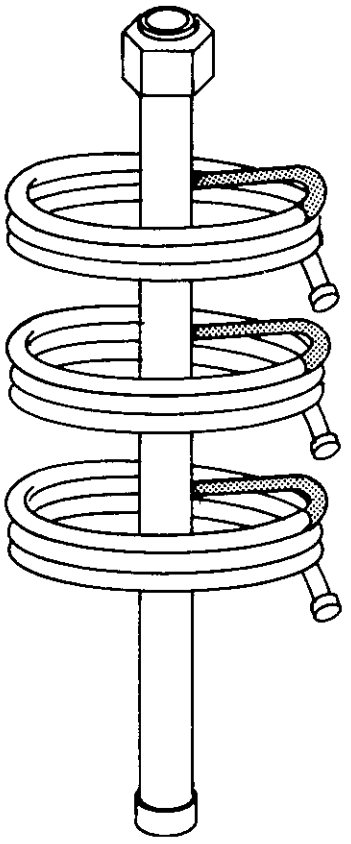

Figure 3–Semipermeable membrane manifold.

interference fit inside the Pd-Ag tube, and greatly increases the tube's "compressive load" strength.

The Pd-Ag tubes each containing a coiled spring, were then formed into five layer coils, approximately 2.5 cm long with a maximum outside coil diameter of 2.5 cm. The coiling process was done on a custom made adjustable length mandrel held in a lathe collet. Extreme care was taken to keep all traces of dirt or oil from contaminating the tubing, since this could result in permanent poisoning of membrane activity [23].

For each manifold (fig. 3), three coils were prepared and wound as described above. One end of each coil (the outside end) was capped off with a custom made 316 stainless steel cap. The other end (the inside end) was fitted into a specially drawn "elbow" made from 0.208 cm o.d. 321 stainless steel tubing, approximately 1.5 cm long. This elbow was, in turn, placed into a drilled hole in a central tube (0.328 cm o.d., 0.089 cm wall thickness). The central tube can be made from either 316 stainless steel or 270 nickel. It is the top of this central tube which is ultimately connected to the pressure measurement manifold using a compression fitting. The bottom of the tube is capped.

The Pd-Ag coils, end caps, elbows, and central tube were assembled in a vibration eliminating fixture to al-

low brazing of all the joints. Due to the chemical sensitivity of Pd-Ag, the use of any kind of flux is impossible. Thus, vacuum brazing was employed. All joints were "dressed" with a single loop of 0.051 cm diameter precious metal (82% gold, 18% nickel) brazing wire. The fixture-held manifold was placed in the vacuum furnace, which was then evacuated to 1.3×10^{-5} Pa. The temperature was then raised to the melting point of the brazing wire, and the system was allowed to "soak" at this temperature for a few minutes. The furnace was then cooled slowly to prevent the development of cracks. The completed manifold was tested for pinholes using a helium leak detector, and for hydrogen diffusion (with pure hydrogen) on both sides of the membrane.

Before the membrane is actually used, the Pd-Ag surface must be activated by repeated oxidation and reduction at elevated temperature (300 °C has proven to be satisfactory). Oxidation is done in a pressurized (6 MPa) environment of oxygen or air; reduction is done in the same way using pure hydrogen [25]. A membrane prepared in this way will quickly reach equilibrium during an experiment. Typically, 45 minutes is adequate to allow 95% of equilibration (pressure stabilization) to take place.

3.3 Pressure Measurements

Measurements of the pressures of the pure hydrogen (from inside the membrane manifold) and the mixture (outside the membrane) were made using a commercial dead weight pressure balance. The balance has an accuracy of 0.015%, and a range of between 0.04 and 82.7 MPa. The pressure of the test fluid (either hydrogen or mixture) is referenced to an inert gas line via a diaphragm type differential pressure transducer. The inert gas communicates its pressure to another differential pressure transducer which is referenced to oil pressure. The oil pressure is generated by weights on a piston table. When both differential pressure transducers are at null condition, one can obtain the pressure of the test fluid by summing the weights pressurizing the piston. Corrections are made for local gravity (979,601.148 milligals at Boulder station B), atmospheric pressure, temperature effect on piston area, elastic distortion of the cylinder, and oil head pressure. Corrections for fluid expansion into valve and transfer line volumes are also required. In actual practice, the differential pressure transducers are first brought to null with equal opposing pressures, to allow the setting of a zero reference point. Hysteresis effects in the transducer are minimized by "rocking" the diaphragm up and down several times before taking a measurement. The effect of temperature on the pressure transfer lines (between differential pressure transducers) is a small source of systematic error, so care was taken to maintain a uniform room temperature.

4. Temperature Control and Measurement

Since the fugacity measurements are made isothermally, adequate temperature control is necessary. Mixed liquid baths are usually the best way to thermostat an experiment of this type. This is impractical in the present work, however, since measurements at high temperatures are anticipated. For this reason, a commercially available vigorously mixed oven was modified to provide a thermostat. The major modifications included the installation of baffles (to promote more uniform mixing of the temperature transmitting fluid), installation of large aluminum thermal masses (to reduce temperature gradients) and the fabrication of a thermally insulated cover plate (from which the pressure vessel and other high temperature components are suspended inside the oven).

The oven is heated by 6.5 kW resistive elements controlled by a proportional SCR circuit, allowing temperature control of the apparatus components to ±0.05 °C. The controller is also equipped with a high temperature limiting cutoff for safety. For additional safety, the temperature transmitting fluid of the oven is maintained at a slight negative pressure, and a low flow rate of nitrogen is continually passed through the hot zone and is exhausted into a fume hood.

Temperature gradients among key components inside the oven are monitored using opposed pairs of J-type (iron-constantan) thermocouples [26,27]. The observed gradients are then minimized using very low power "shimming" heaters located near or in major components.

Temperature measurements are made using a commercial quartz crystal oscillator thermoprobe. The quartz probe is located in a thermowell in the pressure vessel. The immersion error of the probe in this configuration was calculated to be on the order of ±0.003 °C. A single point calibration is performed on a regular basis, using either the triple point or freezing point of water. This single point measurement is for scaling only; the frequency versus temperature table for the quartz probe is stored on a ROM, and is accessed automatically. The probe has an absolute accuracy of ±0.03 °C in the present region of interest. Errors due to long term instability amount to less than ±0.008 °C. Errors due to hysteresis are of a negligible level, since the measurements are made isothermally. Thus, thermometry precision on the order of ±0.05% (coefficient of variation) is easily obtainable.

5. Analytical System

It is necessary to determine the composition of the gas mixture (outside the semipermeable membrane) in order

to deduce fugacity coefficients. A custom designed developmental gas chromatograph and sampling system was built to perform the necessary analyses. This was considered necessary because of some of the unique problems inherent in hazardous gas analysis [28,29].

The analytical system consists of a primary sampling system (which allows removal of a sample from the hostile pressure/temperature environment of the vessel), a secondary sampling system (which allows sample manipulation and injection) and the gas chromatograph, in which the separation and quantitation is actually done. The primary sampling system consists of a 10 port valve (rated for service at 250 °C and 48 MPa), a circulating pump, and necessary valving. This equipment is shown in place in figure 2. The sampling valve is actuated remotely using helium gas (at 0.83 MPa, feeding a pneumatic drive), thus permitting the operator to remain outside the potentially hazardous pressure vessel zone. Helium is used as the actuation fluid to provide very fast valve switching. The evacuable sample loop of this valve has a volume of 0.5 ml. At a mixture pressure of 3.45 MPa, the withdrawal of a sample aliquot of this size causes a mixture pressure drop of 0.0008 MPa, which has a negligible effect upon the equilibrium mixture composition. Before the sampling valve is switched to remove this plug of sample, the mixture gas is circulated through the sample loop using a commercial check valve type pump. This minimizes the problem of concentration gradients, which often plague expansions of gas mixtures from elevated pressures. Only a few minutes of circulation are needed, since the pump is able to move 4.0 ml of fluid per stroke, and a pumping rate of 15 strokes per minute is employed.

Switching of the primary sampling valve results in the transfer of the plug of sample to the secondary sampling manifold, which is shown schematically in figure 4. The sample is held between valves A and B inside a 316L stainless steel bellows. The pressure of the sample may be varied by compressing or expanding the bellows. Valve B allows the sample to be introduced into a 10 port sampling valve, S, equipped with a 50 μl sample loop. Valve D allows the loop to be evacuated before being filled with sample and between analyses. It has been found in this work that loop evacuation before filling leads to a factor of two increase in precision of the measured chromatographic peak area counts. The vent valve, C, allows the sample pressure to be dropped to ambient before injection. The ambient pressure is measured using a fixed cistern mercury barometer, with the appropriate corrections being applied to the readings [30].

The sampling valve, bellows, and valves A through D

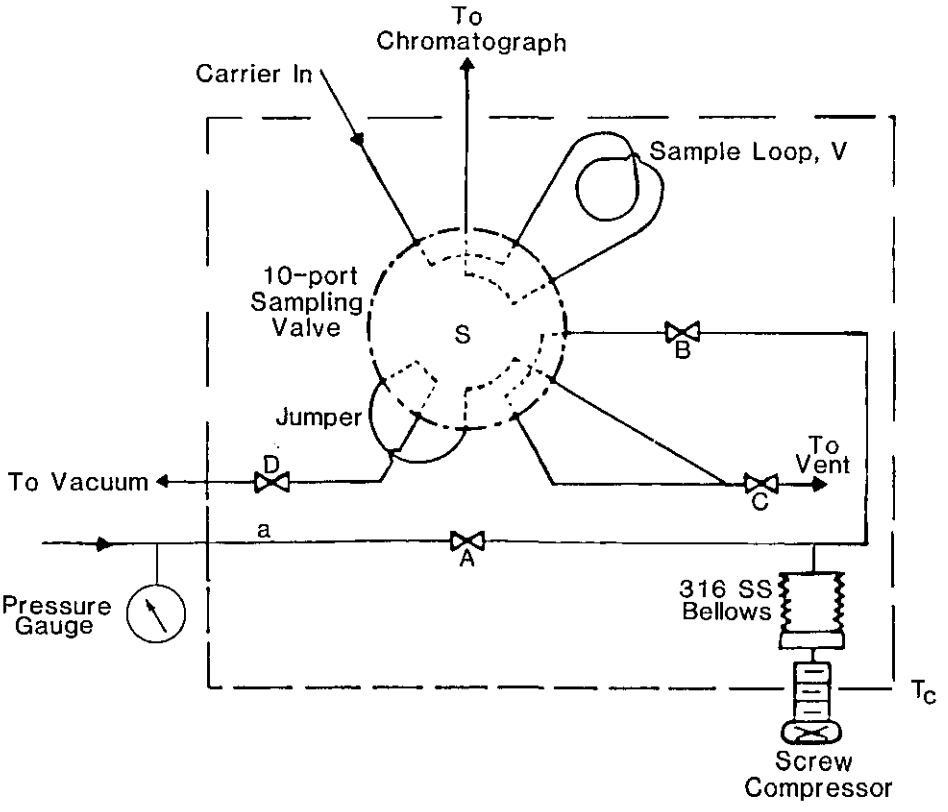

Figure 4–Secondary sampling manifold.

are mounted within a massive (1050 cm^3) aluminum block which is heated (in the present work, to 125±0.3 °C). The aluminum block reduces temperature gradients to a negligible level. Temperature control is provided by a proportional controller which responds to a thermistor sensor. Thus, by controlling the temperature and pressure of the fixed volume sample loop, one is assured of injecting the same quantity of sample for each analysis.

Upon switching the sampling valve of the secondary manifold, the plug of sample is swept from the loop into the chromatograph. This chromatograph has been specially constructed to provide precise control of column temperature and pressure. The column is thermostated in a vigorously stirred oil bath which is maintained to within ±0.02 °C. All analyses are done isothermally to minimize carrier flow rate disruptions. Column pressure is controlled using a fine adjustment pressure regulator (a commercially available unit used for pressure gauge calibration) followed by a fine metering valve. The chromatograph is very similar to units used for precise thermodynamic measurements [31–33]. Mass flow controllers are not used since the column temperature is not programmed. The carrier gas flow rate, measured at the detector exit, is maintained at 40.00±0.05 ml per minute. Since both hydrogen and the mixture gas (in the present case, methane and propane were studied) required detection and quantitation, argon was chosen as the carrier gas [34].

The separation of mixtures of hydrogen-methane and hydrogen-propane is experimentally trivial and will be described later. A micro cell thermal conductivity detector (TCD) at the column exit, connected to a commercial electronic integrator, provided detection and quantitation. Peak area counts as logged by the integrator are corrected for atmospheric pressure (equivalent to sample loop pressure, since injections were done at ambient pressure) and detector aging. The pressure correction is required since the loop pressure affects the quantity of fluid injected, and dividing by the atmospheric pressure normalizes the response. The correction for detector aging is needed since the gold-sheathed tungsten filaments of the TCD run hotter in an argon carrier stream than in the more common carrier gases such as helium and hydrogen. Thus, the filaments undergo accelerated oxidation due to trace amounts of oxygen that are not trapped. This correction is applied by periodically injecting a standard mixture to track signal loss. The corrected peak areas are then converted to mole fractions either by using a calibration equation or the standard bracketing technique [35,36]. After leaving the detector exit, sample and carrier are expelled through a transfer line to a dedicated outside blower, to provide operator safety.

6. Testing and Evaluation

Since the analytical measurements are the greatest single source of error in this experiment, a thorough testing of the sampling and chromatographic systems was needed. Testing of the nonanalytical components of the apparatus was described in the preceding section. In this section, the extensive tests performed on the analytical system will be described.

Due to the complexity of the two sampling systems, with many joints, fittings and valves, correlation between repeated measurements is very possible. For example, if sampling valves are not sufficiently evacuated or purged, residual sample from previous analyses would cause a systematic, additive error. This would be reflected in a definite trend of component areas with analysis repetition or time.

To check for this type of sample correlation, an extended study was done on a standard mixture of 74.8% hydrogen, 25.2% methane. The mixture was prepared as described (for standard calibration mixtures) in the next section. Thirty separate analyses were done on the mixture over a period of two days. The measurements were made in approximately equal intervals of time. Component areas, total areas, and component chromatographic mole fractions were calculated. Chromatographic mole fractions are those determined from the component area and total area, uncorrected for relative detector response. It was then necessary to look for trends in these measured quantities as a function of sample run or time.

Plots of each of the above quantities versus run (or time) revealed no discernible structure. In addition, tables of correlation were calculated, which included Pearson, Spearman, and Kendall correlation coefficients. No unexpected correlations were observed. Related variables, such as component area and total area, showed high correlation as expected [37,38]. Linear regressions were performed in which the measured chromatographic quantities were fit against the repetition number. In each case, little correlation was found. The estimates of the first order parameter were poorly determined (as deduced from the standard errors) and of questionable significance (as deduced from the t values), while the intercepts were well determined and highly significant. This suggests that the proper representation for repeat analysis data is a mean with some measure of dispersion. Since the data were taken at approximately equal intervals of time, time-series statistics are nominally informative. Thus, first order auto-correlation and Durbin-Watson d statistics were calculated, and indicated minimal correlation among errors [39]. Since an average appears to represent repetitive analysis adequately, we can make probability plots to assess the

nature of the distribution of data about the mean. These tests showed that the actual distribution of measurement values deviates negligibly from the normal distribution, and inferences based on the assumption of normality are valid [40].

It may be concluded from the results of foregoing tests that each analysis is an independent measurement of concentration, unaffected by previous measurements, and that an average of repetition measurements will provide an unbiased estimate of concentration, and the standard deviation will provide a measure of the dispersion.

7. Quantitation

Since the sensitivity of the thermal conductivity detector (TCD) is sample material dependent, it is not possible to take the integrator response as a concentration reading. It should be noted that absolute detectors requiring no calibration are available (for example, a gas density balance), and for these instruments *direct integrator response is a valid method of quantitation*. For relative response detectors such as the TCD, one must use either an internal or external standard, or normalization [35,36]. For this type of work, the external standard method is preferable.

To use the external standard method, mixtures of known composition of hydrogen/methane and hydrogen/propane were prepared. These standard gas mixtures were then chromatographed under the same conditions as the experimental mixtures (same conditions of carrier flow rate, injector, column and detector temperature, and TCD bridge current). The standard mixtures were prepared gravimetrically using a commercial 25 kg capacity two pan balance. The sensitivity of this balance is ± 0.0025 g, with an accuracy dependent on calibration with a standard 1 g class S weight (1.0000 ± 0.0005 g) [41]. This uncertainty will propagate an error of approximately 0.4% into a typical gravimetrical mole fraction (a mixture of 0.5 mole fraction hydrogen prepared by three separate weight measurements).

8. Hydrogen-Methane Calibration and Analysis

Nine standard mixtures of hydrogen-methane were prepared for the calibration, along with a sample of pure hydrogen. Pure methane was not used since it represents an experimentally unaccessible point in the mole fraction range. Separation was easily done using a packed column (1.5 m long, 0.32 cm o.d.) of 150–200 mesh 5 Å molecular sieve. The column was maintained at 60 °C, since methane tends to adsorb on the zeolite surface of the molecular sieve at lower temperatures. The elevated temperature also provided for increased speed of analysis without sacrificing baseline resolution of the peaks. A plot of the corrected area counts (detector response) versus mole fraction is provided in figure 5. The slight but noticeable curvature of this plot is not unusual for

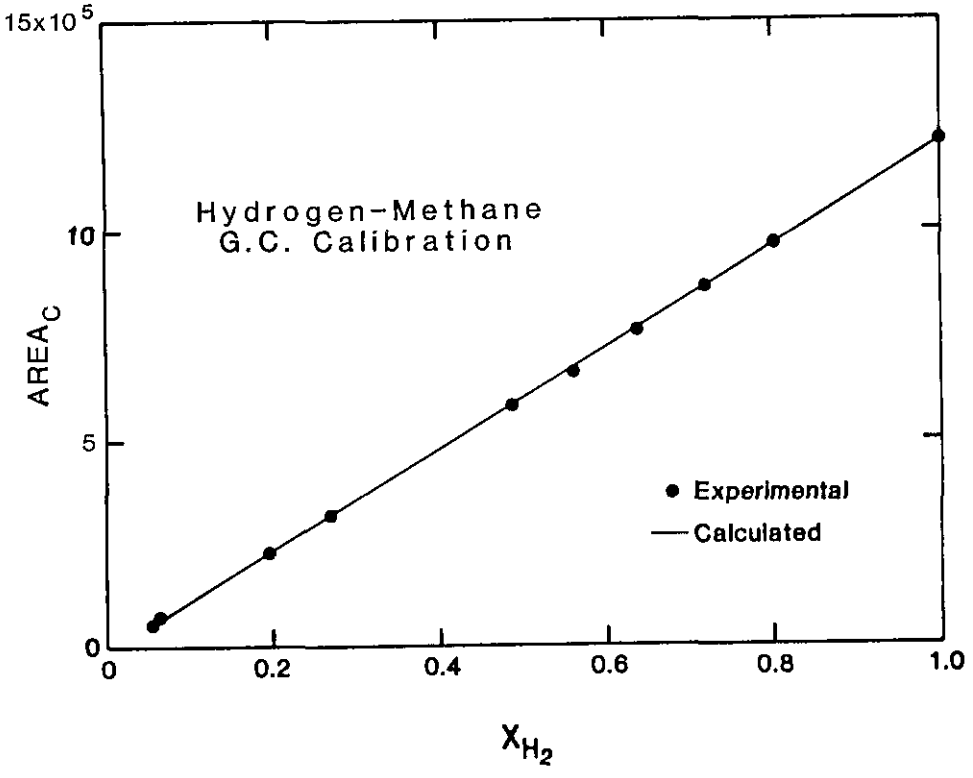

Figure 5–Chromatographic calibration curve for hydrogen-methane binary.

hydrogen-containing binary mixtures.

The data were fitted to a second degree polynomial, with the result that the poorly determined constant term proved to be statistically indistinguishable from zero. This is internally consistent, since the curve must logically pass through the origin. A second degree polynomial constrained to pass through the origin (i.e., the constant term is set equal to zero) was then found to represent the data to within experimental error. The results of the analysis are shown in table 1. The resulting parameters a and b were highly significant (as judged by the t-test and the F-test), although a is far better determined than is b. The percent error in the fit is 0.55, which is comparable to that obtained using other chromatographic quantitation methods. The root mean square error, or overall regression standard deviation, was ± 0.0026 in mole fraction, resulting in an error of 0.52% in mole fraction for an equimolar mixture. A plot of residuals versus mole fraction showed no discernible structure, and a regression found no meaningful correlation. Thus, the model set forth in table 1 accounts for all data structure except random error.

Table 1. Regression results for hydrogen-methane calibration

$$aA + bA^2 = n$$

where A = corrected chromatographic area response
n = mole fraction of hydrogen

regression results:

$a = 8.5764 \times 10^{-7}$	0.56 percent CV
$b = -2.5940 \times 10^{-14}$	38.70 percent CV
$r^2 = 0.99998$	

root mean square error, $n = 0.0026$
coefficient of variation $= 0.5506$

9. Hydrogen Propane Calibration and Analysis

Standard calibration mixtures were prepared for hydrogen-propane in the same way as for hydrogen-methane. For this system, only four standard mixtures were prepared, and only in the higher hydrogen mole fraction range. Calculations were done using the standard "bracketing" method [29] rather than by determining a calibration equation. The reason for this type of calibration (rather than the more preferable type done for hydrogen-methane) is the very high cost of research grade propane. It is, however, not unreasonable to expect mole fraction accuracy of better than 1.0% for the hydrogen-propane system.

This mixture is easily separated using a packed column (1.5 m long, 0.32 cm o.d.) containing porapak-Q[2]. The column was maintained at 80 °C, since the porous polymer packing was observed to entrain hydrogen at lower temperatures. It should be noted that elevated temperatures cause the polymer beads to swell, resulting in an increase in the retention time of hydrogen and a decrease of that of propane. Thus, the temperature at which the two peaks merge is lowered by these additive effects.

10. Results for Hydrogen/Propane and Hydrogen/Methane

Plots of the fugacity coefficient of hydrogen in mixture with propane, $\phi^m_{H_2}$, as deduced from eqs (2), (3), and (4), are shown in figures 6 and 7. The data shown in figure 6 were taken at 80 °C (353 K), and those in figure 7 were taken at 130 °C (403 K). The nominal mixture (total) pressure in each case was 3.45 MPa. The actual data are listed in tables 2 and 3. The error bars represent the uncertainty of a typical $\phi^m_{H_2} - x_{H_2}$ pair, and will be discussed in more detail later. The data represented by the triangles on figure 6 are the results of an earlier study [17]. Although the earlier data were taken at a slightly different temperature (345 K instead of the 353 K in the present work), the agreement is striking.

In both plots, the change in $\phi^m_{H_2}$ is most pronounced at lower values of x_{H_2}. This behavior is consistent for a low molecular weight gas (at a relatively high reduced temperature) in a binary mixture with a heavier gas. It should also be noted that the data at 130 °C show a more gentle increase in slope than the data at 80 °C. This is consistent with the expectation that $\phi^m_{H_2}$ be closer to unity at higher temperatures, for a given composition. The slight upturn at the high hydrogen mole fraction range is probably due to the upturn in molar volume in this region. This behavior of $\phi^m_{H_2}$ is also suggested in an earlier study done under approximately the same conditions [15]. A study comparing the measured values of $\phi^m_{H_2}$ with predictions of several equations of state is ongoing and will be reported later [42].

A plot of $\phi^m_{H_2}$ for hydrogen/methane at 80 °C (353 K) and 3.45 MPa is provided in figure 8. The actual data are listed in table 4. The total change of $\phi^m_{H_2}$ over the hydrogen mole fraction range studied is 13%, compared to

[2]Certain commercial equipment, instruments, or materials are identified in this paper in order to adequately specify the experimental procedure. Such identification does not imply recommendation or endorsement by the National Bureau of Standards, nor does it imply that the materials or equipment identified are necessarily the best available for the purpose.

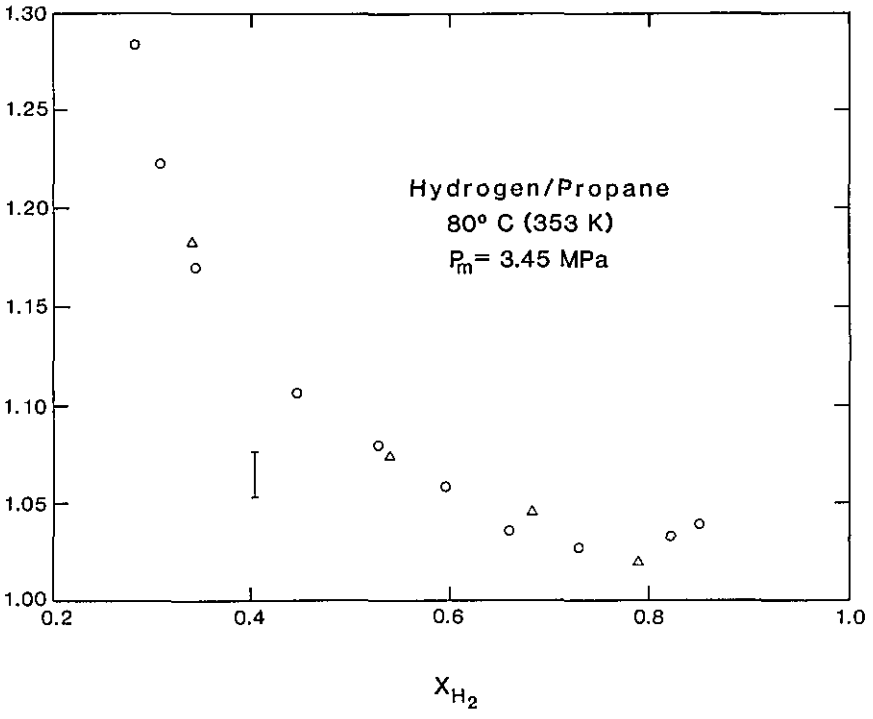

Figure 6–Fugacity coefficient of hydrogen, $\phi^m_{H_2}$, versus mole fraction of hydrogen, in propane at 80 °C (353 K). A typical error bar is shown at the lower left.
o — this work
Δ — previous data of Antezana [17], taken at 345 K.

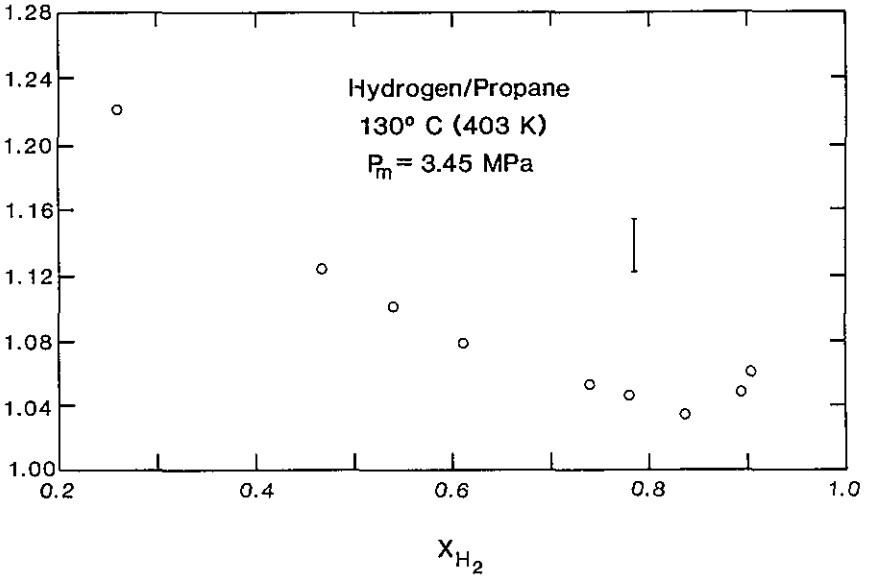

Figure 7–Fugacity coefficient of hydrogen, $\phi^m_{H_2}$, versus mole fraction of hydrogen, in propane at 130 °C (403 K). A typical error bar is shown at upper right.

23% in the hydrogen-propane mixture at 353 K. This is expected because of the higher reduced temperature of methane. The value of $\phi^m_{H_2}$ changes most sharply in the region of low hydrogen mole fraction, as expected [10]. Data on this system were not taken above 353 K since the change in $\phi^m_{H_2}$ would probably not be detected. As with the hydrogen-propane system, work on predictions and comparison with equation of state results is in progress and will be reported on later.

The error bars shown in figures 6–8 represent random propagated errors in $\phi^m_{H_2}$ and x_{H_2}. From eq (2), only the first term on the righthand side was considered, since the contribution of the second order term is small. Errors in temperature, hydrogen partial pressure, and the second virial coefficient were then considered. Strictly, the error in B might properly be considered systematic, however enough data are available on hydrogen to ascribe a measure of dispersion about B [43–45]. The error propagation for eqs (3) and (4) was carried out in the usual manner [46]. The recognized sources of systematic error, along with countermeasures, have been described in the experimental section.

Table 2. Hydrogen/propane at 80 °C (353 K)

Mole fraction, H_2	Partial pressure, H_2 (MPa)	Fugacity coefficient, $\phi^m_{H_2}$
0.848	3.01	1.040
0.822	2.91	1.033
0.730	2.73	1.028
0.659	2.33	1.036
0.594	2.15	1.058
0.526	1.96	1.080
0.445	1.69	1.106
0.344	1.39	1.170
0.309	1.33	1.230
0.280	1.25	1.283

Table 3. Hydrogen/propane at 130 °C (403 K)

Mole fraction, H_2	Partial pressure, H_2 (MPa)	Fugacity coefficient, $\phi^m_{H_2}$
0.904	3.29	1.058
0.897	3.23	1.054
0.835	2.96	1.038
0.783	2.81	1.047
0.738	2.66	1.047
0.618	2.28	1.077
0.545	2.06	1.096
0.472	1.82	1.116
0.265	1.12	1.220

Table 4. Hydrogen/methane at 80 °C (353 K)

Mole fraction, H_2	Partial pressure, H_2 (MPa)	Fugacity coefficient, $\phi^m_{H_2}$
0.849	3.17	1.121
0.790	2.92	1.115
0.764	2.80	1.097
0.652	2.40	1.115
0.536	1.99	1.125
0.459	1.75	1.134
0.307	1.19	1.166
0.216	0.88	1.223

The author would like to thank Drs. Gerald C. Straty and Howard J. M. Hanley for many helpful discussions, and Gretchen L. Hume for her assistance in performing some of the measurements.

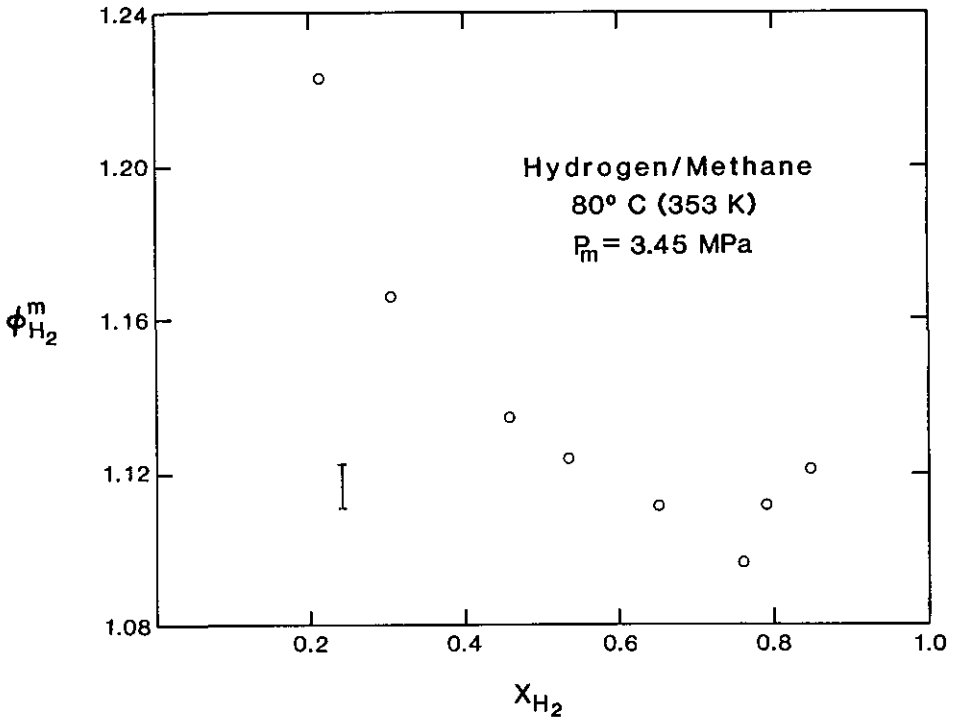

Figure 8–Fugacity coefficient of hydrogen $\phi^m_{H_2}$, versus mole fraction of hydrogen, in methane at 80 °C (353 K). A typical error bar is shown at the lower left.

12. References

[1] Lewis, G. N., Proc. Am. Acad. **37**, 49 (1901).
[2] Lewis, G. N., Z. Physik. Chem. **38**, 205 (1901).
[3] Lewis, G. N., and M. Randall, *Thermodynamics*. New York: McGraw-Hill Book Co. (1961–revised).
[4] Sandler, S. I., *Chemical and Engineering Thermodynamics*. New York: John Wiley and Sons (1977).
[5] Kyle, B. G., *Chemical and Process Thermodynamics*. Englewood Cliffs: Prentice Hall, Inc. (1984).
[6] Prausnitz, J. M., *Molecular Thermodynamics of Fluid-Phase Equilibria*. Englewood Cliffs: Prentice Hall, Inc. (1969).
[7] Prausnitz, J. M., A.I.Ch.E. J. **5**, 3 (1959).
[8] Chao, K. C., and R. A. Greenkorn, *Thermodynamics of Fluids*. New York: Marcel Dekker, Inc. (1975).
[9] Denbigh, K., *The Principles of Chemical Equilibrium*. Cambridge University Press (1971 3rd Ed.).
[10] Cheh, H. Y., Proceedings of the 6th symposium on thermophysical properties. ASME, *256* (1973).
[11] Ramsay, W., Phil. Mag. **38**(5), 206 (1894).
[12] Tsakalotos, D., Proc. Chem. Soc. London **24**, 208 (1908).
[13] Krishnamurty, V. V. G., doctoral dissertation. New York: Columbia University (1963).
[14] Cooper, H. W., doctoral dissertation. New York: Columbia University (1967).
[15] Ghosal, A. B., doctoral dissertation. New York: Columbia University (1971).
[16] Klink, A. E.; H. Y. Cheh and E. H. Amick, A.I.Ch.E. J. **21**, 1142 (1975).
[17] Antezana, F., and H. Y. Cheh, Ind. Eng. Chem. Fundam. **14**, 224 (1975).
[18] Antezana, F., and H. Y. Cheh, Ind. Eng. Chem. Fundam. **15**, 95 (1976).
[19] Klink, A. E., private communication (1981).
[20] Antezana, F., private communication (1981).
[21] ASME boiler and pressure vessel code, Sec. VIII: Unfired pressure vessels. New York: American Society of Mechanical Engineers (1965).
[22] Oberg, E., and F. D. Jones, Machinery's Handbook, H. L. Horton, ed. New York: The Industrial Press (1964, 2104 p.).
[23] Smith, D. P., *Hydrogen in Metals*. Chicago: University of Chicago Press (1948).
[24] Wise, E. M., *Palladium*. New York: Academic Press (1968).
[25] McGee, W., private communication (1981).
[26] Sparks, L. L., private communication (1982).
[27] Powell, R. L.; W. J. Hall, C. H. Hyink, L. L. Sparks, G. W. Burns, M. G. Scroger, and H. H. Plumb, Thermocouple reference tables based on the IPTS-68. Natl. Bur. Stand. (U.S.) Monogr. 125 (1974).
[28] Jeffery, P. G., and P. J. Kipping, *Gas Analysis by Gas Chromatography*. Oxford: Pergamon Press (1972).
[29] Cowper, C. J., and A. J. DeRose, *The Analysis of Gases by Chromatography*. Oxford: Pergamon Press (1983).
[30] Brombacher, W. G.; D. P. Johnson, and J. L. Cross, Mercury barometers and manometers. Natl. Bur. Stand. (U.S.) Monogr. 8 (1964).
[31] Conder, J., and R. Young, *Physicochemical Measurement by Gas Chromatography*. Chichester: John Wiley and Sons (1979).
[32] Laub, R. J., and R. L. Pecsok, *Physicochemical Applications of Gas Chromatography*. New York: Wiley Interscience (1978).
[33] Bruno, T. J.; D. E. Martire, M. W. P. Harbison, A. Nikolic, and C. F. Hammer, J. Phys. Chem. **87**, 2425 (1983).
[34] Heftmann, E., *Chromatography; A Laboratory Handbook of Chromatographic and Electrophoretic Methods*. New York: Van Nostrand Reinhold (1975, 3rd Ed.).
[35] McNair, H. M. and E. J. Bonnelli, *Basic Gas Chromatography*. Varian Aerograph (1969).
[36] Grant, D. W., *Gas Liquid Chromatography*. London: Van Nostrand Reinhold (1971).
[37] *S.A.S. Users Guide: Statistics*. Cary, NC: SAS Institute (1982).
[38] Langley, R., *Practical Statistics*. New York: Dover (1970).
[39] Ostle, B., and R. W. Mensing, *Statistics in Research*. Ames, IA: Iowa State University Press (1975).
[40] Vecchia, D. L., private communication (1984).
[41] Battino, R., and A. G. Williamson, J. Chem. Ed. **61**, 51 (1984).
[42] Ely, J. F., to be published.
[43] Levelt-Sengers, J. M. H.; M. Klein, and J. S. Gallagher, AEDC-TR-71-39; USAF (1971).
[44] Goodwin, R. D., private communication (1984).
[45] McCarty, R. D., private communication (1984).
[46] Meyer, S. L., *Data Analysis for Scientists and Engineers*. New York: John Wiley and Sons (1975).

conference report

PROGRAMS CONSIDERED IN RADIATION INSTRUMENTS AND LABORATORY SYSTEM

The NBS-hosted Workshop on Radiation Survey Instruments and Calibrations brought together representatives of the public and private sectors to discuss possible future national programs in two related areas. The first program would test the performance of radiation survey instruments and would be based on performance criteria and test methods contained in a standard now under development. The second would establish a system of secondary standards laboratories that could provide instrument calibrations and related services including, for example, instrument performance testing and measurement quality assurance.

Joining with NBS as sponsors of the July 10–12 workshop were the Department of Defense, the Department of Energy, the Center for Devices and Radiological Health in the Food and Drug Administration, the Nuclear Regulatory Commission, the Conference of Radiation Control Program Directors, the Nuclear Suppliers Association, and the Health Physics Society. This represents a balance among interested agencies and organizations in the private, state, and federal sectors. The workshop program was structured to present each of these three perspectives, and the 160 registrants represented a similar wide range of interests and concerns.

Measurement Incentive

To establish the proper perspective for discussions that were to follow, the workshop began with a few papers that emphasized the increasing importance of making accurate measurements of radiation. It was generally agreed that new legislation, and a steady growth in litigation related to personnel exposure, provide strong incentive for improved reliability and defendability of measurement results.

Discussion of the first major topic (survey instrument performance) began with a series of papers that described operational problems with instruments over a broad range of user interests and conditions of use. Possible solutions of these problems were then considered, including a draft American National Standard that would establish detailed instrument performance requirements and would prescribe testing procedures used to determine whether those requirements have been met by a particular instrument. The possibility of a national instrument testing and certification program, based on the draft standard, was discussed by a panel including instrument users and manufacturers. It was generally agreed that development of the standard should continue, but that implementation of a national program would require much additional planning and study of various alternative approaches.

The second major topic (secondary standards laboratories) was introduced by several papers that described a limited number of ongoing programs resulting in secondary laboratories, and the operational criteria for those laboratories. Several representatives of national user sectors then expressed their interest in, and support for, development of a system of secondary laboratories in the private sector. Representatives of national professional societies and organizations participated in a panel discussion that was intended to identify an organization that would coordinate private-sector development, and conceivably accredit secondary laboratories that satisfy established performance criteria in the future. A clear majority of the workshop attendees indicated a preference to have the Health Physics Society perform this function.

National Committee Established

In a final session, speakers described relevant recent technical work relating to either of the two major topics, such as studies of instrument performance and specialized calibration facilities.

The interactions and discussions that began during the workshop will be continued in a national committee for which NBS will serve as the secretariat. This committee will consist of members who will represent all the major interests. It will plan and guide implementation of a national instrument testing program and the establishment of a system of private-sector secondary standards laboratories. After the committee has developed specific plans that represent the consensus of the various interests, a second workshop will be held to present the plans to the general community of instrument users, manufacturers, and other concerned parties.

The proceedings of the workshop are to be published by the Department of Energy.

Prepared by *Elmer H. Eisenhower, chief of the Office of Radiation Measurement, NBS.*